Mathematical Modeling of the Diffusion of Magnetic Particles in a Ferrofluid Seal under Magnetic and Centrifugal Forces

Dissertation

zur Erlangung des akademischen Grades

doctor rerum naturalium
(Dr. rer. nat.)

von **Dipl.-Math. Klim Kavaliou**
geb. am 8. May 1987 in Elisenvaara, Russische Föderation

genehmigt durch die Fakultät für Mathematik
der Otto-von-Guericke-Universität Magdeburg

Gutachter: **Prof. Dr. rer. nat. habil. Lutz Tobiska**
Prof. Dr. Viktor Polevikov

eingereicht am: 01.12.2015
Verteidigung am: 06.04.2016

Acknowledgements

I would like to express my deepest gratitude to my supervisor Prof. Dr. Lutz Tobiska for giving me the opportunty to study for my PhD at the Otto-von-Guericke University of Magdeburg. I am highly thankful for remarkable discussions and valuable suggestions, which came always in time. He encouraged me and provided constant support in all what conserned my studies and beyound. His marvelous interest to mathematics inspired me during all these years. This invaluable experience opened the door to my academic research career.

I am very gratefull to Prof. Viktor Polevikov from Belarusian State University for fruitful discussions and sharing the ideas. I appreciate his criticism and valuable suggestions on the topic of my research. All meetings with him inspered me and provided lots of new ideas.

I would like to acknowledge the DFG-Graduiertenkolleg 1554 "Micro-Macro-Interactions in Structured Media and Particle Systems" for granting me the scholarship to pursue my doctoral studies. I am grateful to all professors and members of the Graduiertenkolleg for helpfull discussions and introduction into new fields of science.

I would like to thank my friends Dr. Piotr Skrzypacz and Dr. Naveed Ahmed for their support, especially at the beginning of my studies. I am grateful to all members of Prof. Tobiska's research group for sharing their researche experience and providing with the new ideas. I appreciate my colleges Alina Bondarava and Kristin Simon, who every day improved my mood, were ready to help in any situation and always open for discussion.

I am grateful to my friends in Minsk, Ivan Bachtin and Volha Linkevich, for their belief in me and encouragement. I express wholehearted gratitude to my parents, my brother and all my family. Their unlimited love and support gave me the power to bring the efforts to complete my doctoral studies.

Abstract

The main objective of this thesis is to derive a mathematical model of a ferrofluid seal which can be used for an accurate and robust numerical simulation. The mathematical model considers the effect of redistribution of magnetic particles in a moving ferrofluid, which stays in presence of a strong outer magnetic field. The presence of fluid-gas surfaces implies the free surface problem to be taken into consideration. Numerical tests determine the parameter range at which the mathematical model is applicable and answer the main question, how the effects of fluid motion and particle concentration interact.

The derivation of a mathematical model starts with a system of 3D partial-differential equations. Different assumptions, such as an axial symmetry of the external forces etc., allows to write the system in a 2D cross-section and simplify it. The simplified mathematical model is a partially coupled system of three partial differential equations and an integro-differential equation. For solution of the resulting mathematical model a decoupling strategy is suggested. Each equation is considered and discretized as a separate problem. In most cases the standard theory for unique solvability and stability of the discretization can be applied. Some of the problems, however, need a special treatment. For example, the discretization of the convective-diffusive problem describing the particle concentration. The mixed Finite Element–Finite Volume discretization is introduced, for which the stability can be shown. In the literature this type of discretizations is usually performed on weakly acute triangulation of the domain. The presented analysis allows to extend it to a more general Delaunay triangulation with preserving properties of the discretization. The numerical computations confirm the theoretical predictions.

The decoupling strategy for the solution of the considered mathematical model is as follows. The four equations of the system are split into two pairs. The pairs of the equations are solved sequentially, the coupled solution of each pair is obtained by iteration technique. The numerical computations provide a better understanding of the interaction of particle distribution and fluid motion, which is quite strong and cannot be neglected. The mathematical model is appropriate for modeling of rotary ferrofluid-based seals. Moreover, under seal conditions the fluid motion effect is dominating, i.e. the particle concentration stays close to uniform.

Zusammenfassung

Das Hauptziel der vorliegenden Arbeit ist die Herleitung eines mathematischen Models für Magnetfluiddichtungen, welches akkurate und robuste numerische Simulationen ermöglicht. Dieses Model berücksichtigt den Einfluss der Umverteilung magnetischer Partikel in bewegenten Magnetfluiden unter dem Einfluss äußerer Magnetfelder. Die vorhandene Fluid-Gas-Oberfläche ist als freie Oberfläche Teil des Problems. Mit Hilfe numerischer Tests wird der Parameterbereich bestimmt, in welchem das mathematische Model anwendbar ist. Von besonderem Interesse ist dabei inwieweit sich die Fluidbewegung und die Konzentration der magnetischen Partikel gegenseitig beeinflussen.

Die Herleitung des mathematischen Models geht von einem System dreidimensionaler partieller Differentialgleichungen aus. Verschiedene Annahmen, wie Achsensymmetrie der äußeren Kräfte, ermöglichen die Vereinfachung des Systems in eine zweidimensionale achsensymmetrische Formulierung. Das vereinfachte Model ist ein partiell gekoppeltes System dreier partieller Differentialgleichungen und einer Integrodifferentialgleichung. Zur Lösung dieses Problems wird eine Entkopplungsstrategie vorgeschlagen, bei der jede Gleichung separat betrachtet und diskretisiert wird. Für die meisten dieser Gleichungen kann Standardtheorie für die eindeutige Lösbarkeit und Stabilität der Diskretisierung verwandt werden. Einige Teilprobleme bedürfen jedoch spezieller Techniken. Für die Konvektions-Diffusions-Gleichung der Partikelkonzentration wird die gemischte Finite Elemente-Finite Volumen-Diskretisierung eingeführt, für welche Stabilität gezeigt werden kann. In der Literatur werden für diese Form der Diskretisierung nichtstumpfe Triangulierungen des Gebietes genutzt. Die hier präsentierte Analysis ermöglicht den Übergang zu allgemeineren Delaunay-Triangulierungen. Die mathematischen Berechnungen bestätigen hierbei die theoretischen Ergebnisse.

Die Entkopplungsstrategie sieht vor das System aus vier Gleichungen in zwei Gleichungspaare zu teilen. Diese Paare werden sequentiell bearbeitet. Die Lösung jedes solchen Paares aus gekoppelten Gleichungen geschieht dabei mit Hilfe einer Iterationstechnik. Die numerischen Simulationen bieten einen besseren Einblick in die Interaktion von Partikelverteilung und Fluidbewegung. Diese erweist sich als ziemlich stark und kann nicht vernachlässigt werden. Das gewonnene mathematische Model kann zur Beschreibung von rotierenden ferrofluidbasierten Dichtungen verwendet werden. Unter realistischen Anwendungsbedingungen wird das Problem durch die Fluidbewegung dominiert und die Partikelkonzentration bleibt nahezu konstant.

Contents

Chapter 1

Introduction

Overview

A ferrofluid is a liquid which becomes strongly magnetized in the presence of a magnetic field, so that magnetic moment of a ferrofluid is only one order lower than that of a solid magnetic material. This property is provided by a nanoscaled – around 10 nm – ferri- or ferromagnetic particles suspended throughout the basic liquid. The carrier fluid can be some type of hydrocarbons, water or organic solvent. Magnetic particles are covered by a surfactant, which keeps them dispersed and prevents sedimentation. For detailed overview of ferrofluids and their properties see [6, 37].

Ferrofluids found wide application in engineering, biology and medicine [6, 37]. This can be explained by a combination of two properties, usually excluding each other, magnetization and fluidity. One of the most successful applications of the ferrofluids are ferrofluid seals, also called magneto-fluid seals. These are rotary seals with a ferrofluid being a sealing material, which is held in the gap by a high gradient magnetic field. The main advantage is a very low leakage, which remains a problem of sealing, especially for rotary seals [17, 19]. Ferrofluid seal can be used to separate liquids or gases. For both types of isolated media the main question is how to estimate the stability limits of a ferrofluid seal under different operation conditions. For liquids the interaction of a magnetic fluid and a fluid being sealed on a liquid–liquid interface is a point of great importance for modeling and application [19]. For gases this problem does not arise, what decreases the number of effects to be taken into account and simplifies modeling.

There is a number of experimental [1, 35] and numerical studies [16, 22, 29, 31, 33, 47, 48] on ferrofluid seals separating two gas regions. Theoretical and numerical investigations regarding the magnetophoresis and Brownian motion in ferrofluids are presented in [4, 5, 32, 34]. We should take into account a number of effects. In particular, shaft rotation brings fluid in motion, the shape of a gas-liquid surface is determined by the force balance on it, the non-uniform magnetic field leads to non-uniform distribution of magnetic particles. In the following we discuss the related studies, which lead us to a new model. It is worth mentioning that all these studies consider the steady state of a

ferrofluid seal. A special geometry of structural elements of a ferrofluid seal and its main advantage were introduced in [47]. The authors neglected the magnetization of a ferrofluid, what allowed to obtain an analytical expression for the magnetic field in the gap. This approach was used in series of works, where either hydrodynamic effects [31, 47, 48] or redistribution of particles [33] were taken into account. In [22] the authors attempted to estimate the influence of the fluid velocity on the particle concentration. However, the backward interaction was not investigated.

Modeling aspects and discretization strategy

In this thesis we are interested in modeling a ferrofluid seal taking into account the effect of a non-uniform particle distribution in a moving liquid. The interrelation of a fluid velocity and a particle concentration is considered as well. Following the ideas in the above mentioned studies and classical literature on ferrofluids [6, 37], we formulate a complex mathematical model in the three-dimensional Cartesian space. Assuming axisymmetry of magnetic and velocity fields as well as the smallness of the gap size to the shaft radius, the system can be approximated by a two-dimensional system in a cross-section. The relevance of this approximation was shown in [31].

The introduced system can be described as follows. Maxwell's equations set the magnetic fields in the gap. Neglecting the influence of magnetization on the magnetic field allows us to simplify and solve them analytically. The hydrodynamic properties are described by the incompressible Navier-Stokes equation, which is split into two equations. Specifically, the Laplace equation for the azimuthal component of the velocity and Navier-Stokes-type equation for the planar velocity component in a cross section. Young-Laplace equation determines the free surface shape. Moreover, the redistribution of magnetic particles is described by a convective-diffusive type problem.

Our goal is to obtain a robust numerical solution of the system. The Laplace equation is solved by two different methods, namely by Finite Elements and Boundary Elements. We use the boundary element discretization in order to provide a simple coupling with the Young-Laplace equation. The finite element method is used due to a good connection to the other discrete problems. The Young-Laplace equation is a complex integro-differential equation, for which we discuss only the discretization technique not considering its properties. The slip boundary conditions of the Navier-Stokes equation are not easy to handle, so we refer to the literature [2, 3] in order to provide a robust numerical scheme. Convection-diffusion equation leads to a noncoercive elliptic problem and needs a special treatment. The continuous convective-diffusive type problem was studied in [12]. The authors proved the unique solvability along with some interesting properties, such as positivity of a solution. The Finite Volume, discretization preserving important properties of the continuous problem, was first introduced in [10]. In [21] we suggested the Finite Element–Finite Volume discretization. The final structure of this scheme is related to the one in [10]. Due to the similarity of two above schemes, the majority of properties were inherited. Moreover, in [21] we have shown the stability of the discretization. The disadvantage of the numer-

ical scheme in [21] is discretization on a weakly acute type triangulation. In this work we extended it to a more general Delauney triangulation with preserving discretization properties.

Structure of the thesis

The thesis is outlined as follows. We begin Chapter 2 by presenting some well-known results of the vector calculus. In particular, the transformations form the three-dimensional Cartesian coordinates to cylindrical coordinates are given. We proceed this chapter with the derivation of above mentioned equations, which are written in 3D Cartesian coordinates and then transformed into cylindrical ones. Neglecting particular effects allows us to provide a planar approximation of the system. We assume the existence of a steady state of the system and Newtonian behavior of a ferrofluid. Moreover, we neglect the influence of a fluid magnetization on a magnetic field strength as well as the interparticle dipole-dipole interaction. At the end of the section the full mathematical model is formulated.

In Chapter 3, the considered model is split into an integro-differential equation and three partial differential equations, which are studied separately. We analyze the integro-differential equation and derive the variational formulation of the partial differential equations. Finally, the existing solvability results for the variational problems are presented.

The discretization of the continuous subproblems is introduced in Chapter 4. We present Boundary Element and Finite Element method for the Laplace equation, which describes the azimuthal velocity. The Young-Laplace equation is discretized following the ideas in [31]. Next, we provide a discretization of the Navier-Stokes equation by the Finite Element method in velocity-pressure formulation. For the convection-diffusion equation three methods are discussed. The first one is the Finite-Volume method [10], whereas the other two are the mixed Finite Element–Finite Volume method on a weakly acute triangulation [21] and its extension to the Delauney triangulation. The former one is used for the discretization of the convection-diffusion equation. The solution strategy for partially coupled system completes this chapter.

The numerical tests are presented in Chapter 5. Here, we compare our numerical results with the ones obtained in the related study [31]. In order to demonstrate the properties of the discretization of the convection-diffusion equation some model problems are considered. Finally, we solve the coupled subsystem of the Navier-Stokes and the convection-diffusion equations and systemize the results.

1. Introduction

Chapter 2

Mathematical model and simplifications

We derive a mathematical model of a ferrofluid rotary seal, which you can see on Figure 2.1. The basic seal consists of a ferrofluid, annular permanent magnet, an annular pole piece and a magnetically permeable shaft [17]. The shaft is a rotating cylinder around which the coaxial magnet and pole pieces are placed. We consider a model with a pole having a hyperboloidal profile, which is quiet close to a triangular shape. According to [35] the optimal tapering angle lies in between 30 and 45 grad.

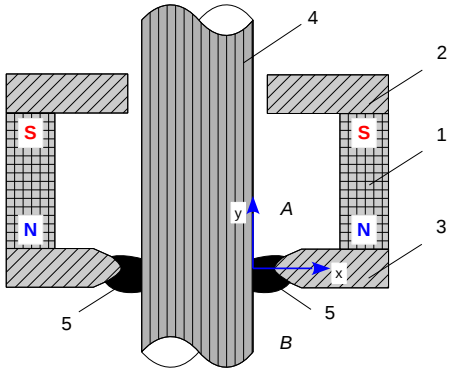

Figure 2.1: Schematic view of the magnetic fluid seal: 1 – magnet, 2 – core, 3 – magnetic flux concentrator, 4 – shaft, 5 – magnetic fluid, A – region of high pressure, B – region of low pressure.

The narrow gap between the pole and the shaft is filled with a ferrofluid which forms a hermetic barrier between two areas of different pressure. The state of ferrofluid in the seal is determined by the balance of three forces: magnetic force, centrifugal force, and the pressure drop.

2. Mathematical model and simplifications

The general 3D model consists of the following equations. The system of the Maxwell equations describes the magnetic field for nonconducting media

$$\nabla \cdot \mathbf{B} = \mathbf{0},$$
$$\nabla \times \mathbf{H} = \mathbf{0}.$$

The Navier-Stokes equation expresses the flow of the incompressible Newtonian ferrofluid

$$\rho\left(\mathbf{v} \cdot \nabla\right)\mathbf{v} = \nabla \cdot \mathbb{T}(\mathbf{v}, p, \mathbf{H}, \mathbf{B}) + \rho\mathbf{g},$$
$$\nabla \cdot \mathbf{v} = 0.$$

The Young-Laplace equation describes the force balance on the free surface Γ_f and determines its shape

$$\mathbf{n} \cdot [|\mathbb{T}(\mathbf{v}, p, \mathbf{H}, \mathbf{B}) \cdot \mathbf{n}|] = \alpha\mathcal{K} \quad \text{on } \Gamma_f.$$

The concentration of ferromagnetic particles is obtained as a solution of a convection-diffusion problem for the Brownian motion of particles

$$\rho\mathbf{v} \cdot \nabla c = -\nabla \cdot \mathbf{i},$$
$$\frac{1}{|\Omega|}\int_\Omega c\,dx = 1.$$

All the equations are supplemented with boundary conditions which will be given later. Here $\mathbf{H}$ and $\mathbf{B}$ denote the magnetic field intensity and the magnetic induction, respectively, ρ the fluid density, $\mathbf{v}$ the fluid velocity, p the hydrodynamic pressure, $\mathbf{g}$ the acceleration of gravity, $\mathbb{T}$ the combined hydrodynamic and magnetic stress tensor, $\mathbf{n}$ a unit normal to Γ_f, α the surface tension, $\mathcal{K}$ the sum of principal curvatures, c the particle concentration, $\mathbf{i}$ the mass flux density.

The derived mathematical model is partially investigated in a series of works [27, 31, 33, 47, 48]. On Figure 2.2 one can see the schematic view of these studies (arrows 1-3) and the improvement provided by current work (4). Arrows on the figure shows the dependencies between equations for different models. Let us discuss them in details.

One should note that the effects of particle redistribution and fluid motion were not considered together in that series of studies [27, 31, 33, 47, 48]. It means in case of moving liquid the particle concentration was assumed to be uniform, so the convection-diffusion equation was omitted. The change of particle concentration [33] was investigated for no flow case, i.e. the Navier-Stokes equation was omitted.

In all above mentioned studies Maxwell equations ignore the fluid magnetization so the solution is equivalent to gap with no fluid at all. Having in addition the hyperboloid profile of the concentrator allows to find an analytical expression of magnetic field intensity, which reduces the system of equations. That is why it is also skipped in the scheme. The Young-Laplace equation is needed to fix the domain shape, which is used by all the other equations.

Let us make more clear the split of Navier-Stokes equation, which you can see on the Figure 2.2. In case of a moving fluid the system of Navier-Stokes and Young-Laplace

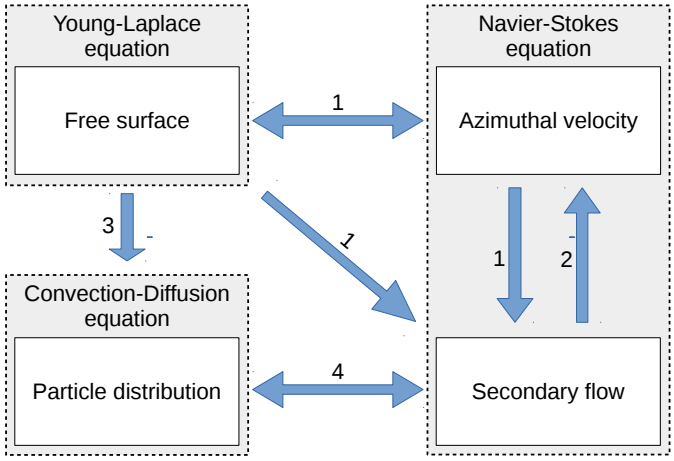

Figure 2.2: Effects taken into account in different studies: 1 - [31, 47, 48]; 1,2 - [27]; 3 - [33]; 1,3,4 - present work.

equations is investigated [27, 31, 47, 48]. The Navier-Stokes equation is split into two equations for different velocity components: the azimuthal velocity describing liquid rotation around the shaft and the secondary flow expressing fluid motion into 2-dimensional cross-section. Azimuthal velocity has a great influence on the free surface shape, i.e. the corresponding problems are strongly coupled.

Influence of the secondary flow on the azimuthal velocity was neglected in [31, 47, 48] (model 1). That neglecting was studied in [27] (model 1-2), where the numerical tests have shown its validity. The particle redistribution in case of a non-moving fluid was observed in [33] (model 3). The aim of the present research is to take into account fluid motion and nonuniform particle distribution, i.e. to solve the system of Young-Laplace, Navier-Stokes and convection-diffusion equations (model 1,3,4).

The mathematical model which is used for the numerical simulations is derived in the following steps. At first we formulate general 3-dimensional equations in Cartesian coordinates. We investigate the steady state of the system, i.e. the solution does not depend on time. Also we assume that the system is isothermal, i.e. the temperature of the system is uniform and constant. Assuming a laminar flow and axially magnetization of the magnet allows us to consider the rotation symmetry of the system. Further we can write equations in 3-dimensional cylindrical coordinates with z axis coinciding with the axis of symmetry. Along that axis the system has rotational invariance. Moving the origin to the shaft surface along the r axis and taking into consideration the smallness of the gap we simplify the 3-dimensional system to a 2-dimensional one written in the cross-section. In the following we describe all these steps in detail for each equation separately.

2.1 Curvilinear coordinates

We present at the first part of this section the transformation from 3D Cartesian coordinates to general curvilinear coordinates. Then formulas for the transformation to cylindrical coordinates are given. These expressions are later used for the partial differential equations.

2.1.1 Vector Calculus

Let us consider some basic vector calculus in general 3-dimensional curvilinear coordinates. We generally follow the description in [25].

Every point in 3-dimensional space is given by three numbers or Cartesian coordinates x_1, x_2, x_3. Also it can be represented by three other numbers or curvilinear coordinates q_1, q_2, q_3 which are related to previous ones by the invertible transformations

$$\begin{aligned} x_i &= x_i(q_1, q_2, q_3), \qquad i = \overline{1,3}, \\ q_j &= q_j(x_1, x_2, x_3), \qquad j = \overline{1,3}. \end{aligned}$$

Every point can also be written as a position vector

$$\mathbf{r}(x_1, x_2, x_3) = x_1\mathbf{e}_1 + x_2\mathbf{e}_2 + x_3\mathbf{e}_3,$$

where $\mathbf{e}_1, \mathbf{e}_2, \mathbf{e}_3$ are standard basis vectors in Cartesian coordinates. Each unit vector can be evaluated by differentiation of a position vector with respect to corresponding variable, e.g.

$$\mathbf{e}_i = \frac{\partial \mathbf{r}}{\partial x_i} \Bigg/ \left| \frac{\partial \mathbf{r}}{\partial x_i} \right|, \quad i = \overline{1,3}.$$

Following these rules we can define the basis vectors in a fixed point of a curvilinear coordinate system

$$\mathbf{k}_i = \frac{1}{H_i} \frac{\partial \mathbf{r}}{\partial q_i} \quad i = \overline{1,3},$$

where

$$H_i = \left| \frac{\partial \mathbf{r}}{\partial q_i} \right| = \sqrt{\left(\frac{\partial x_1}{\partial q_i}\right)^2 + \left(\frac{\partial x_2}{\partial q_i}\right)^2 + \left(\frac{\partial x_3}{\partial q_i}\right)^2} \tag{2.1}$$

are the scale factors which are called Lamé coefficients. Differential changes along the unit vectors $\mathbf{k}_i$ can be evaluated as

$$ds_i = |d_{q_i}\mathbf{r}| = \left| \frac{\partial \mathbf{r}}{\partial q_i} \right| dq_i = H_i dq_i.$$

In case the vectors $\mathbf{k}_i$ are orthogonal at all points, the differential of the arc length is calculated as a space diagonal

$$d\mathbf{s}^2 = ds_1^2 + ds_2^2 + ds_3^2 = H_1^2 dq_1^2 + H_2^2 dq_2^2 + H_3^2 dq_3^2.$$

The gradient of a scalar or vector valued function f in curvilinear coordinates is derived by the definition

$$(\text{grad } f)_i = \text{grad } f \cdot \mathbf{k}_i = \frac{1}{H_i}\left(\frac{\partial f}{\partial x_1}\frac{\partial x_1}{\partial q_i} + \frac{\partial f}{\partial x_2}\frac{\partial x_2}{\partial q_i} + \frac{\partial f}{\partial x_3}\frac{\partial x_3}{\partial q_i}\right) = \frac{1}{H_i}\frac{\partial f}{\partial q_i}. \tag{2.2}$$

The divergence of a vector field $\mathbf{a}$ is given by

$$\text{div } \mathbf{a} = \frac{1}{H_1 H_2 H_3}\left(\frac{\partial (a_1 H_2 H_3)}{\partial q_1} + \frac{\partial (a_2 H_1 H_3)}{\partial q_2} + \frac{\partial (a_3 H_1 H_2)}{\partial q_3}\right). \tag{2.3}$$

Combining equations (2.2) and (2.3) we obtain the formula for the Laplace operator applied to a scalar function f

$$\begin{aligned}\Delta f &= \text{div grad } f \\ &= \frac{1}{H_1 H_2 H_3}\left(\frac{\partial (\frac{H_2 H_3}{H_1}\frac{\partial f}{\partial q_1})}{\partial q_1} + \frac{\partial (\frac{H_1 H_3}{H_2}\frac{\partial f}{\partial q_2})}{\partial q_2} + \frac{\partial (\frac{H_1 H_2}{H_3}\frac{\partial f}{\partial q_3})}{\partial q_3}\right).\end{aligned} \tag{2.4}$$

2.1.2 From Cartesian to cylindrical coordinates

We apply the general vector calculus in order to obtain representation of differential operators in cylindrical coordinates, namely the Laplace operator and material derivative. We consider the case when the z axis in cylindrical coordinates coincides with the x_3 axis in Cartesian ones. We remind that a point in cylindrical coordinates is determined by three numbers (r, ϕ, z) which are related to Cartesian coordinates

$$\begin{aligned} r &= \sqrt{x_1^2 + x_2^2}, & x_1 &= r\cos\phi, \\ \phi &= \arctan\frac{x_2}{x_1}, & x_2 &= r\sin\phi, \\ z &= x_3, & x_3 &= z. \end{aligned} \tag{2.5}$$

The cylindrical coordinates x, y, z correspond to the general curvilinear coordinates q_1, q_2, q_3 from previous section. The basis vectors of the cylindrical coordinate system at arbitrary point $\mathrm{P} = (x_1, x_2, x_3)$ are given as follows

$$\begin{aligned} \hat{\mathbf{r}} &= \cos\phi\,\mathbf{e}_1 + \sin\phi\,\mathbf{e}_2 = \frac{x}{\sqrt{x_1^2 + x_2^2}}\mathbf{e}_1 + \frac{x_2}{\sqrt{x_1^2 + x_2^2}}\mathbf{e}_2, \\ \hat{\boldsymbol{\phi}} &= -\sin\phi\,\mathbf{e}_1 + \cos\phi\,\mathbf{e}_2 = -\frac{x_2}{\sqrt{x_1^2 + x_2^2}}\mathbf{e}_1 + \frac{x_1}{\sqrt{x_1^2 + x_2^2}}\mathbf{e}_2, \\ \hat{\mathbf{z}} &= \mathbf{e}_3, \end{aligned} \tag{2.6}$$

which correspond to $\mathbf{k}_1, \mathbf{k}_2, \mathbf{k}_3$, respectively. Lamé coefficients in point P are evaluated by (2.1)

$$\begin{aligned} H_r &= \sqrt{(\cos\phi)^2 + (\sin\phi)^2 + 0} = 1, \\ H_\phi &= \sqrt{(-r\sin\phi)^2 + (r\cos\phi)^2 + 0} = r, \\ H_z &= \sqrt{0 + 0 + 1} = 1. \end{aligned} \tag{2.7}$$

One can notice that vectors $\mathbf{e}_1, \mathbf{e}_2, \mathbf{e}_3$ are constant in every point of $\mathbb{R}^3$. That is why vectors $\hat{\mathbf{r}}$ and $\hat{\boldsymbol{\phi}}$ depend only on ϕ in cylindrical coordinates, while $\hat{\mathbf{z}}$ is a constant vector.

Every vector field $\mathbf{a}$ can be expressed as a linear combination of vectors (2.6) in some fixed point P

$$\mathbf{a} = a_r\hat{\mathbf{r}} + a_\phi\hat{\boldsymbol{\phi}} + a_z\hat{\mathbf{z}}.$$

Applying Laplace operator to $\mathbf{a}$ and writing it in cylindrical coordinates via (2.4), substituting Lamé coefficients (2.7) leads us to

$$\begin{aligned}
\Delta\mathbf{a} &= \frac{1}{r}\frac{\partial}{\partial r}\left(r\frac{\partial\mathbf{a}}{\partial r}\right) + \frac{1}{r^2}\frac{\partial^2\mathbf{a}}{\partial\phi^2} + \frac{\partial^2\mathbf{a}}{\partial z^2} \\
&= \frac{1}{r}\frac{\partial}{\partial r}\left[r\left(\frac{\partial a_r}{\partial r}\hat{\mathbf{r}} + \frac{\partial a_\phi}{\partial r}\hat{\boldsymbol{\phi}} + \frac{\partial a_z}{\partial r}\hat{\mathbf{z}}\right)\right] \\
&\quad + \frac{1}{r^2}\frac{\partial}{\partial\phi}\left(\frac{\partial a_r}{\partial\phi}\hat{\mathbf{r}} + a_r\frac{\partial\hat{\mathbf{r}}}{\partial\phi} + \frac{\partial a_\phi}{\partial\phi}\hat{\boldsymbol{\phi}} + a_\phi\frac{\partial\hat{\boldsymbol{\phi}}}{\partial\phi} + \frac{\partial a_z}{\partial\phi}\hat{\mathbf{z}}\right) \\
&\quad + \frac{\partial}{\partial z}\left(\frac{\partial a_r}{\partial z}\hat{\mathbf{r}} + \frac{\partial a_\phi}{\partial z}\hat{\boldsymbol{\phi}} + \frac{\partial a_z}{\partial z}\hat{\mathbf{z}}\right) \\
&= \frac{1}{r}\left[\left(\frac{\partial a_r}{\partial r}\hat{\mathbf{r}} + \frac{\partial a_\phi}{\partial r}\hat{\boldsymbol{\phi}} + \frac{\partial a_z}{\partial r}\hat{\mathbf{z}}\right) + r\left(\frac{\partial^2 a_r}{\partial r^2}\hat{\mathbf{r}} + \frac{\partial^2 a_\phi}{\partial r^2}\hat{\boldsymbol{\phi}} + \frac{\partial^2 a_z}{\partial r^2}\hat{\mathbf{z}}\right)\right] \\
&\quad + \frac{1}{r^2}\left(\frac{\partial^2 a_r}{\partial\phi^2}\hat{\mathbf{r}} + 2\frac{\partial a_r}{\partial\phi}\frac{\partial\hat{\mathbf{r}}}{\partial\phi} + a_r\frac{\partial^2\hat{\mathbf{r}}}{\partial\phi^2}\right. \\
&\qquad \left. + \frac{\partial^2 a_\phi}{\partial\phi^2}\hat{\boldsymbol{\phi}} + 2\frac{\partial a_\phi}{\partial\phi}\frac{\partial\hat{\boldsymbol{\phi}}}{\partial\phi} + a_\phi\frac{\partial^2\hat{\boldsymbol{\phi}}}{\partial\phi^2} + \frac{\partial^2 a_z}{\partial\phi^2}\hat{\mathbf{z}}\right) \\
&\quad + \left(\frac{\partial^2 a_r}{\partial z^2}\hat{\mathbf{r}} + \frac{\partial^2 a_\phi}{\partial z^2}\hat{\boldsymbol{\phi}} + \frac{\partial^2 a_z}{\partial z^2}\hat{\mathbf{z}}\right).
\end{aligned} \tag{2.8}$$

Using representation (2.6) one can evaluate

$$\begin{aligned}
\frac{\partial\hat{\mathbf{r}}}{\partial\phi} &= -\sin\phi\ \mathbf{e}_1 + \cos\phi\ \mathbf{e}_2 = \hat{\boldsymbol{\phi}}, \\
\frac{\partial^2\hat{\mathbf{r}}}{\partial\phi^2} = \frac{\partial\hat{\boldsymbol{\phi}}}{\partial\phi} &= -\cos\phi\ \mathbf{e}_1 - \sin\phi\ \mathbf{e}_2 = -\hat{\mathbf{r}}, \\
\frac{\partial^2\hat{\boldsymbol{\phi}}}{\partial\phi^2} &= \sin\phi\ \mathbf{e}_1 - \cos\phi\ \mathbf{e}_2 = -\hat{\boldsymbol{\phi}}.
\end{aligned} \tag{2.9}$$

Substituting (2.9) to (2.8) we end up with the Laplace operator of $\mathbf{a}$ written in cylindrical coordinates

$$\Delta\mathbf{a} = \left(\Delta a_r - \frac{a_r}{r^2} - \frac{2}{r^2}\frac{\partial a_\phi}{\partial\phi}\right)\hat{\mathbf{r}} + \left(\Delta a_\phi - \frac{a_\phi}{r^2} + \frac{2}{r^2}\frac{\partial a_r}{\partial\phi}\right)\hat{\boldsymbol{\phi}} + \left(\Delta a_z\right)\hat{\mathbf{z}}. \tag{2.10}$$

The material derivative of $\mathbf{a}$ is derived in the same way using formula for gradient (2.2)

with coefficients (2.7)

$$\begin{aligned}(\mathbf{a}\cdot\nabla)\,\mathbf{a} =& \left(a_r\frac{\partial}{\partial r}+\frac{a_\phi}{r}\frac{\partial}{\partial\phi}+a_z\frac{\partial}{\partial z}\right)\left(a_r\hat{\mathbf{r}}+a_\phi\hat{\boldsymbol{\phi}}+a_z\hat{\mathbf{z}}\right)\\ =&a_r\left(\frac{\partial a_r}{\partial r}\hat{\mathbf{r}}+\frac{\partial a_\phi}{\partial r}\hat{\boldsymbol{\phi}}+\frac{\partial a_z}{\partial r}\hat{\mathbf{z}}\right)\\ &+\frac{a_\phi}{r}\left(\frac{\partial a_r}{\partial\phi}\hat{\mathbf{r}}+a_r\frac{\partial\hat{\mathbf{r}}}{\partial\phi}+\frac{\partial a_\phi}{\partial\phi}\hat{\boldsymbol{\phi}}+a_\phi\frac{\partial\hat{\boldsymbol{\phi}}}{\partial\phi}+\frac{\partial a_z}{\partial\phi}\hat{\mathbf{z}}\right)\\ &+a_z\left(\frac{\partial a_r}{\partial z}\hat{\mathbf{r}}+\frac{\partial a_\phi}{\partial z}\hat{\boldsymbol{\phi}}+\frac{\partial a_z}{\partial z}\hat{\mathbf{z}}\right)\\ =&\left(a_r\frac{\partial a_r}{\partial r}+\frac{a_\phi}{r}\frac{\partial a_r}{\partial\phi}+a_z\frac{\partial a_r}{\partial z}-\frac{a_\phi^2}{r}\right)\hat{\mathbf{r}}\\ &+\left(a_r\frac{\partial a_\phi}{\partial r}+\frac{a_\phi}{r}\frac{\partial a_\phi}{\partial\phi}+a_z\frac{\partial a_\phi}{\partial z}+\frac{a_r a_\phi}{r}\right)\hat{\boldsymbol{\phi}}\\ &+\left(a_r\frac{\partial a_z}{\partial r}+\frac{a_\phi}{r}\frac{\partial a_z}{\partial\phi}+a_z\frac{\partial a_z}{\partial z}\right)\hat{\mathbf{z}}.\end{aligned}\tag{2.11}$$

The divergence of $\mathbf{a}$ is evaluated according to (2.3)

$$\nabla\cdot\mathbf{a}=\frac{1}{r}\left(\frac{\partial(r\,a_r)}{\partial r}+\frac{\partial(a_\phi)}{\partial\phi}+\frac{\partial(r\,a_z)}{\partial z}\right).\tag{2.12}$$

Applying (2.2) to $\mathbf{a}$ componentwise we obtain a gradient of a vector valued function

$$\nabla\mathbf{a}=\begin{pmatrix}\dfrac{\partial a_r}{\partial r} & \dfrac{\partial a_\phi}{\partial r} & \dfrac{\partial a_z}{\partial r}\\ \dfrac{1}{r}\dfrac{\partial a_r}{\partial\phi} & \dfrac{1}{r}\dfrac{\partial a_\phi}{\partial\phi} & \dfrac{1}{r}\dfrac{\partial a_z}{\partial\phi}\\ \dfrac{\partial a_r}{\partial z} & \dfrac{\partial a_\phi}{\partial z} & \dfrac{\partial a_z}{\partial z}\end{pmatrix}.\tag{2.13}$$

Using the Lamé coefficients (2.7) the gradient and the Laplace operator of a scalar function f can be evaluated according to (2.2) and (2.4)

$$\nabla f=\begin{pmatrix}\dfrac{\partial f}{\partial r}\\ \dfrac{1}{r}\dfrac{\partial f}{\partial\phi}\\ \dfrac{\partial f}{\partial z}\end{pmatrix},\tag{2.14}$$

$$\Delta f=\frac{1}{r}\frac{\partial}{\partial r}\left(r\frac{\partial f}{\partial r}\right)+\frac{1}{r^2}\frac{\partial^2 f}{\partial\phi^2}+\frac{\partial^2 f}{\partial z^2}.\tag{2.15}$$

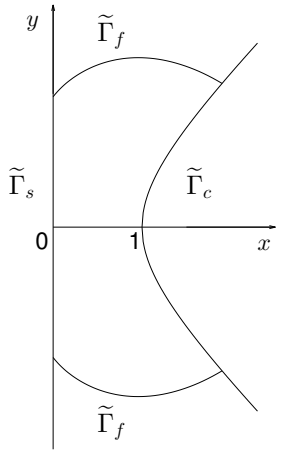

Figure 2.3: Domain $\widetilde{\Omega}$ and its boundary $\partial\widetilde{\Omega} = \widetilde{\Gamma}_f \cup \widetilde{\Gamma}_s \cup \widetilde{\Gamma}_c$.

2.2 Deriving a simplified mathematical model

Let $\Omega \subset \mathbb{R}^3$ be a bounded domain whose boundary $\partial\Omega$ contains the free surface of a ferrofluid and partially the surface of the shaft and the concentrator where ferrofluid touches them. We split the boundary $\partial\Omega$ to the free surface Γ_f, the surface on the shaft Γ_s and the surface on the concentrator Γ_c, which are pairwise disjoint and $\Gamma_f \cup \Gamma_s \cup \Gamma_c = \partial\Omega$.

After introducing a set of equations in Ω we apply the cylindrical coordinates and write all the equations in cross-section of Ω with the half-plane Orz. Then the dimensionless coordinates

$$x = \frac{r - R}{a}, \quad y = \frac{z}{a}, \quad \phi = \phi \tag{2.16}$$

are applied. Here R denotes the radius of the shaft, $a \ll R$ the width of the gap. The cross-section of Ω in half-plane of Oxy ($x > 0$) for angle $\phi = 0$ is denoted by $\widetilde{\Omega}$. Its boundary $\partial\widetilde{\Omega}$ is split into three parts $\partial\widetilde{\Omega} = \widetilde{\Gamma}_f \cup \widetilde{\Gamma}_s \cup \widetilde{\Gamma}_c$ like $\partial\Omega$, where $\widetilde{\Gamma}_f$ $\widetilde{\Gamma}_s$ $\widetilde{\Gamma}_c$ are pairwise disjoint. Thanks to the axial symmetry functions written in the cross-section $\widetilde{\Omega}$ do not depend on ϕ, so we can consider $\widetilde{\Omega}$ corresponding to any angle ϕ. On Figure 2.3 one can see the schematic view of the domain $\widetilde{\Omega}$ and its boundary.

During simplifications we will use the following approximation. As $r \in (R, R + a)$ and $R \gg a$, we can approximate the ratio a/r by the first term of Taylor series

$$\frac{a}{r} = \frac{a}{R + ax} = \frac{a}{R}\left(1 - \frac{a}{R}x + o\left(\frac{a}{R}\right)\right) \approx \frac{a}{R} = \delta. \tag{2.17}$$

2.2.1 Maxwell's equations

Maxwell's equations form the foundation of classical electrodynamics. We apply them to ferrofluids following Rosensweig [37].

Assuming that a ferrofluid is nonconducting, the free current density and the displacement current are negligible, the system of Maxwell's equations is simplified in the magnetostatic limit to

$$\begin{cases} \nabla \cdot \mathbf{B} = 0, \\ \nabla \times \mathbf{H} = 0 \end{cases} \quad \text{in } \Omega, \tag{2.18}$$

where $\mathbf{H}$ and $\mathbf{B}$ denote the magnetic field intensity and the magnetic induction, respectively. These functions are related to each other by the following identity

$$\mathbf{B} = \mu_{\mathbf{0}}(\mathbf{H} + \mathbf{M}), \tag{2.19}$$

where $\mu_0 = 4\pi \times 10^{-7}$ V·s/(A·m) is the vacuum permeability. Since a ferrofluid is a "soft" material [37], the magnetization vector is parallel to the vector of applied magnetic field

$$\mathbf{M} = M\frac{\mathbf{H}}{H}. \tag{2.20}$$

Here M and H are the moduli of vectors $\mathbf{M}$ and $\mathbf{H}$, respectively. In that situation using $\nabla \times \mathbf{H} = \mathbf{0}$ one can show that

$$(\mathbf{M} \cdot \nabla)\,\mathbf{H} \equiv M\nabla H. \tag{2.21}$$

The second equation of the Maxwell's system (2.18) provides curl of $\mathbf{H}$ equal to zero. Therefore one can introduce a function $\psi : \mathbb{R}^3 \to \mathbb{R}$ such that

$$\mathbf{H} \equiv -\nabla\psi, \tag{2.22}$$

which satisfies this equation automatically. Using (2.19) and (2.20) and substituting (2.22) one can rewrite the Maxwell's system (2.18) as

$$\operatorname{div}\left(\left[1 + \frac{M}{H}\right]\nabla\psi\right) = 0 \quad \text{in } \Omega.$$

If M is homogeneous, i.e. M/H and $\partial M/\partial H$ are small enough, one can neglect the term M/H. That simplification is valid since under seal conditions the magnetic field strength is several orders higher than the saturation magnetization M_s of a ferrofluid. That means M is very close to M_s and almost constant. We finally obtain

$$\Delta\psi = 0 \quad \text{in } \Omega.$$

Evaluating the Laplace operator in cylindrical coordinates by (2.15) and vanishing the derivatives with respect to ϕ due to the axial symmetry we come to

$$\frac{1}{r}\frac{\partial}{\partial r}\left(r\frac{\partial\psi}{\partial r}\right) + \frac{\partial^2\psi}{\partial z^2} = 0. \tag{2.23}$$

Changing the variables by (2.16) and using the approximation (2.17) the equation is simplified to

$$\delta\frac{\partial\psi}{\partial x}+\frac{\partial^2\psi}{\partial x^2}+\frac{\partial^2\psi}{\partial y^2}=0.$$

Neglecting the term with δ due to its smallness we obtain the Laplace equation for a 2-dimensional potential.

$$\Delta\widetilde{\psi}=0 \quad \text{in } \widetilde{\Omega}. \tag{2.24}$$

Here $\widetilde{\psi}$ is a potential ψ restricted to the cross-section $\widetilde{\Omega}$.

In final equation for Maxwell's potential (2.24) there is no magnetization, so one can conclude that the used model neglects the presence of a ferrofluid in the gap. Linear sizes of the concentrator are much larger than the gap length between the shaft and the concentrator. That allows us to extend domain $\widetilde{\Omega}$ in y axis to infinity and look for a solution in infinite domain. The magnetic permeability of the shaft and the concentrator is much higher than that of the ferrofluid. Under these assumption the boundary conditions only on solid surfaces $\widetilde{\Gamma}_s$ and $\widetilde{\Gamma}_c$ are sufficient, which are given according to [47]

$$\widetilde{\psi}=\widetilde{\psi}_0=\text{const} \quad \text{on } \widetilde{\Gamma}_s, \quad \widetilde{\psi}=0 \quad \text{on } \widetilde{\Gamma}_c. \tag{2.25}$$

Hyperboloidal profile of the concentrator is given by

$$y^2=\tan^2\beta(x^2-1), \tag{2.26}$$

where β denotes an angle formed by an asymptote. One should note that curve (2.26) is an origin-centered East-West opening hyperbola. The center of that hyperbola coincides with the origin, and distance from its center to a vertex on x axis is fixed to 1.

Applying elliptic coordinates as it was done in [47] we obtain an analytical expression for the magnetic field strength in the gap between the shaft and the concentrator as a solution of the equation (2.24) with boundary conditions (2.25). Making the backward transformation we get the solution given in the cross-section

$$h_s=h_s(x,y)=\frac{\sin\beta}{\left[\left((x^2+y^2)\cos^2\beta+1\right)^2-4x^2\cos^2\beta\right]^{1/4}}, \tag{2.27}$$

where h_s is a dimensionless magnetic field intensity given in $\widetilde{\Omega}$, index s means that it corresponds to a ferroofluid seal with the prescribed geometry.

2.2.2 Magnetic force density

The magnetic force acting on a ferrofluid is an object of special interest, since it describes the magnetic properties of the material. We follow Rosensweig [37] in order to define a magnetic force density.

Let us first introduce magnetic stress tensor

$$\mathbb{T}_m(\mathbf{H},\mathbf{B}):=-\left(\int_0^H\mu_0\left(\frac{\partial(M\mathrm{v})}{\partial\mathrm{v}}\right)_H dH+\frac{\mu_0}{2}H^2\right)\mathbb{I}+\mathbf{H}\otimes\mathbf{B}, \tag{2.28}$$

where $\mathbb{I}$ denotes an identity tensor, $M\mathrm{v}$ the magnetic moment of a volume unit v of colloid. The integral term here describes the inter-particle or dipole-dipole interaction, which can be neglected for dilute ferrofluids [37]. So we use a simplified magnetic stress tensor

$$\mathbb{T}_m(\mathbf{H}, \mathbf{B}) := -\frac{\mu_0}{2} H^2 \mathbb{I} + \mathbf{H} \otimes \mathbf{B}.$$

The magnetic force density is given by

$$\mathbf{f}_m = \nabla \cdot \mathbb{T}_m = \mu_0 \left(\mathbf{M} \cdot \nabla\right) \mathbf{H}.$$

As we said before a ferrofluid is a "soft" material [37], which implies that magnetization vector is parallel to a magnetic field intensity and therefore (2.21) holds. Then the magnetic force density for a volume unit can be written as follows

$$\mathbf{f}_m = \mu_0 M \nabla H, \tag{2.29}$$

which is equal to the Kelvin force density for H being an outer magnetic field.

According to standard models for ferrofluids [6, 37], magnetization is usually taken as a function of magnetic field strength and temperature. According to our assumptions the system is isothermal so the temperature is omitted. The classic approximation of magnetization is done with the Langevin function

$$M = M_s L(\xi h) \quad \text{with} \quad L(t) = \coth(t) - 1/t, \tag{2.30}$$

where M_s denotes saturation magnetization, h a dimensionless magnetic field strength

$$h = \frac{H}{H_0},$$

ξ the Langevin parameter given by

$$\xi = \frac{\mu_0 m H_0}{kT}. \tag{2.31}$$

Here m is a magnetic moment of a single particle, H_0 a maximum of the magnetic field strength, k the Boltzmann constant, T absolute temperature.

According to [37] the saturation magnetization of a ferrofluid is a product of a saturation magnetization of a ferrite and a volume fraction of magnetic particles in a base liquid. It means, it is a function of particle concentration. We can interpret this as

$$M_s = \overline{M_s} c, \tag{2.32}$$

where M_s denotes saturation magnetization of a ferrofluid at current particle concentration c, $\overline{M_s}$ is saturation magnetization of a uniform colloid. Substituting (2.30) and (2.32) into (2.29) we end up with the final expression for the magnetic force density

$$\mathbf{f}_{m,\mathrm{v}} = \nabla \cdot \mathbb{T}_m = \mu_0 \overline{M_s} H_0 L(\xi h)\, c \nabla h. \tag{2.33}$$

Force applied to a single particle is obtained by multiplying (2.29) by a volume of that particle taken as an average volume v_p. According to definition

$$\mathbf{M} = \frac{d\mathbf{m}}{d\mathrm{v}},$$

where $d\mathbf{m}$ is a magnetic moment of the volume element $d\mathrm{v}$. It is important to note, that here $\mathbf{M}$ is understood as a magnetization of the ferrite material of some particle and not of a ferrofluid. We assume that magnetic moment is uniform with respect to the volume and write

$$\mathbf{m}_p = \mathbf{M}\mathrm{v}_p.$$

Here v_p is an average particle volume, and $\mathbf{m}_p$ the corresponding magnetic moment. It holds also for saturation magnetization of ferrite $M_{s,f}$ and $m = |\mathbf{m}_p|$ being the absolute value of a magnetic moment of a particle

$$m = M_{s,f}\mathrm{v}_p. \tag{2.34}$$

Multiplying (2.29) by v_p, substituting there (2.30) with (2.34) we obtain the average magnetic force applied to a single particle

$$\mathbf{f}_{m,p} = \mu_0 m L\left(\xi h\right) H_0 \nabla h. \tag{2.35}$$

2.2.3 Navier-Stokes equation

The stationary Navier-Stokes equation for an incompressible ferrofluid is given by [37]

$$\begin{aligned} \rho\left(\mathbf{v}\cdot\nabla\right)\mathbf{v} &= \nabla\cdot\mathbb{T}(\mathbf{v},p,\mathbf{H},\mathbf{B}) + \rho\mathbf{g}, \\ \nabla\cdot\mathbf{v} &= 0, \end{aligned} \tag{2.36}$$

where $\mathbf{v}$ denotes the velocity field, η the dynamic viscosity, ρ the density of a ferrofluid, p the total pressure, $\mathbf{g}$ the acceleration of gravity. The stress tensor $\mathbb{T}(\mathbf{v},p,\mathbf{H},\mathbf{B})$ is given by

$$\mathbb{T}(\mathbf{v},p,\mathbf{H},\mathbf{B}) = \mathbb{T}_v + \mathbb{T}_m. \tag{2.37}$$

Here tensors $\mathbb{T}_v$ and $\mathbb{T}_m$ incorporate hydrodynamic and magnetic stresses, respectively. The magnetic stress tensor $\mathbb{T}_m$ was already defined in (2.28). The hydrodynamic one has the following form

$$\mathbb{T}_v(\mathbf{v},p) := 2\eta\mathbb{D}(\mathbf{v}) - p\mathbb{I}, \tag{2.38}$$

where the velocity deformation tensor $\mathbb{D}(\mathbf{v})$ is defined by

$$\mathbb{D}(\mathbf{v}) := \frac{1}{2}\left(\nabla\mathbf{v} + \nabla\mathbf{v}^T\right).$$

The boundary conditions are given as follows. At fluid-solid boundaries Γ_s, Γ_c the fluid velocity is equal to that on solid surfaces. On the free surface the slip boundary conditions

are imposed. Full set of boundary conditions looks as follows

$$\begin{aligned} \mathbf{v} &= 0 && \text{on } \Gamma_c, \\ \mathbf{v} &= \mathbf{v_0} && \text{on } \Gamma_s, \\ \mathbf{v}\cdot\mathbf{n} = 0, \quad \mathbf{n}\cdot[|\mathbb{T}(\mathbf{v},p,\mathbf{H},\mathbf{B})|]\cdot\boldsymbol{\tau} &= 0 && \text{on } \Gamma_f, \end{aligned} \tag{2.39}$$

where $\mathbf{v_0}$ denotes the rotation velocity of the shaft, $\mathbf{n}$ is the unit normal to Γ_f, $\boldsymbol{\tau}$ the unit tangent, and $[|\cdot|]$ the jump over the surface.

Before applying transformation to cylindrical coordinates we want to rewrite the Navier-Stokes equation in an alternative form. For incompressible Newtonian fluids it holds

$$\nabla\cdot\mathbb{T}_v(\mathbf{u},p) \equiv \eta\left(\Delta\mathbf{u} + \nabla\text{div }\mathbf{u}\right) - \nabla p = \eta\Delta\mathbf{u} - \nabla p.$$

Substituting it into the Navier-Stokes equation (2.36) we obtain

$$\begin{aligned} -\eta\Delta\mathbf{v} + \rho\left(\mathbf{v}\cdot\nabla\right)\mathbf{v} + \nabla p^* &= \mathbf{f}_{m,\mathrm{v}}, \\ \nabla\cdot\mathbf{v} &= 0, \end{aligned} \tag{2.40}$$

where p^* is the pressure which incorporates the gravity force, $f_{m,v} = \nabla\cdot\mathbb{T}_m$ is given by (2.33). We recall the axial symmetry of the system, that means the acceleration of gravity $\mathbf{g}$ is parallel to the axis of symmetry Oz. Without loss of generality we direct it against the axis, i.e. $p^* = p + \rho g z$ with $g = |\mathbf{g}|$.

Now we apply the cylindrical coordinates (2.10), (2.11), (2.12) to the Navier-Stokes equation in form (2.40). Due to the axisymmetry all the derivatives with respect to ϕ vanish. We write a vector equation coordinatewise

$$\begin{aligned} -\eta\left(\frac{1}{r}\frac{\partial}{\partial r}\left(r\frac{\partial v_r}{\partial r}\right) + \frac{\partial^2 v_r}{\partial z^2} - \frac{v_r}{r^2}\right) + \rho\left(v_r\frac{\partial v_r}{\partial r} + v_z\frac{\partial v_r}{\partial z} - \frac{v_\phi^2}{r}\right) + \nabla_r p^* &= \mathbf{f}_{m,\mathrm{v}}\cdot\mathbf{e}_1, \\ -\eta\left(\frac{\partial^2 v_\phi}{\partial r^2} + \frac{\partial^2 v_\phi}{\partial z^2} - \frac{v_\phi}{r^2}\right) + \rho\left(v_r\frac{\partial v_\phi}{\partial r} + v_z\frac{\partial v_\phi}{\partial z} + \frac{v_r v_\phi}{r}\right) &= 0, \\ -\eta\left(\frac{\partial^2 v_z}{\partial r^2} + \frac{\partial^2 v_z}{\partial z^2}\right) + \rho\left(v_r\frac{\partial v_z}{\partial r} + v_r\frac{\partial v_z}{\partial z}\right) + \nabla_z p^* &= \mathbf{f}_{m,\mathrm{v}}\cdot\mathbf{e}_3, \\ \frac{1}{r}\left(v_r + r\frac{\partial v_r}{\partial r} + r\frac{\partial v_z}{\partial z}\right) &= 0. \end{aligned} \tag{2.41}$$

We introduce the dimensionless functions given in Ω

$$v_x = \frac{v_r}{v_0}, \quad \omega = \frac{v_\phi}{v_0}, \quad v_y = \frac{v_z}{v_0}, \quad \widehat{\mathbf{v}} = (v_x,\omega,v_y), \quad \widehat{p} = \frac{p^*}{\rho v_0^2}, \tag{2.42}$$

where v_0 is the linear velocity of the shaft rotation. We substitute dimensionless coordinates and variables (2.16), (2.42), and expression for magnetic force density (2.33) into (2.41). Then we apply transformation (2.14) together with the approximation (2.17),

which gives

$$\begin{aligned}
&\frac{\eta v_0}{a^2}\left(\delta\frac{\partial v_x}{\partial x}+\frac{\partial^2 v_x}{\partial x^2}+\frac{\partial^2 v_x}{\partial y^2}-\delta^2 v_x\right)\\
&\qquad\qquad+\frac{\rho v_0^2}{a}\left(v_x\frac{\partial v_x}{\partial x}+v_y\frac{\partial v_x}{\partial y}-\delta\omega^2\right)+\frac{1}{a}\frac{\partial \widehat{p}}{\partial x}=\frac{\mu_0\overline{M_s}H_0}{\rho v_0^2}\,L\left(\xi h\right)c\,\frac{\partial h}{\partial x},\\
&\frac{\eta v_0}{a^2}\left(\frac{\partial^2\omega}{\partial x^2}+\frac{\partial^2\omega}{\partial y^2}-\delta^2\omega\right)+\frac{\rho v_0^2}{a}\left(v_x\frac{\partial\omega}{\partial x}+v_y\frac{\partial\omega}{\partial y}+\delta v_x\omega\right)=0,\\
&\frac{\eta v_0}{a^2}\left(\frac{\partial^2 v_y}{\partial x^2}+\frac{\partial^2 v_y}{\partial y^2}\right)+\frac{\rho v_0^2}{a}\left(v_x\frac{\partial v_y}{\partial x}+v_y\frac{\partial v_y}{\partial y}\right)+\frac{1}{a}\frac{\partial \widehat{p}}{\partial y}=\frac{\mu_0\overline{M_s}H_0}{\rho v_0^2}\,L\left(\xi h\right)c\,\frac{\partial h}{\partial y},\\
&\qquad\qquad\delta v_x+\frac{\partial v_x}{\partial x}+\frac{\partial v_y}{\partial y}=0.
\end{aligned}\tag{2.43}$$

We recall that the point of our interest is a flow between two coaxial surfaces of revolution. The distance between the surfaces is much smaller than their radii, this relation can be approximated by δ according to (2.17). The domain shape causes the rotation component of the velocity to be two to three orders higher than two other components [31]. Having in addition $\delta \sim 10^{-2}$ we can neglect almost all terms with factor δ due to their smallness except the term $\delta\omega^2$, which has the same order as the main term of the corresponding equation.

Now we can write equations (2.43) in 2D. Grouping terms by using differential operators one obtains

$$\begin{aligned}
-\frac{1}{\mathrm{Re}}\Delta\widetilde{\mathbf{v}}+\left(\widetilde{\mathbf{v}}\cdot\nabla\right)\widetilde{\mathbf{v}}+\nabla\widetilde{p}&=\delta\widetilde{\omega}^2\mathbf{e}_1+\frac{\delta}{\mathrm{Fr}_m}L(\xi\widetilde{h})\,\widetilde{c}\,\nabla\widetilde{h},\\
\nabla\cdot\widetilde{\mathbf{v}}&=0,\\
\Delta\widetilde{\omega}+\widetilde{\mathbf{v}}\cdot\nabla\widetilde{\omega}&=0,
\end{aligned}\tag{2.44}$$

where $\widetilde{\mathbf{v}}$, $\widetilde{\omega}$, $\widetilde{p}$, $\widetilde{c}$, and $\widetilde{h}$ are the dimensionless functions defined in the cross-section $\widetilde{\Omega}$, which correspond to (v_x, v_y), ω, $\widehat{p}$, c, and h, respectively. The used constants are standard for Navier-Stokes equations Reynolds number

$$\mathrm{Re}=\frac{a\rho v_0}{\eta}\tag{2.45}$$

and the magnetic Froude number, which is chosen in the same manner as in [31]

$$\mathrm{Fr}_m=\frac{\rho v_0^2\delta}{\mu_0\overline{M_s}H_0}.\tag{2.46}$$

Remark 2.2.1. *The term $\widetilde{\mathbf{v}}\cdot\nabla\widetilde{\omega}$ describes the influence of the secondary flow on the azimuthal velocity. It was neglected in [31, 47, 48] since $\widetilde{\mathbf{v}}$ was estimated to be several orders smaller in magnitude than ω. Later it was considered in [27] and the coupled system* (2.44) *was solved numerically. However, the computations have shown that this term is negligible. That is why we also omit it in the mathematical model.*

We introduce a stress tensor useful for writing Navier-Stokes equation in dimensionless form

$$\sigma(\mathbf{v}, p) := \frac{2}{\mathrm{Re}}\mathbb{D}(\mathbf{v}) - p\mathbb{I}. \tag{2.47}$$

One can note that it differs from $\mathbb{T}_v$ (2.38) only by multiplicative constant at velocity term. Using the incompressibility condition $\nabla \cdot \widetilde{\mathbf{v}} = 0$ and taking into account the remark 2.2.1 one can write (2.44) as follows

$$\begin{aligned} (\widetilde{\mathbf{v}} \cdot \nabla)\,\widetilde{\mathbf{v}} - \nabla \cdot \sigma(\widetilde{\mathbf{v}}, \widetilde{p}) = \mathbf{e}_1 \delta \widetilde{\omega}^2 + \frac{\delta}{\mathrm{Fr}_m} L\left(\xi \widetilde{h}\right) c \nabla \widetilde{h} \qquad & \text{in } \Omega, \\ \nabla \cdot \widetilde{\mathbf{v}} = 0 \qquad & \text{in } \Omega, \\ \Delta \widetilde{\omega} = 0 \qquad & \text{in } \Omega. \end{aligned} \tag{2.48}$$

Now we can apply the same transformations to the boundary conditions (2.39). Using the fact that the jumps of $\mathbf{H} \cdot \boldsymbol{\tau}$ and $\mathbf{B} \cdot \mathbf{n}$ vanish and there is no viscous media out of the ferrofluid seal, one can show that

$$\mathbf{n} \cdot [|\mathbb{T}(\mathbf{v}, p, \mathbf{H}, \mathbf{B})|] \cdot \boldsymbol{\tau} = \mathbf{n} \cdot [|\mathbb{T}_v(\mathbf{v}, p)|] \cdot \boldsymbol{\tau} = \mathbf{n} \cdot \mathbb{T}_v(\mathbf{v}, p) \cdot \boldsymbol{\tau} \quad \text{on } \Gamma_f.$$

We recall that all the applied forces and the domain Ω have the axial symmetry around z axis. In that case the rotation velocity $\mathbf{v}_0$, the normal $\mathbf{n}$, and the tangent $\boldsymbol{\tau}$ have the following form in cylindrical coordinates

$$\mathbf{v}_0 = (0, v_0, 0)\,, \quad \mathbf{n} = (n_r, 0, n_z)\,, \quad \boldsymbol{\tau} = (-n_z, \tau_\phi, n_r)\,,$$

where $v_0 = |\mathbf{v}_0|$ and τ_ϕ is an arbitrary constant. After applying the cylindrical coordinates (2.13) the boundary conditions (2.39) will look as follows

$$\begin{aligned} v_r = v_\phi = v_z = 0 \qquad & \text{on } \Gamma_c, \\ v_r = v_z = 0, \quad v_\phi = v_0 \qquad & \text{on } \Gamma_s, \\ v_r n_r + v_z n_z = 0, \quad (n_r, 0, n_z) \cdot \mathbb{T}_v(\mathbf{v}, p) \cdot (-n_z, \tau_\phi, n_r) = 0 \qquad & \text{on } \Gamma_f. \end{aligned}$$

Let us consider the last term in more details. Using the representation of $\mathbb{T}_v(\mathbf{v}, p)$ (2.38) and transformation formula (2.10), then vanishing all derivatives with respect to ϕ, we obtain

$$\mathbf{n} \cdot \mathbb{T}_v(\mathbf{v}, p) \cdot \boldsymbol{\tau} = \eta\,(n_r, 0, n_z) \cdot \begin{bmatrix} 2\dfrac{\partial v_r}{\partial r} + \dfrac{1}{\eta}\,p & \dfrac{\partial v_\phi}{\partial r} & \dfrac{\partial v_z}{\partial r} + \dfrac{\partial v_r}{\partial z} \\ \dfrac{\partial v_\phi}{\partial r} & \dfrac{1}{\eta}\,p & \dfrac{\partial v_\phi}{\partial z} \\ \dfrac{\partial v_z}{\partial r} + \dfrac{\partial v_r}{\partial z} & \dfrac{\partial v_\phi}{\partial z} & 2\dfrac{\partial v_z}{\partial z} + \dfrac{1}{\eta}\,p \end{bmatrix} \cdot (-n_z, \tau_\phi, n_r)$$

$$= \eta\,(n_r, n_z) \cdot \begin{bmatrix} 2\dfrac{\partial v_r}{\partial r} + \dfrac{1}{\eta}\,p & \dfrac{\partial v_z}{\partial r} + \dfrac{\partial v_r}{\partial z} \\ \dfrac{\partial v_z}{\partial r} + \dfrac{\partial v_r}{\partial z} & 2\dfrac{\partial v_z}{\partial z} + \dfrac{1}{\eta}\,p \end{bmatrix} \cdot (-n_z, n_r) + \eta\tau_\phi \left(\frac{\partial v_\phi}{\partial r} n_r + \frac{\partial v_\phi}{\partial z} n_z\right) = 0.$$

Since τ_ϕ is an arbitrary constant it must hold

$$\frac{\partial v_\phi}{\partial r} n_r + \frac{\partial v_\phi}{\partial z} n_z = 0.$$

Using the stress tensor $\sigma(\mathbf{v}, p)$ (2.47) we obtain for dimensionless variables in a cross-section the following boundary conditions

$$\begin{aligned} \widetilde{\mathbf{v}} = 0, \quad \widetilde{\omega} = 0 \qquad & \text{on } \widetilde{\Gamma}_c, \\ \widetilde{\mathbf{v}} = 0, \quad \widetilde{\omega} = 1 \qquad & \text{on } \widetilde{\Gamma}_s, \\ \widetilde{\mathbf{v}} \cdot \widetilde{\mathbf{n}} = 0, \quad \widetilde{\mathbf{n}} \cdot \sigma(\widetilde{\mathbf{v}}, \widetilde{p}) \cdot \widetilde{\boldsymbol{\tau}} = 0, \quad \frac{\partial \widetilde{\omega}}{\partial \widetilde{\mathbf{n}}} = 0 \qquad & \text{on } \widetilde{\Gamma}_f, \end{aligned} \tag{2.49}$$

where $\widetilde{\mathbf{n}}$ and $\widetilde{\boldsymbol{\tau}}$ are a unit normal and a tangent to $\widetilde{\Gamma}_f$, respectively. Functions $\widetilde{\mathbf{v}}$, $\widetilde{\omega}$, $\widetilde{p}$ are given in cross-section $\widetilde{\Omega}$.

2.2.4 Convection-Diffusion equation

A magnetic fluid is a stable colloid of ferromagnetic particles dispersed within the carrier liquid. According to [4] the classical theory for diffusion of Brownian particles can be applied. Then the stationary convection-diffusion equation has the following form [23]

$$\rho \mathbf{v} \cdot \nabla c = -\nabla \cdot \mathbf{i}, \tag{2.50}$$

where c is the particle concentration, the mass flux density $\mathbf{i}$ is given by

$$\mathbf{i} = -\rho \mathrm{D} \nabla c + \rho c b \mathbf{f}. \tag{2.51}$$

Here D denotes the diffusion coefficient, b particle mobility, f an average force affecting a single particle. The force f consists of magnetic and gravity parts. Under seal conditions the magnetic force is several orders higher than the gravity, therefore the gravity effects can be neglected. In this case f is equal to $\overline{f}_{m,p}$, which is defined by (2.35). The Einstein relation gives the correspondence between the particle mobility and the diffusion coefficient

$$b = \frac{\mathrm{D}}{kT}. \tag{2.52}$$

Substituting (2.52) into (2.51) we obtain

$$\mathbf{i} = -\rho \mathrm{D} \left(\nabla c - \frac{1}{kT} c \, \overline{\mathbf{f}}_{m,p} \right). \tag{2.53}$$

Combining (2.35), (2.50), (2.53) and assuming density ρ to be constant we come to

$$-\mathrm{D} \nabla \cdot (\nabla c - c \, \xi L(\xi h) \nabla h) + \mathbf{v} \cdot \nabla c = 0.$$

Applying the divergence termwise we get

$$-\Delta c + \xi\Big[L(\xi h)\left(\nabla c \cdot \nabla h + c\Delta h\right) + c\nabla L(\xi h)\cdot\nabla h\Big] + \frac{1}{\mathrm{D}}\mathbf{v}\cdot\nabla c = 0.$$

Now applying the cylindrical coordinates (2.5) and vanishing derivatives with respect to ϕ we obtain

$$\begin{aligned} -\left(\frac{1}{r}\frac{\partial c}{\partial r} + \frac{\partial^2 c}{\partial r^2} + \frac{\partial^2 c}{\partial z^2}\right) + \xi\left\{c\frac{dL(\xi h)}{dh}\left[\frac{\partial^2 h}{\partial r^2} + \frac{\partial^2 h}{\partial z^2}\right]\right. \\ \left. + L(\xi h)\left[\frac{\partial c}{\partial r}\frac{\partial h}{\partial r} + \frac{\partial c}{\partial z}\frac{\partial h}{\partial z} + c\left(\frac{1}{r}\frac{\partial h}{\partial r} + \frac{\partial^2 h}{\partial r^2} + \frac{\partial^2 h}{\partial z^2}\right)\right]\right\} \\ + \frac{1}{D}\left(v_r\frac{\partial c}{\partial r} + v_z\frac{\partial c}{\partial z}\right) = 0. \end{aligned} \tag{2.54}$$

Using the dimensionless variables (2.16) and dimensionless velocity (2.42) the convection-diffusion equation (2.54) can be written as

$$\begin{aligned} -\frac{1}{a^2}\left(\frac{a}{r}\frac{\partial c}{\partial x} + \frac{\partial^2 c}{\partial x^2} + \frac{\partial^2 c}{\partial y^2}\right) + \frac{\xi}{a^2}\left\{\frac{c}{H_0}\frac{dL(\xi h)}{dh}\left[\frac{\partial^2 h}{\partial x^2} + \frac{\partial^2 h}{\partial y^2}\right]\right. \\ \left. + L(\xi h)\left[\frac{\partial c}{\partial x}\frac{\partial h}{\partial x} + \frac{\partial c}{\partial y}\frac{\partial h}{\partial y} + c\left(\frac{a}{r}\frac{\partial h}{\partial x} + \frac{\partial^2 h}{\partial x^2} + \frac{\partial^2 h}{\partial y^2}\right)\right]\right\} \\ + \frac{v_0}{a\mathrm{D}}\left(v_x\frac{\partial c}{\partial x} + v_y\frac{\partial c}{\partial y}\right) = 0. \end{aligned}$$

Using the approximation (2.17) and multiplying the equation by a^2 we obtain

$$\begin{aligned} -\left(\delta\frac{\partial c}{\partial x} + \frac{\partial^2 c}{\partial x^2} + \frac{\partial^2 c}{\partial y^2}\right) + \xi\left\{\frac{c}{H_0}\frac{dL(\xi h)}{dh}\left[\frac{\partial^2 h}{\partial x^2} + \frac{\partial^2 h}{\partial y^2}\right]\right. \\ \left. + L(\xi h)\left[\frac{\partial c}{\partial x}\frac{\partial h}{\partial x} + \frac{\partial c}{\partial y}\frac{\partial h}{\partial y} + c\left(\delta\frac{\partial h}{\partial x} + \frac{\partial^2 h}{\partial x^2} + \frac{\partial^2 h}{\partial y^2}\right)\right]\right\} \\ + \frac{v_0 a}{\mathrm{D}}\left(v_x\frac{\partial c}{\partial x} + v_y\frac{\partial c}{\partial y}\right) = 0. \end{aligned}$$

Neglecting all terms with δ due to their smallness we end up with

$$-\frac{1}{\mathrm{Pe}}\nabla\cdot\left(\nabla\widetilde{c} - \widetilde{c}\xi L\left(\xi\widetilde{h}\right)\nabla\widetilde{h}\right) + \widetilde{\mathbf{v}}\cdot\nabla\widetilde{c} = 0, \tag{2.55}$$

where

$$\mathrm{Pe} = \frac{a\, v_0}{D} \tag{2.56}$$

denotes Péclet number, $\widetilde{c}$ and $\widetilde{h}$ are the dimensionless c and h in coordinates of a cross-section $\widetilde{\Omega}$. The total mass of particles must stay constant. Without loss of generality we fix it to 1

$$\frac{1}{|\widetilde{\Omega}|}\int_{\widetilde{\Omega}}\widetilde{c}\,dx = 1. \tag{2.57}$$

Boundary conditions for the convection-diffusion equation are chosen in sense that there is no flux of particles through the boundary

$$\frac{\partial c}{\partial \mathbf{n}} - \left(\xi L\left(\xi h\right) \frac{\partial h}{\partial \mathbf{n}} + \mathbf{v} \cdot \mathbf{n} \right) c = 0 \quad \text{on } \Gamma,$$

where $\mathbf{n}$ is a unit outer normal to boundary Γ. Since $\mathbf{v}$ satisfies the boundary conditions for the Navier-Stokes equation (2.39) one can conclude that $\mathbf{v} \cdot \mathbf{n}$ vanishes on the whole boundary Γ. Applying the cylindrical coordinates (2.14) we obtain

$$\begin{pmatrix} \dfrac{\partial c}{\partial r} \\ \dfrac{1}{r}\dfrac{\partial c}{\partial \phi} \\ \dfrac{\partial c}{\partial z} \end{pmatrix} \cdot \mathbf{n} - \xi L\left(\xi h\right) c \begin{pmatrix} \dfrac{\partial h}{\partial r} \\ \dfrac{1}{r}\dfrac{\partial h}{\partial \phi} \\ \dfrac{\partial h}{\partial z} \end{pmatrix} \cdot \mathbf{n} = 0 \quad \text{on } \Gamma.$$

Due to the axial symmetry the derivatives with respect to ϕ vanish. Finally one can write the boundary conditions in a cross-section

$$\frac{\partial \widetilde{c}}{\partial \widetilde{\mathbf{n}}} - \xi L\left(\xi \widetilde{h}\right) \frac{\partial \widetilde{h}}{\partial \widetilde{\mathbf{n}}} \widetilde{c} = 0 \quad \text{on } \widetilde{\Gamma}, \tag{2.58}$$

where $\widetilde{\mathbf{n}}$ is a unit outer normal to $\widetilde{\Gamma}$, $\widetilde{c}$ and $\widetilde{h}$ are the functions c and h written in the cross-section $\widetilde{\Omega}$, respectively.

Remark 2.2.2. *The term $\xi L(\xi h)\nabla h$ can also be presented as $\nabla \ln \varphi$ with φ given by*

$$\varphi = \exp \int_0^{\xi h} L(\gamma) d\,\gamma = \frac{\sinh(\xi h)}{\xi h}.$$

Such a representation was used in [32, 33] in order to obtain an analytical solution for the convection-diffusion problem in case of no fluid motion. That corresponds to the choice $\mathbf{v} \equiv \mathbf{0}$ in equation (2.54)*. Then the problem* (2.54), (2.58) *has a unique solution c^*, which has the following form*

$$c^* = \frac{\varphi}{\int_\Omega \varphi \, dx}.$$

2.2.5 Young-Laplace equation

The Young-Laplace equation describes the position of free surfaces depending on the force balance on it. We follow [30] deriving the Young-Laplace equation.

Let us first introduce some useful notation. According to our model the free surface consists of two disconnected parts. It generates the following decomposition

$$\Gamma_f = \Gamma_{f,1} \cup \Gamma_{f,2}, \quad \Gamma_{f,1} \cap \Gamma_{f,2} = \varnothing.$$

We define the pressure in the outer media by $p_{\text{ext}}^{(i)}$, where index i corresponds to the outer media with respect to $\Gamma_{f,i}$. For each part $\Gamma_{f,i}$ we introduce an arc length s of a meridian line ranging from 0 to l_i, $i = 1, 2$. Thanks to the axial symmetry the meridian line does not depend on ϕ and without loss of generality we fix $\phi = 0$. Then each meridian line on $\Gamma_{f,i}$, $i = 1, 2$ is described by two parametric functions $r_i(s)$ and $z_i(s)$, which are related to cylindrical coordinates (2.5). That curve can be defined as

$$\gamma_{f,i} \ : \ s \in [0, l_i] \subset \mathbb{R} \mapsto (r_i(s), 0, z_i(s)) \in \mathbb{R}^3. \tag{2.59}$$

In the same manner we can define meridian lines on solid surfaces Γ_s and Γ_c, respectively

$$\begin{aligned} \gamma_s \ &: \ s \in [0, l_s] \subset \mathbb{R} \mapsto (R, 0, z_s(s)) \in \mathbb{R}^3, \\ \gamma_c \ &: \ s \in [0, l_c] \subset \mathbb{R} \mapsto (r_c(s), 0, z_c(s)) \in \mathbb{R}^3. \end{aligned} \tag{2.60}$$

The contact points of these curves can be defined as follows

$$\begin{aligned} \gamma_s(0) &= \gamma_{f,1}(0), \\ \gamma_s(l_s) &= \gamma_{f,2}(0), \\ \gamma_c(0) &= \gamma_{f,1}(l_1), \\ \gamma_c(l_c) &= \gamma_{f,2}(l_2). \end{aligned} \tag{2.61}$$

One should note that the definition is related to some boundary part. For that reason we denote γ as a curve defined on some boundary part Γ, which allows us to derive more general formulas. Here Γ is understood as one of the boundary parts Γ_s, Γ_c, $\Gamma_{f,1}$, $\Gamma_{f,2}$ to be defined later.

So we derive the Young-Laplace equation for a general meridian curve γ, given by two parametric functions $r(s)$, $z(s)$. Then a unit normal and a tangent are given as follows

$$\boldsymbol{\tau} = (r', 0, z'), \quad \mathbf{n} = (-z', 0, r'), \tag{2.62}$$

where prime denotes derivation with respect to s. Using parametric curves we can write a coordinate depending function $f = f(r, 0, z)$ as functions of parameter s

$$f(s) := f(r(s), 0, z(s)) = f(\gamma(s)) \quad \text{on } \Gamma.$$

Since we investigate meridian curves with contact points, all of them lie in a single cross-section, which according to our assumptions coincides with $\widetilde{\Omega}$. Then the coordinates in the 2D cross-section are related to 3D coordinates of domain Ω via (2.16) and could be written as functions of arc length s, i.e.

$$x(s) = \frac{r(s) - R}{a}, \quad y(s) = \frac{z(s)}{a} \quad \text{on } \Gamma.$$

One can also give a function restricted to Γ in a cross-section as a function of parameter s

$$\widetilde{f}(s) := \widetilde{f}(x(s), y(s)) = f(r(s), 0, z(s)) \text{ on } \Gamma.$$

This notation will be used further in this chapter for the case of simplicity.

The general Young-Laplace equation describes the force balance on a free surface

$$\mathbf{n} \cdot [|\mathbb{T} \cdot \mathbf{n}|] = \alpha \mathcal{K} \quad \text{on } \Gamma_f, \tag{2.63}$$

where $\mathcal{K}$ denotes the sum of principal curvatures on the surface, α the surface tension, $\mathbf{n}$ a unit normal to Γ_f, $\mathbb{T}(\mathbf{v}, p, \mathbf{H}, \mathbf{B})$ the stress tensor defined by (2.37). Substituting the stress tensor to (2.63) we obtain the following equation

$$\mathbf{n} \cdot [|\mathbb{T}(\mathbf{v}, p, \mathbf{H}, \mathbf{B}) \cdot \mathbf{n}|] = \frac{\mu_0}{2}(\mathbf{M} \cdot \mathbf{n})^2 - 2\eta \frac{\partial \mathbf{v}}{\partial \mathbf{n}} \cdot \mathbf{n} + p - p_{\text{ext}} = \alpha \mathcal{K} \quad \text{on } \Gamma_f, \tag{2.64}$$

where $\mathbf{n}$ is a unit normal to the surface, p the total pressure of the ferrofluid, and p_{ext} is the pressure in the outer medium with respect to Γ_f. The total pressure p can be obtained by integration of the Navier-Stokes equation (2.40) on the interval $[0, s^*]$ along γ. We recall that derivatives with respect to ϕ vanish. From boundary conditions (2.39) it follows that $\mathbf{v} \cdot \mathbf{n} = 0$ on $\partial\Omega$ and $\mathbf{v} \cdot \boldsymbol{\tau} = 0$ on $\Gamma_s \cup \Gamma_c$. Then using representation of a normal and a tangent (2.62) we obtain

$$\begin{aligned} p(s^*) = &\int_0^{s^*} \left(\rho \frac{r'}{r} v_\phi^2 - \eta \frac{1}{r} \frac{\partial (rw)}{\partial \mathbf{n}} - \rho g z' \right) ds \\ &- \frac{\rho}{2}(\mathbf{v} \cdot \boldsymbol{\tau})^2 + \mu_0 \int_{H(0)}^{H(s)} M \, dH + p(0) \quad \text{on } \Gamma, \end{aligned} \tag{2.65}$$

where w is the vorticity given by

$$w = \frac{\partial v_z}{\partial r} - \frac{\partial v_r}{\partial z}.$$

Substituting the obtained pressure into (2.64) we gain

$$\begin{aligned} \frac{\mu_0}{2}(\mathbf{M} \cdot \mathbf{n})^2 - 2\eta \frac{\partial \mathbf{v}}{\partial \mathbf{n}} \cdot \mathbf{n} + &\int_0^{s^*} \left(\rho \frac{r'}{r} v_\phi^2 - \eta \frac{1}{r} \frac{\partial (rw)}{\partial \mathbf{n}} - \rho g z' \right) ds \\ &- \frac{\rho}{2}(\mathbf{v} \cdot \boldsymbol{\tau})^2 + \mu_0 \int_{H(0)}^{H(s)} M \, dH = \alpha \mathcal{K} + p_{\text{ext}} - p(0) \quad \text{on } \Gamma_f. \end{aligned}$$

Applying the dimensionless coordinates (2.16) and approximation (2.17) we arrive at

$$\begin{aligned} \int_0^{s^*} \left[\rho \delta v_0^2 x' \omega^2 - \frac{\eta v_0}{R} \left(\frac{1}{\delta} \frac{\partial \widehat{w}}{\partial \mathbf{n}} - \widehat{w} y' \right) - \rho a g y' \right] ds + \frac{\mu_0 M_s^2}{2} (\widehat{\mathbf{M}} \cdot \mathbf{n})^2 - 2 \frac{\eta v_0}{a} \frac{\partial \widehat{\mathbf{v}}}{\partial \mathbf{n}} \cdot \mathbf{n} \\ - \frac{\rho v_0^2}{2} (\widehat{\mathbf{v}} \cdot \boldsymbol{\tau})^2 + \mu_0 M_s H_0 \int_{h(0)}^{h(s)} \widehat{M} \, ds = \alpha \mathcal{K} + p_{\text{ext}} - p(0) \quad \text{on } \Gamma_f, \end{aligned}$$

where dimensionless velocity components ω and $\widehat{\mathbf{v}}$ are defined by (2.42), dimensionless vorticity $\widehat{w}$ and magnetization $\widehat{\mathbf{M}}$ are given as follows

$$\widehat{w} = \frac{a}{v_0} w, \quad \widehat{\mathbf{M}} = \frac{\mathbf{M}}{M_s}.$$

Dividing the equation by $\mu_0 M_s H_0$ we obtain

$$\int_0^{s^*} \left[\mathrm{Fr}_m x' \omega^2 - \frac{\mathrm{Fr}_m}{\mathrm{Re}} \left(\frac{1}{\delta} \frac{\partial \widehat{w}}{\partial \mathbf{n}} - \widehat{w} y' \right) - \frac{\rho a g}{\mu_0 M_s H_0} y' + \widehat{M} \frac{\partial h}{\partial s} \right] ds + \frac{M_s}{2H_0} (\widehat{\mathbf{M}} \cdot \mathbf{n})^2 - \frac{2\mathrm{Fr}_m}{\delta \mathrm{Re}} \frac{\partial \widehat{\mathbf{v}}}{\partial \mathbf{n}} \cdot \mathbf{n} - \frac{\mathrm{Fr}_m}{2\delta} (\widehat{\mathbf{v}} \cdot \boldsymbol{\tau})^2 = \frac{\alpha}{\mu_0 M_s H_0} \mathcal{K} + \frac{p_{\mathrm{ext}} - p(0)}{\mu_0 M_s H_0} \quad \text{on } \Gamma_f.$$

Here, the constants Re and Fr_m are defined by (2.45) and (2.46), respectively.

In order to simplify the obtained equation, we use different arguments following [29, 31, 47, 48]. Using the standard characteristics of ferrofluid seals we obtain the following estimates of the constants: $\mathrm{Pe} \sim 100$, $\mathrm{Fr}_m \leq 1$, $\delta \sim 10^{-2}$ and hence, $\mathrm{Fr}_m/\mathrm{Re} < \delta$. See Section 2.4 for more details. For a common ferrofluid seal H_0 is two orders higher than $M_s/2$. This allows us to ignore the pressure jump $(\widehat{\mathbf{M}} \cdot \mathbf{n})$. The constant in front of the gravity force $\rho a g/(\mu_0 M_s H_0)$ does not exceed 10^{-4}, therefore, this term can be omitted. The capillary jump $\alpha\mathcal{K}$ can be neglected for the case $\mathrm{Bo}_m = \mu_0 M_s H_0 a/\alpha > 400$ [29], which holds for our choice of parameters.

Let us now consider the remaining velocity terms. As mentioned in Section 2.2.3, the secondary flow $\widehat{\mathbf{v}}$ is two to three orders lower than azimuthal velocity ω. Moreover, ω has magnitude of 1 due to the problem statement (2.48), (2.49). The structure of a unit normal and a tangent (2.62) imply all variations of secondary flow $\widehat{\mathbf{v}}$ and vorticity $\widehat{w}$ to be at least two orders lower than ω. Then doing simple calculations one can show that the term with ω^2 is at least two orders higher than all the other velocity terms. It allows us to neglect all velocity terms with exception of the term with ω^2.

After applying the discussed simplifications the Young-Laplace equation can be written as follows

$$\int_0^{s^*} \left(\mathrm{Fr}_m x' \omega^2 + \widehat{M} \frac{\partial h}{\partial s} \right) ds = \frac{p_{\mathrm{ext}} - p(0)}{\mu_0 M_s H_0} \quad \text{on } \Gamma_f. \tag{2.66}$$

Using argumentation above, one can show that the terms of this equation are comparable in magnitude. We now switch to functions written in the cross-section $\widetilde{\Omega}$. Writing equation (2.66) two times for both $\gamma_{f,i}$ we obtain a system of two equations

$$\int_0^{s^*} \left(\mathrm{Fr}_m x' \widetilde{\omega}^2 + \widetilde{M} \frac{\partial \widetilde{h}}{\partial s} \right) ds = \frac{p_{\mathrm{ext}}^{(i)} - \widetilde{p}(0, y_i(0))}{\mu_0 M_s H_0} \quad \text{on } \Gamma_{f,i},$$
$$s^* \in [0, l_i], \quad i = 1, 2.$$

These equations are more complex, than it seems. Since the variable s^* can be arbitrary on interval $[0, l_i]$ we can apply a limit to both sides with $s^* \to 0$. Assuming that ω, M, and $\partial h/\partial s$ are continuous functions, it immediately follows that the right hand side is equal to zero. So the right hand side of the equations can be understood as two additional conditions. The system then can be reformulated as follows

$$\begin{gathered}\int_0^{s^*} \left(\mathrm{Fr}_m x' \widetilde{\omega}^2 + \widetilde{M} \frac{\partial \widetilde{h}}{\partial s} \right) ds = 0, \quad s^* \in [0, l_i], \\ \widetilde{p}(0, y_i(0)) = p_{\text{ext}}^{(i)}, \quad i = 1, 2.\end{gathered} \tag{2.67}$$

The system needs some clarifications. At first, two conditions on pressure are redundant, since pressure as a solution of Navier-Stokes equation is unique up to an additive constant. That is why we consider their difference.

$$\Delta p_{\text{ext}} := p_{\text{ext}}^{(2)} - p_{\text{ext}}^{(1)} = \widetilde{p}(0, y_2(0)) - \widetilde{p}(0, y_i(0)).$$

We can eliminate the difference of pressures on the right hand side using the equation (2.65) one more time with $\gamma = \gamma_s$. Taking into account the boundary conditions for the Navier-Stokes equation (2.39), using a unit normal and a tangent to Γ_s

$$\mathbf{n} = (-1, 0, 0), \quad \boldsymbol{\tau} = (0, 0, 1),$$

and neglecting the gravity force as previously, one can obtain

$$p(s^*) = \mu_0 \int_0^{s^*} M \frac{\partial H}{\partial s} ds + p(0) \quad \text{on } \Gamma_s. \tag{2.68}$$

Since the curve γ_s is a straight line parallel to z axis, the function $r_s(s) \equiv R$. Then one can rewrite (2.68) as

$$p(s^*) = \mu_0 \int_{z(0)}^{z(s^*)} \left(M \frac{\partial H}{\partial z} \right) \Bigg|_{r=R} dz + p(0) \quad \text{on } \Gamma_s.$$

Taking $s^* = l_s$ and using dimensionless variables (2.16) we gain

$$\Delta p_{\text{ext}} = \widetilde{p}(0, y_2(0)) - \widetilde{p}(0, y_1(0)) = \mu_0 M_s H_0 \int_{y_1(0)}^{y_2(0)} \left(\widetilde{M} \frac{\partial \widetilde{h}}{\partial y} \right) \Bigg|_{x=0} dy.$$

Dividing the equation by $\mu_0 M_s H_0$ we obtain it in a dimensionless form

$$\mathrm{Pm} = \int_{y_1(0)}^{y_2(0)} \left(\widetilde{M} \frac{\partial \widetilde{h}}{\partial y} \right) \Bigg|_{x=0} dy \tag{2.69}$$

with Pm denoting the dimensionless pressure drop

$$\mathrm{Pm} = \frac{\Delta p_{ext}}{\mu_0 \overline{M}_s H_0}. \tag{2.70}$$

The second note to system (2.67) is that the values of $y_i(0), i = 1, 2$ are not prescribed, i.e. two conditions are needed. to fix them The equation (2.69) can be used as first one. Indeed, we consider two possible cases

1. The pressure drop Pm is given. Then, defining one point, e.g. $y_1(0)$, the second point $y_2(0)$ can be found from equation (2.69) in a unique way, since

$$\mathrm{sign}(\widetilde{M}\frac{\partial \widetilde{h}}{\partial y}) = \mathrm{sign}(y)$$

   and integration goes along the y-axis.

2. One of the points is given. This occurs only in case of critical pressure drop. Then one of the values $y_i(0)$ reaches zero [33], e.g. $y_1(0) = 0$. The value of critical pressure drop is calculated by (2.69).

The second condition on points of contact $y_i(0), i = 1, 2$ is obtained from the volume conservation. We introduce an operator

$$U : (y_1(0), y_2(0)) \mapsto \mathbb{R}$$

defining the volume of fluid, depending on contact points of free surfaces. We need a condition which makes this dependency unique. Having in mind the symmetry of the domain with respect to x-axis, it is enough to assume that for all $y_1(0)$ an operator $y_2(0) \mapsto U(y_1(0), y_2(0))$ is an isomorphism. The volume conservation is then written as follows

$$U(y_1(0), y_2(0)) = \widetilde{U}_0, \tag{2.71}$$

where $\widetilde{U}_0$ denotes a fixed volume of a ferrofluid in the cross-section.

Remark 2.2.3. *Due to the smallness of $\delta = a/R$ the total fluid volume and its area in a cross-section are related by the following formula $U_0 \approx 2\pi R\widetilde{U}_0$.*

Rewriting the system (2.67) with condition on a pressure drop (2.69) and the volume conservation condition (2.71), the final system of equations will look as follows

$$\begin{gathered}\int_0^{s^*} \left(\mathrm{Fr}_m x' \widetilde{\omega}^2 + \widetilde{M}\frac{\partial \widetilde{h}}{\partial s} \right) ds = 0 \quad \text{on } \Gamma_{f,i}, \quad s^* \in [0, l_i], \quad i = 1, 2, \\ \mathrm{Pm} = \int_{y_1(0)}^{y_2(0)} \left(\widetilde{M}\frac{\partial \widetilde{h}}{\partial y} \right) \Big|_{x=0} dy, \qquad U(y_1(0), y_2(0)) = \widetilde{U}_0.\end{gathered} \tag{2.72}$$

We write equations in an equivalent form, which is more convenient for discretization. Integrating by parts we obtain

$$\int_a^b \widetilde{M}\frac{\partial \widetilde{h}}{\partial s}ds = \widetilde{M}\widetilde{h}\Big|_b - \widetilde{M}\widetilde{h}\Big|_a - \int_a^b \widetilde{h}\frac{\partial \widetilde{M}}{\partial s}ds.$$

Using this and equations for contact points (2.61) we obtain an equivalent formulation of the Young-Laplace equation (2.72)

$$\begin{aligned}\left(\widetilde{M}\widetilde{h}\right)\Big|_{(x(s^*),y_i(s^*))} + \int_0^{s^*}\left(\mathrm{Fr}_m x'\widetilde{\omega}^2 - \frac{\partial \widetilde{M}}{\partial s}\widetilde{h}\right)ds = \left(\widetilde{M}\widetilde{h}\right)\Big|_{(0,y_i(0))} \quad \text{on } \Gamma_{f,i},\\ s^* \in [0, l_i], \quad i = 1, 2,\\ \mathrm{Pm} = \int_{y_1(0)}^{y_2(0)}\left(\widetilde{M}\frac{\partial \widetilde{h}}{\partial y}\right)\Big|_{x=0} dy, \qquad U(y_1(0), y_2(0)) = \widetilde{U}_0.\end{aligned} \tag{2.73}$$

Up to now all derivations were made for a general function M. In other studies [31, 47, 48] the magnetization was assumed to be at saturation M_s. That corresponds to a choice of dimensionless magnetization $\widetilde{M} \equiv 1$, which simplifies the system greatly. But we consider more complex case and use a standard Langevin approximation of the magnetization given by (2.30) and (2.32)

$$M = \overline{M}_s\widehat{M} = \overline{M}_s cL(\xi h) \quad \text{with} \quad L(t) = \coth(t) - 1/t.$$

Using this representation we rewrite the system corresponding to the Young-Laplace equation (2.73). Finally, the whole problem can be formulated as follows

Find two parametrized curves such that at each point $(x(s^*), y_i(s^*))$ it holds

$$\begin{aligned}\left(\widetilde{c}L(\xi\widetilde{h})\widetilde{h}\right)\Big|_{(x(s^*),y_i(s^*))} + \int_0^{s^*}\left(\mathrm{Fr}_m x'\widetilde{\omega}_i^2 - \frac{\partial(\widetilde{c}L(\xi\widetilde{h}))}{\partial s}\widetilde{h}\right)ds = \left(\widetilde{c}L(\xi\widetilde{h})\widetilde{h}\right)\Big|_{(0,y_i(0))}\\ s^* \in [0, l_i], \quad i = 1, 2,\\ \mathrm{Pm} = \int_{y_1(0)}^{y_2(0)}\left(\widetilde{c}L(\xi\widetilde{h})\frac{\partial \widetilde{h}}{\partial y}\right)\Big|_{x=0} dy, \qquad U(y_1(0), y_2(0)) = \widetilde{U}_0.\end{aligned} \tag{2.74}$$

2.3 Complete 2D mathematical model

Combining all of the above we end up with the mathematical model, which is in fact the system of the equations (2.48), (2.55), (2.57), (2.74). For the sake of simplicity from

here and further we use the notation without tilde for the domain in cross-section and its boundary, as well as for functions given there. Then the full mathematical model can be written as

$$\Delta\omega = 0 \quad \text{in } \Omega, \tag{2.75a}$$

$$\begin{aligned}(\mathbf{v}\cdot\nabla)\,\mathbf{v} - \operatorname{div}\,\sigma(\mathbf{v},p) &= \mathbf{e}_1\delta\omega^2 + \frac{\delta}{\mathrm{Fr}_m}L\left(\xi h_s\right)c\nabla h_s \quad \text{in } \Omega,\\ \nabla\cdot\mathbf{v} &= 0 \quad \text{in } \Omega,\end{aligned} \tag{2.75b}$$

$$-\frac{1}{\mathrm{Pe}}\nabla\cdot\left(\nabla c - c\xi L\left(\xi h_s\right)\nabla h_s\right) + \mathbf{v}\cdot\nabla c = 0 \quad \text{in } \Omega, \quad \int\limits_{\Omega} c\,dx = |\Omega|, \tag{2.75c}$$

$$\begin{aligned}&cL(\xi h_s)h_s\Big|_{(x(s^*),y_i(s^*))} + \int\limits_0^{s^*}\Big[\mathrm{Fr}_m x'\omega_i^2 - \frac{\partial(cL(\xi h_s))}{\partial s}h_s\Big]ds = cL(\xi h_s)h_s\Big|_{(0,y_i(0))},\\ &\qquad s^*\in[0,l_i] \quad i=1,2,\\ &\mathrm{Pm} = \int\limits_{y_1(0)}^{y_2(0)} cL(\xi h_s)\frac{\partial h_s}{\partial y}\,dy, \qquad U(y_1(0),y_2(0)) = U_0,\end{aligned} \tag{2.75d}$$

where h_s is the analytical solution of Maxwell's system given by (2.27), stress tensor σ is given by (2.47), constants Fr_m, Pm, Pe, and ξ are defined by (2.46), (2.70), (2.56), (2.31), respectively. The system is supplemented with the boundary conditions (2.49) and (2.58)

$$\begin{aligned}\omega &= 0 \quad \text{on } \Gamma_c,\\ \omega &= 1 \quad \text{on } \Gamma_s,\\ \frac{\partial\omega}{\partial\mathbf{n}} &= 0 \quad \text{on } \Gamma_f,\end{aligned} \tag{2.76a}$$

$$\begin{aligned}\mathbf{v} &= 0 \quad \text{on } \Gamma_c\cup\Gamma_s,\\ \mathbf{v}\cdot\mathbf{n} &= 0 \quad \text{on } \Gamma_f,\\ \mathbf{n}\cdot\sigma(\mathbf{v},p)\cdot\boldsymbol{\tau} &= 0 \quad \text{on } \Gamma_f.\end{aligned} \tag{2.76b}$$

$$\frac{\partial c}{\partial\mathbf{n}} - \xi L(\xi h_s)\frac{\partial h_s}{\partial\mathbf{n}}c = 0 \quad \text{on } \Gamma, \tag{2.76c}$$

The full problem can be described as follows. Find two curves $\gamma_{f,1}$, $\gamma_{f,2}$ defined by the functions $y_i(x)$, $i=1,2$ and the quadruple $\{\omega,\mathbf{v},p,c\}$ in Ω satisfying the system (2.75) with the boundary conditions (2.76). The domain Ω is determined by the functions $y_i(x)$, $i=1,2$ as follows

$$\begin{aligned}\Omega := \big\{(x,y)\in\mathbb{R}^2 \,:\, x>0, \quad &y^2 > (x^2-1)\tan^2\beta,\\ &y > y_1(s) \quad \text{for} \quad s\in(0,l_1), \quad y < y_2(s) \quad \text{for} \quad s\in(0,l_2)\big\}.\end{aligned} \tag{2.77}$$

2.4 Parameter values

In this section we estimate all the dimensionless parameters used in our mathematical model. Our aim is to estimate the parameter values and to reduce the number of varied parameters. We obtain the parameter range for numerical tests, while the smaller number of parameters simplifies classification.

The dimensionless constants are the magnetic Froude number, the Reynolds number, the Péclet number and the Langevin parameter, which are given by (2.46), (2.45), (2.56), and (2.31), respectively

$$\begin{aligned} \mathrm{Fr}_m &= \frac{\rho v_0^2 \delta}{\mu_0 \overline{M_s} H_0}, \\ \mathrm{Re} &= \frac{v_0 a \rho}{\eta}, \\ \mathrm{Pe} &= \frac{a\, v_0}{D} = \mathrm{Re} \cdot \mathrm{Sc}, \\ \xi &= \frac{\mu_0 m H_0}{kT}. \end{aligned} \tag{2.78}$$

Here ρ denotes the density of a ferrofluid, v_0 the rotation velocity of the shaft, δ the relation between the gap width a and the shaft radius R, $\overline{M_s}$ the saturation magnetization of a uniform ferrofluid, H_0 maximum of magnetic field intensity, a the gap width, η the dynamic viscosity, D the diffusion coefficient, m the magnetic moment of a single particle, T the absolute temperature, $\mu_0 = 4\pi \times 10^{-7}$ V·s/(A·m) the vacuum permeability, $k = 1.38 \cdot 10^{-23}$J/K the Boltzmann constant.

As we have shown in (2.78), the Reynolds number and the Péclet number are related through the Schmidt number Sc

$$\mathrm{Sc} = \frac{\eta}{\rho D}.$$

Fixing Schmidt number allows us to consider three independent parameters instead of four. It can be seen in the system (2.75) that the Froude number Fr_m determines the geometry of the domain, whereas the Langevin parameter ξ and the Péclet number Pe are responsible for coupling of the Navier-Stokes and the convection-diffusion equations.

Let us determine the parameter values. We use the Stokes-Einstein relation [9] in order to find the diffusion coefficient

$$D = \frac{kT}{6\pi\eta R_p}$$

with R_p being the radius of a single particle. As it is known from the literature (see [34], e.g.), the Stokes-Einstein relation is not precise for ferrofluids in case of nonuniform particle concentration. However, we aim to estimate this coefficient only to see the order of magnitude. Taking $R_p = 5 \cdot 10^{-9}$ m we obtain

$$D = \frac{1.38 \cdot 10^{-23} \cdot 300}{6\pi \cdot 3 \cdot 10^{-2} \cdot 5 \cdot 10^{-9}} \approx 1.46 \cdot 10^{-12}\ \mathrm{m}^2/\mathrm{s}$$

and

$$\mathrm{Sc} \approx 1.43 \cdot 10^7.$$

For Reynolds number Re not higher than 200 one can guarantee the laminar flow of the fluid [31]. Choosing v_0 we take into consideration that in industry of ferrofluid seals the maximum rotation velocity reaches 500.000 dN [17] with d denoting the diameter of the shaft in mm and N the angular velocity in rev/min, which is equivalent to $v_0 \approx 26.2$ m/s. The other physical characteristics are chosen from their typical ranges for the ferrofluid seals. Such as $a = (1 \div 5) \cdot 10^{-4}$ m, $\delta := a/R = 0.01$, $T = 300$ K, $\rho = (1 \div 1.5) \cdot 10^3$ kg/m^3, $M_s = (4 \div 6) \cdot 10^4$ A/m, $H_0 = 10^5 \div 10^6$ A/m, $\eta = 10^{-3} \div 10^{-1}$ Pa·s, $m = (2 \div 2.5) \cdot 10^{-19}$ A $\cdot$ m^2.

Finally, we present in the table below the observed parameters for different choices of Fr_m and ξ. It can be seen that we do not exceed the maximum industrial velocity of the shaft rotation and the magnetic field intensity is close to real values in magnetic seals.

	$\mathrm{Fr}_m = 0.1$	$\mathrm{Fr}_m = 0.25$	$\mathrm{Fr}_m = 0.5$	$\mathrm{Fr}_m = 0.7$	$\mathrm{Fr}_m = 1$
v_0, m/s	6.63	10.48	14.82	17.54	20.96
Re	63.25	100	141.42	167.33	200
Pe	9.05e+8	1.43e+9	2.02e+9	2.39e+9	2.86e+9

Table 2.1: Parameter values for $\xi = 6$ ($H_0 = 10^5$ A/m).

Chapter 3

Continuous problems

The mathematical model (2.75), (2.76) consists of three elliptic boundary value problems. These problems can be solved numerically using two main approaches: finite difference methods and variational methods. We use different variational methods such as Finite Elements, Boundary Elements, and Finite Volumes for discretization of subproblems. In this chapter we introduce the variational formulation of the problems embedded in the mathematical model and refer to theory guaranteeing their unique solvability. Each PDE of the model (2.75), (2.76) is investigated separately. The coupling strategy is discussed in the next chapter with respect to the discretization method.

3.1 Azimuthal velocity

The problem for azimuthal velocity is given by the equation (2.75a)

$$\Delta\omega = 0 \quad \text{in } \Omega \in \mathbb{R}^2 \tag{3.1}$$

together with the boundary conditions (2.76a)

$$\begin{aligned} \omega &= 0 \quad \text{on } \Gamma_c, \\ \omega &= 1 \quad \text{on } \Gamma_s, \\ \frac{\partial\omega}{\partial\mathbf{n}} &= 0 \quad \text{on } \Gamma_f, \end{aligned} \tag{3.2}$$

where $\mathbf{n}$ is a unit outer normal to Γ.

We use two different discrete methods for the problem (3.1), (3.2). Namely the finite element and the boundary element method. At first one should consider the coupling of the problem (3.1), (3.2) with the problem for the Young-Laplace equation. The Young-Laplace equation (2.75d) is formulated on the free surface. The boundary element method allows to solve problem (3.1), (3.2) only on the boundary, which is enough for coupling. But it also decreases the number of degrees of freedom comparing to the finite element method. The azimuthal velocity also appears on the right-hand side of the Navier-Stokes

equation (2.75b), so discretization of both problems with the finite elements on the same mesh makes implementation easier. These two methods need different problem formulation and we present them both.

We start with the weak formulation of the problem. Multiplying by a test function $\mathrm{w} \in H^1(\Omega)$ and integrating by parts we obtain for a new solution function $\omega \in H^1(\Omega)$

$$(\nabla\omega, \nabla\mathrm{w}) - \int_\Gamma \frac{\partial\omega}{\partial\mathbf{n}}\,\mathrm{w}\,d\gamma = 0.$$

We introduce a bilinear form

$$a_\omega(\omega, \mathrm{w}) := (\nabla\omega, \nabla\mathrm{w})$$

and two spaces incorporating homogeneous and inhomogeneous boundary conditions

$$W := \{\mathrm{w} \in H^1(\Omega) \mid \mathrm{w} = 0 \text{ on } \Gamma_c,\ \mathrm{w} = 1 \text{ on } \Gamma_s\},$$
$$W_0 := \{\mathrm{w} \in H^1(\Omega) \mid \mathrm{w} = 0 \text{ on } \Gamma_c \cup \Gamma_s\}.$$

Then the weak-formulated problem looks as follows:

Find $\omega \in W$ such that

$$a_\omega(\omega, \mathrm{w}) = 0 \quad \forall \mathrm{w} \in W_0. \tag{3.3}$$

The integral over the boundary vanishes due to the boundary conditions and the structure of the space W_0. It follows from the inverse trace theorem that there exists an extension ω_D satisfying the nonhomogeneous boundary conditions [42]. So it remains to find $\omega_0 \in W_0$ such that

$$a_\omega(\omega_0, \mathrm{w}) = -a_\omega(\omega_D, \mathrm{w}) \quad \forall \mathrm{w} \in W_0 \tag{3.4}$$

holds. According to Poincaré-Friedrich's inequality the semi-norm $|\cdot|_{1,W_0}$ is equivalent to the norm $\|\cdot\|_{1,W_0}$. This means that the bilinear form $a_\omega(\cdot,\cdot)$ is coercive on W_0. So the Lax-Milgram theorem can be applied, which guarantees the unique solvability of the problem (3.3) [8].

The boundary element method needs a reformulation in form of a boundary integral equation. The problem for the azimuthal velocity (3.1), (3.2) is described by the Laplace equation with mixed Dirichlet and Neumann boundary conditions. The Laplace equation is the most standard for the boundary element method and is widely studied in the literature, for example in [42]. We use the direct formulation of the boundary integral equations, and collocation method for the discretization.

The boundary value problem is reformulated to a boundary integral equation for two unknown functions. This reformulation is based on properties of the fundamental solution which for 2-dimensional Laplace equation is given by

$$u^*(\xi^0, \xi) = -\ln\left(|\xi^0 - \xi|\right) = -\frac{1}{2}\ln\left(\left(x^0 - x\right)^2 + \left(y^0 - y\right)^2\right), \tag{3.5}$$

where $\xi = (x, y), \xi^0 = (x^0, y^0) \in \mathbb{R}^2$. The solution of the problem is then given by the following representation formula

$$\int_\Gamma \left(u(\xi) \frac{\partial u^*}{\partial \mathbf{n}}(\xi^0, \xi) - u^*(\xi^0, \xi) \frac{\partial u}{\partial \mathbf{n}}(\xi) \right) d\gamma = -\pi b u(\xi^0) \tag{3.6}$$

with

$$b = \begin{cases} 1, & \xi^0 \in \Gamma, \\ 2, & \xi^0 \in \Omega. \end{cases} \tag{3.7}$$

We introduce the following notation for the sake of simplicity. We change the boundary decomposition

$$\Gamma_D = \Gamma_s \cup \Gamma_c, \quad \Gamma_N = \Gamma_f, \tag{3.8}$$

denote

$$q := \frac{\partial u}{\partial \mathbf{n}}, \quad q^* := \frac{\partial u^*}{\partial \mathbf{n}}, \tag{3.9}$$

and write the boundary conditions according to this notation

$$\begin{aligned} u &= \overline{u} \text{ on } \Gamma_D, \\ q &= \overline{q} \text{ on } \Gamma_N. \end{aligned} \tag{3.10}$$

We choose the point ξ^0 on the boundary Γ. Then we split the boundary integral equation (3.6) into two parts for $b = 1$ according to (3.7)

$$\begin{aligned} \int_{\Gamma_D} u^* \, q \, d\gamma - \int_{\Gamma_N} u \, q^* \, d\gamma &= \pi \overline{u}(\xi^0) + \int_{\Gamma_D} \overline{u} \, q^* \, d\gamma - \int_{\Gamma_N} u^* \, \overline{q} \, d\gamma \quad \xi^0 \in \Gamma_D, \\ \int_{\Gamma_D} u^* \, q \, d\gamma - \int_{\Gamma_N} u \, q^* \, d\gamma - \pi u(\xi^0) &= \int_{\Gamma_D} \overline{u} \, q^* \, d\gamma - \int_{\Gamma_N} u^* \, \overline{q} \, d\gamma \quad \xi^0 \in \Gamma_N. \end{aligned} \tag{3.11}$$

We put on the left hand side the unknown functions and skip the argument lists for simplicity. The solution of the problem is sought in the form

$$(u, q) \in H^{-1/2}(\Gamma_D) \times H^{1/2}(\Gamma_N).$$

The problem (3.11) is the direct formulation of the boundary integral equations. We refer to [42, Chapter 7.3] for the unique solvability of the continuous problem.

3.2 Secondary flow

The 2D Navier-Stokes-type equation is given by (2.75b)

$$\begin{aligned} (\mathbf{v} \cdot \nabla) \, \mathbf{v} - \operatorname{div} \sigma(\mathbf{v}, p) &= \mathbf{e}_x \delta \omega^2 + \frac{\delta}{\mathrm{Fr}_m} L \left(\xi h_s \right) \nabla h_s \, c, \\ \nabla \cdot \mathbf{v} &= 0 \end{aligned} \qquad \text{in } \Omega \tag{3.12}$$

and is supplemented with the boundary conditions (2.76b). The boundary conditions include the Dirichlet type condition on solid surfaces

$$\mathbf{v} = 0 \quad \text{on } \Gamma_c \cup \Gamma_s \tag{3.13}$$

and the slip boundary condition on a free surface, consisting of a condition on tangential stresses

$$\mathbf{n} \cdot \sigma(\mathbf{v}, p)\boldsymbol{\tau} = 0 \quad \text{on } \Gamma_f \tag{3.14}$$

and a no penetration condition

$$\mathbf{v} \cdot \mathbf{n} = 0 \quad \text{on } \Gamma_f. \tag{3.15}$$

There are two common ways of applying boundary conditions. One can incorporate them into ansatz space. The other way is to enforce conditions weakly as a constraint by Lagrangian multiplier technique. The first approach is classical and in most cases is more convenient. However, the Lagrange multiplier is more flexible and allows to handle very complex conditions. The no penetration condition (3.15) was imposed weakly in [45, 46] and in classical way in [2, 44]. The comparison of these two techniques in [3] has shown that the incorporation into ansatz space is usually less complex and numerically cheaper. Therefore, this approach was chosen for the current problem.

For the sake of simplicity we denote

$$\mathbf{f} := \mathbf{e}_x \delta\omega^2 + \frac{\delta}{\mathrm{Fr}_m} L\left(\xi h_s\right) c \nabla h_s. \tag{3.16}$$

We multiply the equation (3.12) by a vector valued test function $\mathbf{w}$ and integrate over the domain Ω. The equation will look as follows

$$\left((\mathbf{v} \cdot \nabla)\,\mathbf{v}, \mathbf{w}\right) - \left(\operatorname{div} \sigma(\mathbf{v}, p), \mathbf{w}\right) = \langle \mathbf{f}, \mathbf{w} \rangle \quad \text{in } \Omega.$$

Taking into account boundary condition (3.14) one can write

$$\sigma(\mathbf{v}, p)\mathbf{n} = (\mathbf{n} \cdot \sigma(\mathbf{v}, p)\mathbf{n})\mathbf{n} + (\boldsymbol{\tau} \cdot \sigma(\mathbf{v}, p)\mathbf{n})\boldsymbol{\tau} = (\mathbf{n} \cdot \sigma(\mathbf{v}, p)\mathbf{n})\mathbf{n}.$$

Then using Green's formula we obtain

$$\begin{aligned} -\int_\Omega \operatorname{div} \sigma(\mathbf{v}, p) \cdot \mathbf{w}\, dx &= \frac{2}{\mathrm{Re}} \int_\Omega \mathbb{D}(\mathbf{v}) : \mathbb{D}(\mathbf{w}) dx - \int_\Omega p \operatorname{div} \mathbf{w}\, dx - \int_{\partial\Omega} \mathbf{w} \cdot \sigma(\mathbf{v}, p)\mathbf{n}\, d\gamma \\ &= \frac{2}{\mathrm{Re}} \int_\Omega \mathbb{D}(\mathbf{v}) : \mathbb{D}(\mathbf{w}) dx - \int_\Omega p \operatorname{div} \mathbf{w}\, dx - \int_{\partial\Omega} \mathbf{w} \cdot \mathbf{n} \left(\mathbf{n} \cdot \sigma(\mathbf{v}, p)\mathbf{n}\right) d\gamma. \end{aligned}$$

We introduce two solution spaces for velocity and pressure, respectively

$$\begin{aligned} X &:= \{\mathbf{w} \in \left(H^1(\Omega)\right)^2 \ : \ \mathbf{w} \cdot \mathbf{n} = 0 \text{ on } \Gamma_f, \quad \mathbf{w} = 0 \text{ on } \Gamma_s \cup \Gamma_c\}, \\ M &:= \{q \in L^2(\Omega) \ : \ \int_\Omega q\, dx = 0\} = L_0^2(\Omega), \end{aligned}$$

two bilinear forms and a trilinear form, respectively

$$a(\mathbf{u},\mathbf{w}) := \frac{2}{\mathrm{Re}}\int_\Omega \mathbb{D}(\mathbf{u}) : \mathbb{D}(\mathbf{w})\, dx,$$
$$b(p,\mathbf{w}) := -\int_\Omega p \ \mathrm{div}\ \mathbf{w}\, dx,$$
$$N(\mathbf{u},\mathbf{v},\mathbf{w}) := \int_\Omega [(\mathbf{u}\cdot\nabla)\mathbf{v}]\,\mathbf{w}\, dx.$$

Using this notation we give a weak formulation of the problem (3.12), (3.13), (3.14), (3.15) according to [44]:

Find a pair $(\mathbf{v},p) \in X \times M$ such that

$$\begin{aligned} a(\mathbf{v},\mathbf{w}) + N(\mathbf{v},\mathbf{v},\mathbf{w}) + b(p,\mathbf{w}) &= \langle f,\mathbf{w}\rangle \qquad \forall \mathbf{w}\in X,\\ b(q,\mathbf{v}) &= 0 \qquad\qquad \forall q \in M. \end{aligned} \tag{3.17}$$

The solvability of the problem (3.17) is usually studied by means of the following problem

Find $\mathbf{v} \in X_0$ such that

$$a(\mathbf{v},\mathbf{w}) + N(\mathbf{v},\mathbf{v},\mathbf{w}) = \langle f,\mathbf{w}\rangle \qquad \forall \mathbf{w}\in X_0, \tag{3.18}$$

where X_0 is defined as follows

$$X_0 := \{v \in X \ :\ \mathrm{div}\ v = 0\}. \tag{3.19}$$

Existence of a solution of the problem (3.18) is guaranteed by [18, Theorem 4.1.2] and the estimate provided by the Korn's second inequality and Poincaré-Morrey inequality [45]

$$a(\mathbf{w},\mathbf{w}) \geq C_1\|\mathbf{w}\|_1^2 - C_2\int_\Gamma |\mathbf{w}\cdot\mathbf{n}|^2 d\gamma \quad \forall \mathbf{w}\in X. \tag{3.20}$$

One can see that $\mathbf{w}\cdot\mathbf{n} = 0$ on Γ for all $\mathbf{w}\in X$ due to the structure of the space X. So it follows

$$a(\mathbf{w},\mathbf{w}) \geq C_1\|\mathbf{w}\|_1^2 \quad \forall \mathbf{w}\in X.$$

Then [18, Theorem 4.1.3] proves that solution is unique if $\mathrm{Re}^2\|f\|_0$ is sufficiently small.

The final step is to show that for each solution $\mathbf{v}$ of the problem (3.18) there exist $p \in M$ such that the pair $(\mathbf{v},p)$ is a solution of (3.17). This is proven in [18, Theorem 4.1.4] by using the LBB-condition

$$\beta\|q\|_0 \leq \sup_{\mathbf{w}\in H_0^1(\Omega)^2} \frac{|b(\mathbf{w},q)|}{\|\mathbf{w}\|_1} \leq \sup_{\mathbf{w}\in X} \frac{|b(\mathbf{w},q)|}{\|\mathbf{w}\|_1} \quad \forall q \in M.$$

3.3 Particle concentration

The convection-diffusion problem (2.75c) consists of the convective-diffusive type equation

$$-\frac{1}{\mathrm{Pe}}\nabla\cdot\Big(\nabla c - c\xi L(\xi h_s)\nabla h_s\Big) + \mathbf{v}\cdot\nabla c = 0 \quad \text{in } \Omega \tag{3.21}$$

the integral condition, fixing the mass of particles

$$\frac{1}{|\Omega|}\int_\Omega c\,dx = 1, \tag{3.22}$$

and is supplemented by the boundary condition (2.76c)

$$\frac{\partial c}{\partial \mathbf{n}} - \xi L(\xi h_s)\frac{\partial h_s}{\partial \mathbf{n}}c = 0 \quad \text{on } \Gamma. \tag{3.23}$$

For simplicity we introduce the following notation

$$\boldsymbol{\alpha} := \xi L(\xi h_s)\nabla h_s + \mathrm{Pe}\ \mathbf{v}. \tag{3.24}$$

Since $\mathbf{v}$ is a solution of the planar Navier-Stokes equation (3.12) it is a divergence-free function which satisfies boundary conditions (3.13), (3.15). It means that the boundary condition can be written as follows

$$\frac{\partial c}{\partial \mathbf{n}} - \xi L(\xi h_s)\frac{\partial h_s}{\partial \mathbf{n}}c = \frac{\partial c}{\partial \mathbf{n}} - c\boldsymbol{\alpha}\cdot\mathbf{n} = 0.$$

Then one can write the problem (3.21), (3.23) in a general nonhomogeneous form

$$\begin{aligned} -\nabla\cdot(\nabla c - \boldsymbol{\alpha}c) &= f \quad \text{in } \Omega,\\ (\nabla c - \boldsymbol{\alpha}c)\cdot\mathbf{n} &= 0 \quad \text{on } \Gamma. \end{aligned} \tag{3.25}$$

Multiplying by a test function $\mathrm{w} \in H^1(\Omega)$ and integrating by parts we write the problem for the unknown function $c \in H^1(\Omega)$

Find $c \in H^1(\Omega)$ such that

$$a_c(c,\mathrm{w}) := (\nabla c - \boldsymbol{\alpha}c, \nabla \mathrm{w}) = \langle f, \mathrm{w}\rangle \quad \text{for all } \mathrm{w} \in H^1(\Omega). \tag{3.26}$$

The integral over the boundary vanishes due to the boundary conditions (3.23). One immediately can see that for the choice $\mathrm{w} = \mathrm{const}$ the homogeneous problem is satisfied for any $c \in H^1(\Omega)$. This induces the necessary solvability condition for the general problem, i.e. $\langle f, 1\rangle = 0$. In addition solution of a homogeneous problem remains a solution being multiplied by a constant, i.e. the solution of (3.26) is not unique if it exists.

We start with analysis of coercivity of the bilinear form $a_c(\cdot,\cdot)$. If it holds, then the Lax-Milgram theorem implies the unique solvability of the problem. Let us introduce a general factorized space

$$V_n := \left\{ \mathrm{w} \in H^1(\Omega) \ :\ \frac{1}{|\Omega|}\int_\Omega \mathrm{w}\,dx = n \right\}, \quad n \in \{0,1\}.$$

The space V_1 incorporates the integral condition (3.22), and the space $V_0 = H^1(\Omega) \cap L_0^2(\Omega)$. Using this space definition we write the problem (3.26) together with the integral condition (3.22) as follows

Find $c \in V_1$ such that

$$a_c(c, \mathrm{w}) = \langle f, \mathrm{w} \rangle \quad \text{for all } \mathrm{w} \in V_0, \tag{3.27}$$

Homogenizing the integral condition (3.22) we can choose equal ansatz and test spaces. We obtain the equivalent formulation

Find $c \in V_0$ such that

$$a_c(c, \mathrm{w}) = \langle f, \mathrm{w} \rangle - a_c(1, \mathrm{w}) \quad \text{for all } \mathrm{w} \in V_0. \tag{3.28}$$

As one can see, the bilinear form $a_c(\cdot, \cdot)$ is not coercive on $H^1(\Omega)$ for an arbitrary $\boldsymbol{\alpha}$ because of the constant functions. In view of problem (3.28) it is interesting whether $a_c(\cdot, \cdot)$ is coercive on the factorized space $V_0 = H^1(\Omega) \cap L_0^2(\Omega)$. Integrating by parts we find

$$a_c(\mathrm{w}, \mathrm{w}) = |\mathrm{w}|_1^2 + \frac{1}{2}(\operatorname{div} \boldsymbol{\alpha}, \mathrm{w}^2) - \frac{1}{2}\langle \boldsymbol{\alpha} \cdot \mathbf{n}, \mathrm{w}^2 \rangle_\Gamma \quad \text{for all } \mathrm{w} \in H^1(\Omega).$$

Thus, holding

$$\operatorname{div} \boldsymbol{\alpha} \geq 0 \quad \text{in } \Omega, \tag{3.29a}$$

$$\boldsymbol{\alpha} \cdot \mathbf{n} \leq 0 \quad \text{on } \partial\Omega \tag{3.29b}$$

guarantees coercivity on V_0 [21]. In that case Lax-Milgram theorem proves the unique solvability of the problem (3.28).

Conditions (3.29) are satisfied for $\boldsymbol{\alpha} \equiv 0$ on $\overline{\Omega}$. That leads us to the Neumann problem for the Poisson equation. One can also specify a class of nonzero functions, satisfying (3.29). Integrating both terms over the domain and the boundary, respectively, we obtain

$$\int_\Omega \operatorname{div} \boldsymbol{\alpha} \, dx \geq 0,$$

$$\int_{\partial\Omega} \boldsymbol{\alpha} \cdot \mathbf{n} \, d\gamma \leq 0.$$

Applying the Gauss theorem we conclude

$$\int_\Omega \operatorname{div} \boldsymbol{\alpha} \, dx = \int_{\partial\Omega} \boldsymbol{\alpha} \cdot \mathbf{n} \, d\gamma = 0.$$

Together with conditions (3.29) and under certain regularity assumptions on $\boldsymbol{\alpha}$ it is equivalent to

$$\operatorname{div} \boldsymbol{\alpha} = 0 \quad \text{in } \Omega,$$

$$\boldsymbol{\alpha} \cdot \mathbf{n} = 0 \quad \text{on } \partial\Omega.$$

Here the conditions can be understood either pointwise or almost everywhere. This means that velocity part of any solution of the Stokes problem with, for example, homogeneous Dirichlet or slip boundary conditions is a class of functions satisfying (3.29) and, therefore, guaranteeing the coercivity of the bilinear form $a_c(\cdot,\cdot)$ on V_0.

Remark 3.3.1. *One can show that for* $\boldsymbol{\alpha}$ *defined by* (3.24) *statement* (3.29a) *holds, while* (3.29b) *does not. Indeed, taking into account the boundary conditions for the Navier-Stokes equation* (3.13) *and* (3.15)*, and using exact representation for* h_s (2.27) *one can get the following*

$$\operatorname{div}\boldsymbol{\alpha} = \operatorname{div}\left(\xi L(\xi h_s)\nabla h_s + \ \mathrm{Pe}\ \mathbf{v}\right) = \xi\frac{\partial L(\xi h_s)}{\partial h_s}(\nabla h_s)^2 + \xi L(\xi h_s)\Delta h_s.$$

Since the Langevin function $L(\cdot)$ *is monotonically increasing, its derivative is positive. A direct computation for* $h_s(x,y) = \sin\beta\left[\left((x^2+y^2)\cos^2\beta+1\right)^2 - 4x^2\cos^2\beta\right]^{-1/4}$ *given by* (2.27) *shows that* $\Delta h_s \geq 0$ *for* $\beta \in [0,\pi/2]$*. It provides* $\operatorname{div}\boldsymbol{\alpha} \geq 0$*, and moreover, for* $\beta \in (0,\pi/2)$ *it holds* $\operatorname{div}\boldsymbol{\alpha} > 0$ *in* Ω*. Gauss's theorem then implies* $\int_{\partial\Omega}\boldsymbol{\alpha}\cdot\mathbf{n}\,d\gamma > 0$ *which shows that* (3.29b) *cannot be satisfied. However, let us have a closer look at the statement* (3.29b)

$$\boldsymbol{\alpha}\cdot\mathbf{n} = \left(\xi L(\xi h_s)\nabla h_s + \ \mathrm{Pe}\ \mathbf{v}\right)\cdot\mathbf{n} = \xi L(\xi h_s)\nabla h_s\cdot\mathbf{n}.$$

Taking into account that h_s *decreases while moving away from the magnet, we conclude that* ∇h_s *is directed toward it. That is why the statement* (3.29b) *can only be satisfied if magnetic field source is placed inside the domain* Ω*. But that comes into contradiction with the basics of the mathematical model. Hence* $\boldsymbol{\alpha}\cdot\mathbf{n}$ *has no certain sign.*

The question of existence and uniqueness of a solution of the general convective-diffusive type problem (3.26) was investigated in [12]. There the problem was studied as a special case of a one parameter family

Find $c \in H^1(\Omega)$ such that

$$a_\gamma(c,\mathrm{w}) := a_c(c,\mathrm{w}) + \gamma(c,\mathrm{w}) = \langle f,\mathrm{w}\rangle \quad \text{for all } \mathrm{w}\in H^1(\Omega). \tag{3.30}$$

The problem (3.26) is then considered as a special case of (3.30) with $\gamma = 0$. The bilinear form a_γ appears to be coercive on $H^1(\Omega)$. Indeed, using the Hölder's inequality we can estimate

$$\begin{aligned} a_\gamma(\mathrm{w},\mathrm{w}) &\geq |\mathrm{w}|_1^2 - \|\boldsymbol{\alpha}\|_{0,\infty}\|\mathrm{w}\|_0|\mathrm{w}|_1 + \gamma\|\mathrm{w}\|_0^2 \\ &\geq \frac{1}{2}|\mathrm{w}|_1^2 + \left(\gamma - \frac{\|\boldsymbol{\alpha}\|_\infty^2}{2}\|\mathrm{w}\|\right)\|\mathrm{w}\|_0^2. \end{aligned} \tag{3.31}$$

From this one can conclude that a_γ is coercive on $H^1(\Omega)$ having $\boldsymbol{\alpha}\in L^\infty$ and γ sufficiently large. A more detailed analysis shows that the regularity assumption on $\boldsymbol{\alpha}$ can be relaxed to $\boldsymbol{\alpha}\in L^p$, $p>2$ [12].

Summarizing the mentioned above we obtain the following statements

- If $\boldsymbol{\alpha}$ satisfies conditions (3.29), i.e. $\operatorname{div}\boldsymbol{\alpha} \geq 0$ and $\boldsymbol{\alpha}\cdot\mathbf{n} \leq 0$, the bilinear form $a_c(\cdot,\cdot)$ is coercive on $V_0 = H^1(\Omega) \cap L^2_0(\Omega)$, the bilinear form $a_\gamma(\cdot,\cdot)$ is coercive on $H^1(\Omega)$ for $\gamma \in \mathbb{R}^+$.
- Solutions of the Stokes problem with homogeneous Dirichlet or slip boundary conditions provide a wide class of $\boldsymbol{\alpha}$ satisfying (3.29).
- The bilinear form $a_\gamma(\cdot,\cdot)$ is coercive on $H^1(\Omega)$ for the choice of γ being sufficiently large and $\boldsymbol{\alpha} \in L^p$, $p > 2$.

The general result for solvability of the problems (3.26) and (3.30) is proven in [12] and can be given in a single theorem

Theorem 3.3.2 (simplification of Theorem 1.1 [12])**.** *Let $\Omega \subset \mathbb{R}^2$ be a domain with a Lipschitz-continuous boundary and $\boldsymbol{\alpha} \in L^p(\Omega)$, $p > 2$ then it holds*

(i) The problem (3.30) *is uniquely solvable for any $\gamma > 0$ for all $f \in H^{-1}(\Omega)$.*

(ii) The problem (3.26) *has a solution if and only if $\langle f, 1\rangle = 0$.*

(iii) In case $f = 0$ problem (3.26) *has a solution $\widehat{c}$ unique up to a multiplicative constant, such that $\widehat{c} > 0$.*

(iv) If $\langle f, 1\rangle = 0$ problem (3.26) *has a unique solution $c^* \in V_0$. Set of all solutions of the problem* (3.26) *can be written as $c^* + \mathbb{R}\widehat{c} \in H^1(\Omega)$.*

The detailed proof of it can be found in [12].

Chapter 4

Discretization

In this section we continue the study of the mathematical model (2.75), (2.76). We present the discretization of the continuous problems studied in previous chapter. As it was mentioned before, we solve each equation separately. The coupling strategy will be introduced at the end of the chapter.

However we want to mention one important moment. The Young-Laplace equation determines the force balance on the free surface, so it is given only on the boundary. The Navier-Stokes and convection-diffusion equations are discretized by the finite element and finite volume methods on the whole domain. The Laplace equation for azimuthal velocity is coupled with the Young-Laplace equation, and azimuthal velocity appears on the right-hand side of the Navier-Stokes equation. Since Laplace equation is standard and the simplest one in our system, we decided to use for it different numerical methods to better fit each specific case. Namely, the boundary element discretization for better coupling with the Young-Laplace equation and finite element discretization for easier incorporation into Navier-Stokes equation.

We discretize the domain with admissible and shape-regular triangulation $\mathcal{T}_h$ of Ω [8]. The discrete polygonal domain $\Omega_h = \bigcup_{T \in \mathcal{T}_h} T$ is chosen such that all vertices on $\partial\Omega_h$ lie on $\partial\Omega$. The decomposition $\partial\Omega = \Gamma_s \cup \Gamma_c \cup \Gamma_f$ implies the decomposition of the discrete boundary $\partial\Omega_h = \Gamma_{s,h} \cup \Gamma_{c,h} \cup \Gamma_{f,h}$.

4.1 Laplace equation for azimuthal velocity

We discuss here two possible discretizations of the mixed boundary value problem for the Laplace equation (3.1) with boundary conditions (3.2)

$$\begin{aligned} \Delta\omega &= 0 \quad && \text{in } \Omega, \\ \omega &= 0 \quad && \text{on } \Gamma_c, \\ \omega &= 1 \quad && \text{on } \Gamma_s, \\ \frac{\partial\omega}{\partial\mathbf{n}} &= 0 \quad && \text{on } \Gamma_f, \end{aligned} \tag{4.1}$$

where $\mathbf{n}$ is a unit outer normal to Γ.

The finite elements for the Poisson equation are quite standard, so we present here only the general points. The weak formulation of the problem (4.1) is given by (3.3)

Find $\omega \in W$ such that

$$a_\omega(\omega, \mathrm{w}) = 0 \quad \forall \mathrm{w} \in W_0 \tag{4.2}$$

with spaces given by

$$\begin{aligned} W &:= \{\mathrm{w} \in H^1(\Omega) \mid \mathrm{w} = 0 \text{ on } \Gamma_c,\ \mathrm{w} = 1 \text{ on } \Gamma_s\}, \\ W_0 &:= \{\mathrm{w} \in H^1(\Omega) \mid \mathrm{w} = 0 \text{ on } \Gamma_c \cup \Gamma_s\}. \end{aligned}$$

We discretize the variational problem (4.2) with standard Galerkin $\mathcal{P}^2$ conforming finite elements. We define the discrete space by

$$W_h := \{\mathrm{w}_h \in C^0(\Omega_h) \,:\, \mathrm{w}\big|_T \in \mathcal{P}^2(T),\ \text{for all } T \in \mathcal{T}_h,\ \mathrm{w}_h = 1 \text{ on } \Gamma_s,\ \mathrm{w}_h = 0 \text{ on } \Gamma_c\} \subset W.$$
$$W_{h0} := \{\mathrm{w}_h \in C^0(\Omega_h) \,:\, \mathrm{w}\big|_T \in \mathcal{P}^2(T),\ \text{for all } T \in \mathcal{T}_h,\ \mathrm{w}_h = 0 \text{ on } \Gamma_s \cup \Gamma_c\} \subset W_0.$$

Then the nonhomogeneous discrete problem can be written as follows

Find $\omega_h \in W_h$ such that

$$a(\omega_h, \mathrm{w}_h) := (\nabla\omega_h, \nabla\mathrm{w}_h) = 0 \quad \forall \mathrm{w}_h \in W_{h0}. \tag{4.3}$$

Like for the continuous problem we apply the inverse trace theorem in order to switch to the problem with homogeneous boundary conditions. The conforming finite element space $W_{h0} \subset W_0(\Omega)$ provides the coercivity of $a(\cdot,\cdot)$ on W_{h0}. Then the Lax-Milgram theorem can be applied, which guaranties the unique solvability of the discrete problem (4.3).

The boundary element discretization of the boundary integral equations (3.11)

$$\begin{aligned} \int_{\Gamma_D} u^*\, q\, d\gamma - \int_{\Gamma_N} u\, q^*\, d\gamma &= \pi\overline{u}(\xi^0) + \int_{\Gamma_D} \overline{u}\, q^*\, d\gamma - \int_{\Gamma_N} u^*\, \overline{q}\, d\gamma \quad \xi^0 \in \Gamma_D, \\ \int_{\Gamma_D} u^*\, q\, d\gamma - \int_{\Gamma_N} u\, q^*\, d\gamma - \pi u(\xi^0) &= \int_{\Gamma_D} \overline{u}\, q^*\, d\gamma - \int_{\Gamma_N} u^*\, \overline{q}\, d\gamma \quad \xi^0 \in \Gamma_N. \end{aligned}$$

is observed in more details. We recall useful notation from the continuous case (3.8), (3.9), (3.10). Namely, the boundary decomposition

$$\Gamma_D = \Gamma_s \cup \Gamma_c, \quad \Gamma_N = \Gamma_f,$$

functions

$$q := \frac{\partial u}{\partial \mathbf{n}}, \quad q^* := \frac{\partial u^*}{\partial \mathbf{n}}$$

and boundary conditions

$$u = \overline{u} \text{ on } \Gamma_D,$$
$$q = \overline{q} \text{ on } \Gamma_N.$$

Function u^* is a fundamental solution of the Laplace equation given by (3.5). We introduce a sequence of boundary points

$$\Xi := \{\xi_j = (x_j, y_j)\}_{j=1}^N \tag{4.4}$$

and two index sets

$$I_D = \{j \ : \ (x_j, y_j) \in \Gamma_D\}, \quad I_N = \{j \ : \ (x_j, y_j) \in \Gamma_N\}.$$

The sequence Ξ generates the discrete boundary

$$\widehat{\Gamma}_h := \cup \tau_i, \quad j = 1, \cdots, N,$$

where τ_i are the boundary parts, which are also called boundary elements, with grid points (x_{j-1}, y_{j-1}), (x_j, y_j) being their end points.

We choose piecewise constant boundary elements, which means each τ_i is a line segment and the discrete solution is sought in the following form

$$(u_h, q_h) \in S_h^0(\widehat{\Gamma}_{h,N}) \times S_h^0(\widehat{\Gamma}_{h,D}),$$

where $S_h^0(\widehat{\Gamma}_h) := \text{span } \{\varphi_i^0\}_{j=1}^N$ with

$$\varphi_k^0(\xi) = \begin{cases} 1 & \text{for } \xi \in \tau_i, \\ 0 & \text{otherwise.} \end{cases}$$

We introduce in addition

$$\Delta x_j = x_j - x_{j-1}, \quad \Delta y_j = y_j - y_{j-1}.$$

The length of j-th boundary element is given by

$$l_j = \sqrt{{\Delta x_j}^2 + {\Delta y_j}^2}, \quad j = 1, \cdots, N.$$

The parameter s is related to the length of $\widehat{\Gamma}_h$ so

$$s_j = \sum_{i=1}^{j} l_i, \quad |\widehat{\Gamma}_h| = s_N.$$

The nodal point on each boundary element τ_i is chosen as the center of this element, it can be defined by $\xi_{i-\frac{1}{2}}$. Now we can write the parametric representation of the boundary

$$\begin{cases} x(s) = (s - s_{j-\frac{1}{2}})x'_j + x_{j-\frac{1}{2}}, \\ y(s) = (s - s_{j-\frac{1}{2}})y'_j + y_{j-\frac{1}{2}}, \end{cases} \tag{4.5}$$
$$s_{j-1} \le s \le s_j, \quad j = 1, \cdots, N,$$

where $s_{j-\frac{1}{2}} = s_j - \frac{l_j}{2} = s_{j-1} + \frac{l_j}{2}$, $x'_j = \frac{\Delta x_j}{l_j}$, $y'_j = \frac{\Delta y_j}{l_j}$.

Taking $\xi^0 = \xi_{i-\frac{1}{2}} \in \widehat{\Gamma}_h$, $i \in \{1, \cdots, N\}$ we can write the system of N linear equations

$$\begin{cases} \displaystyle\sum_{\tau_j \subset \widehat{\Gamma}_{h,D}} \int_{s_{j-1}}^{s_j} u^*\, q_h\, ds - \sum_{\tau_j \subset \widehat{\Gamma}_{h,N}} \int_{s_{j-1}}^{s_j} u_h\, q^*\, ds \\ \quad = \pi \overline{u}(\xi_{i-\frac{1}{2}}) + \displaystyle\sum_{\tau_j \subset \widehat{\Gamma}_{h,D}} \int_{s_{j-1}}^{s_j} \overline{u}\, q^*\, ds - \sum_{\tau_j \subset \widehat{\Gamma}_{h,N}} \int_{s_{j-1}}^{s_j} u^*\, \overline{q}\, ds, & i \in I_D, \\ -\pi u_h(\xi_{i-\frac{1}{2}}) + \displaystyle\sum_{\tau_j \subset \widehat{\Gamma}_{h,D}} \int_{s_{j-1}}^{s_j} u^*\, q_h\, ds - \sum_{\tau_j \subset \widehat{\Gamma}_{h,N}} \int_{s_{j-1}}^{s_j} u_h\, q^*\, ds \\ \quad = \displaystyle\sum_{\tau_j \subset \widehat{\Gamma}_{h,D}} \int_{s_{j-1}}^{s_j} \overline{u}\, q^*\, ds - \sum_{\tau_j \subset \widehat{\Gamma}_{h,N}} \int_{s_{j-1}}^{s_j} u^*\, \overline{q}\, ds, & i \in I_N. \end{cases}$$

Further we assume that on every boundary element τ_j boundary value functions $\overline{u}, \overline{q}$ are constants. We introduce the coefficients v_i of the decomposition such that

$$u_h = \sum_{j \in I_N} v_j \varphi_j^0, \quad q_h = \sum_{j \in I_D} v_j \varphi_j^0.$$

The discrete problem can be written as a system of linear equations

$$\begin{cases} \displaystyle\sum_{\tau_j \subset \widehat{\Gamma}_{h,D}} v_j \int_{s_{j-1}}^{s_j} u^*\, ds - \sum_{\tau_j \subset \widehat{\Gamma}_{h,N}} v_j \int_{s_{j-1}}^{s_j} q^*\, ds = \pi \overline{u}_{i-\frac{1}{2}} \\ \quad + \displaystyle\sum_{\tau_j \subset \widehat{\Gamma}_{h,D}} \overline{u}_{j-\frac{1}{2}} \int_{s_{j-1}}^{s_j} q^*\, ds - \sum_{\tau_j \subset \widehat{\Gamma}_{h,N}} \overline{q}_{j-\frac{1}{2}} \int_{s_{j-1}}^{s_j} u^*\, ds, & i \in I_D, \\ -\pi v_i + \displaystyle\sum_{\tau_j \subset \widehat{\Gamma}_{h,D}} v_j \int_{s_{j-1}}^{s_j} u^*\, ds - \sum_{\tau_j \subset \widehat{\Gamma}_{h,N}} v_j \int_{s_{j-1}}^{s_j} q^*\, ds \\ \quad = \displaystyle\sum_{\tau_j \subset \widehat{\Gamma}_{h,D}} \overline{u}_{j-\frac{1}{2}} \int_{s_{j-1}}^{s_j} q^*\, ds - \sum_{\tau_j \subset \widehat{\Gamma}_{h,N}} \overline{q}_{j-\frac{1}{2}} \int_{s_{j-1}}^{s_j} u^*\, ds, & i \in I_N. \end{cases} \tag{4.6}$$

For more compact view we introduce

$$a_{ij} = \int_{s_{j-1}}^{s_j} u^*(\xi_{i-\frac{1}{2}}, \xi(s))\, ds, \quad b_{ij} = \int_{s_{j-1}}^{s_j} q^*(\xi_{i-\frac{1}{2}}, \xi(s))\, ds.$$

So finally system (4.6) looks like

$$\begin{cases} \sum\limits_{\tau_j \subset \widehat{\Gamma}_{h,D}} a_{ij} v_j - \sum\limits_{\tau_j \subset \widehat{\Gamma}_{h,N}} b_{ij} v_j = \pi \overline{u}_{i-\frac{1}{2}} \\ \qquad\qquad + \sum\limits_{\tau_j \subset \widehat{\Gamma}_{h,D}} \overline{u}_{j-\frac{1}{2}} b_{ij} - \sum\limits_{\tau_j \subset \widehat{\Gamma}_{h,N}} \overline{q}_{j-\frac{1}{2}} a_{ij}, \quad i \in I_D, \\ \sum\limits_{\tau_j \subset \widehat{\Gamma}_{h,D}} a_{ij} v_j - \sum\limits_{\tau_j \subset \widehat{\Gamma}_{h,N}} \left(b_{ij} + \pi \delta_{ij}\right) v_j \\ \qquad\qquad = \sum\limits_{\tau_j \subset \widehat{\Gamma}_{h,D}} \overline{u}_{j-\frac{1}{2}} b_{ij} - \sum\limits_{\tau_j \subset \widehat{\Gamma}_{h,N}} \overline{q}_{j-\frac{1}{2}} a_{ij}, \quad i \in I_N, \end{cases} \tag{4.7}$$

where δ_{ij} is the Kronecker delta.

To simplify the integrals a_{ij} and b_{ij} we write u^* and q^* as functions of parameter s and represent $\rho(\xi^0, \xi(s))$ in parametric coordinates $x(s)$, $y(s)$ on interval $s \in [s_{j-1}, s_j]$. Using the fact that $\left(x'_j\right)^2 + \left(y'_j\right)^2 = 1$ by the definition (4.5) we obtain

$$\begin{aligned} &\rho^2(\xi^0, \xi(s)) = \left(x^0 - x(s)\right)^2 + \left(y^0 - y(s)\right)^2 \\ &= \left(x^0 - x_{j-\frac{1}{2}} + (s_{j-\frac{1}{2}} - s) x'_j\right)^2 + \left(y^0 - y_{j-\frac{1}{2}} + (s_{j-\frac{1}{2}} - s) y'_j\right)^2 \\ &= \left(s_{j-\frac{1}{2}} - s\right)^2 + \left(y^0 - y_{j-\frac{1}{2}}\right)^2 + \left(x^0 - x_{j-\frac{1}{2}}\right)^2 \\ &\quad + 2\left(s_{j-\frac{1}{2}} - s\right)\left[x'_j\left(x^0 - x_{j-\frac{1}{2}}\right)) + y'_j\left(y^0 - y_{j-\frac{1}{2}}\right)\right] \\ &= \left((s_{j-\frac{1}{2}} - s) + \left[x'_j\left(x^0 - x_{j-\frac{1}{2}}\right) + y'_j\left(y^0 - y_{j-\frac{1}{2}}\right)\right]\right)^2 \\ &\quad - \left[x'_j\left(x^0 - x_{j-\frac{1}{2}}\right) + y'_j\left(y^0 - y_{j-\frac{1}{2}}\right)\right]^2 \\ &\quad + \left(y^0 - y_{j-\frac{1}{2}}\right)^2 + \left(x^0 - x_{j-\frac{1}{2}}\right)^2 \\ &= \left(s - s_{j-\frac{1}{2}} - \left[x'_j\left(x^0 - x_{j-\frac{1}{2}}\right) + y'_j\left(y^0 - y_{j-\frac{1}{2}}\right)\right]\right)^2 \\ &\quad + \left(y'_j\left(x^0 - x_{j-\frac{1}{2}}\right)\right)^2 + \left(x'_j\left(y^0 - y_{j-\frac{1}{2}}\right)\right)^2 \\ &\quad - 2x'_j y'_j\left(x^0 - x_{j-\frac{1}{2}}\right)\left(y^0 - y_{j-\frac{1}{2}}\right) \\ &= \left(s - s_{j-\frac{1}{2}} - \left[x'_j\left(x^0 - x_{j-\frac{1}{2}}\right) + y'_j\left(y^0 - y_{j-\frac{1}{2}}\right)\right]\right)^2 \\ &\quad + \left(y'_j\left(x^0 - x_{j-\frac{1}{2}}\right) - x'_j\left(y^0 - y_{j-\frac{1}{2}}\right)\right)^2. \end{aligned}$$

In case $\xi^0 = \xi_{i-\frac{1}{2}}$ we can write it in a short form

$$\rho^2(\xi_{i-\frac{1}{2}}, \xi(s)) = \left(s - s_{j-\frac{1}{2}} - c_{ij}\right)^2 + {d_{ij}}^2 \tag{4.8}$$

with

$$\begin{aligned} c_{ij} &= x'_j \left(x_{i-\frac{1}{2}} - x_{j-\frac{1}{2}} \right) + y'_j \left(y_{i-\frac{1}{2}} - y_{j-\frac{1}{2}} \right), \\ d_{ij} &= y'_j \left(x_{i-\frac{1}{2}} - x_{j-\frac{1}{2}} \right) - x'_j \left(y_{i-\frac{1}{2}} - y_{j-\frac{1}{2}} \right). \end{aligned} \tag{4.9}$$

Integrals in coefficients a_{ij} and b_{ij} are evaluated analytically. Before calculating b_{ij} let us simplify the integrand

$$\frac{\partial u^*}{\partial \mathbf{n}}(\xi_{i-\frac{1}{2}}, \xi(s)) = \cos(\widehat{x(s), n_j}) \frac{x_{i-\frac{1}{2}} - x(s)}{\rho^2 \left(\xi_{i-\frac{1}{2}}, \xi(s) \right)} + \cos(\widehat{y(s), n_j}) \frac{y_{i-\frac{1}{2}} - y(s)}{\rho^2 \left(\xi_{i-\frac{1}{2}}, \xi(s) \right)}. \tag{4.10}$$

Choosing the direction of the circuit counterclockwise the outer normal determined by the derivatives of x and y is given by $n_j = \left(y'_j, -x'_j \right)^T$. Cosine of an angle between the x and n_j is

$$\cos(\widehat{x(s), n_j}) = \cos\left(\widehat{\begin{pmatrix} x'_j \\ 0 \end{pmatrix}, \begin{pmatrix} y'_j \\ -x'_j \end{pmatrix}} \right) = \frac{x'_j y'_j}{x'_j \sqrt{\left(x'_j \right)^2 + \left(y'_j \right)^2}} = y'_j. \tag{4.11}$$

In the same way we can get $\cos(\widehat{y(s), n_j}) = -x'_j$. Substituting this values to (4.10) we obtain

$$\begin{aligned} \frac{\partial u^*}{\partial \mathbf{n}}(\xi_{i-\frac{1}{2}}, \xi(s)) =& \frac{y'_j \left(x_{i-\frac{1}{2}} - x(s) \right) - x'_j \left(y_{i-\frac{1}{2}} - y(s) \right)}{\rho^2 \left(\xi_{i-\frac{1}{2}} \xi(s) \right)} \\ =& \frac{y'_j \left(x_{i-\frac{1}{2}} - x_{j-\frac{1}{2}} - (s - s_{j-\frac{1}{2}}) x'_j \right)}{\rho^2 \left(\xi_{i-\frac{1}{2}}, \xi(s) \right)} \\ & - \frac{x'_j \left(y_{i-\frac{1}{2}} - y_{j-\frac{1}{2}} - (s - s_{j-\frac{1}{2}}) y'_j \right)}{\rho^2 \left(\xi_{i-\frac{1}{2}}, \xi(s) \right)} \\ =& \frac{d_{ij}}{\rho^2 \left(\xi_{i-\frac{1}{2}}, \xi(s) \right)}, \quad s \in [s_{j-1}, s_j]. \end{aligned} \tag{4.12}$$

Using (4.12) as integrand in b_{ij} we end up with

$$\begin{aligned} b_{ij} &= \int_{s_{j-1}}^{s_j} q^*(\xi_{i-\frac{1}{2}}, \xi(s))\, ds = d_{ij} \int_{s_{j-1}}^{s_j} \frac{ds}{\rho^2 \left(\xi_{i-\frac{1}{2}}, \xi(s) \right)} \\ &= d_{ij} \int_{s_{j-1}}^{s_j} \frac{ds}{\left(s - s_{j-\frac{1}{2}} - c_{ij} \right)^2 + {d_{ij}}^2} = \arctan\left(\frac{s - s_{j-\frac{1}{2}} - c_{ij}}{d_{ij}} \right) \Bigg|_{s_{j-1}}^{s_j} \\ &= \arctan\left(\frac{\frac{l_j}{2} - c_{ij}}{d_{ij}} \right) + \arctan\left(\frac{\frac{l_j}{2} + c_{ij}}{d_{ij}} \right). \end{aligned} \tag{4.13}$$

Coefficients a_{ij} can be evaluated straightly

$$\begin{aligned} a_{ij} &= \int_{s_{j-1}}^{s_j} u^*(\xi_{i-\frac{1}{2}}, \xi(s))\, ds = -\frac{1}{2}\int_{s_{j-1}}^{s_j} \ln\Big(\rho(\xi_{i-\frac{1}{2}}, \xi(s))\Big)\, ds \\ &= -\frac{1}{2}\int_{s_{j-1}}^{s_j} \ln\left(\left(s - s_{j-\frac{1}{2}} - c_{ij}\right)^2 + {d_{ij}}^2\right) ds \\ &= -\frac{1}{2}\left(s - s_{j-\frac{1}{2}} - c_{ij}\right)\ln\left(\left(s - s_{j-\frac{1}{2}} - c_{ij}\right)^2 + {d_{ij}}^2\right)\Big|_{s_{j-1}}^{s_j} \\ &\quad + s|_{s_{j-1}}^{s_j} - d_{ij}\arctan\left(\frac{s - s_{j-\frac{1}{2}} - c_{ij}}{d_{ij}}\right)\Big|_{s_{j-1}}^{s_j} \\ &= -\frac{1}{2}\left(\frac{l_j}{2} - c_{ij}\right)\ln\left(\left(\frac{l_j}{2} - c_{ij}\right)^2 + {d_{ij}}^2\right) \\ &\quad - \frac{1}{2}\left(\frac{l_j}{2} + c_{ij}\right)\ln\left(\left(\frac{l_j}{2} + c_{ij}\right)^2 + {d_{ij}}^2\right) + l_j - d_{ij}b_{ij}. \end{aligned} \tag{4.14}$$

The numerical solution of the problem (4.2) is given as a solution of the system (4.7) with coefficients specified by (4.13), (4.14).

4.2 Young-Laplace equation

Here we discuss the discretization of the Young-Laplace equation (2.75d)

$$\begin{gathered} cL(\xi h_s)h_s\Big|_{(x(s^*),y_i(s^*))} + \int_0^{s^*}\Big[\mathrm{Fr}_m x'\omega_i^2 - \frac{\partial(cL(\xi h_s))}{\partial s}h_s\Big]ds = cL(\xi h_s)h_s\Big|_{(0,y_i(0))}, \\ s^* \in [0, l_i] \quad i = 1, 2, \\ \mathrm{Pm} = \int_{y_1(0)}^{y_2(0)} cL(\xi h_s)\frac{\partial h}{\partial y}\, dy, \qquad U(y_1(0), y_2(0)) = U_0, \end{gathered} \tag{4.15}$$

One can see that the main equation is a nonlinear integro-differential equation with respect to y. We propose the solution technique which was used for a simpler equation in [31]. It uses the fact that function h_s (2.27) is invertible as function of y. This allows us to write integrals in (4.15) as follows

$$\int_0^{s^*} \mathrm{Fr}_m x'\omega_i^2 ds = \int_0^{x(s^*)} \mathrm{Fr}_m \omega_i^2 dx,$$

$$\int_0^{s^*} \frac{\partial(cL(\xi h_s))}{\partial s}h_s ds = \int_0^{x(s^*)} \frac{\partial(cL(\xi h_s))}{\partial x}h_s dx + \int_{y(0)}^{y(s^*)} \frac{\partial(cL(\xi h_s))}{\partial y}h_s dy.$$

One should note that integrals on the right hand side remain curve integrals with respect to s. We introduce new parametrization for more simple discretization.

We recall the expression of the magnetic field intensity (2.27)

$$h_s(x,y) = \frac{\sin\beta}{\left[\left((x^2+y^2)\cos^2\beta+1\right)^2 - 4x^2\cos^2\beta\right]^{1/4}}.$$

Then for equation

$$h(x,y) = \Phi(x)$$

we invert $h(x,y)$ with respect to y and obtain

$$\begin{aligned} y(x) &= \pm g(x,\Phi(x)), \text{ where} \\ g(x,\Phi(x)) &:= \sqrt{\sqrt{\frac{\tan^4\beta}{\Phi^4(x)} + \frac{4x^2}{\cos^2\beta}} - \frac{1}{\cos^2\beta} - x^2}. \end{aligned} \tag{4.16}$$

The sign of y is chosen depending on the free surface part. Following further the ideas of [31] we introduce parametrization of a curve with respect to x instead of arc length s. It is possible if we assume that functions $x_i(s)$ corresponding to $r_i(s)$ in (2.59) are bijective. Then we are able to change the integration variable in (2.66) from $s \in [0, l_i]$ to $x_i \in [0, x_i(l_i)]$ or $y_i \in [0, y_i(l_i)]$. For further simplicity we also define

$$\zeta_i := x_i(l_i). \tag{4.17}$$

Moreover, functions y_i can be understood as functions of x, i.e. we redefine $y_i(x) := y_i(x_i^{-1}(x)) = y_i(s)$, $i = 1, 2$.

At this point we assume that each part of free surface preserves the sign, i.e. y_i can be either non-negative or non-positive. So, assuming that $i = 1$ corresponds to the upper part, we can write

$$y_i(x) = (-1)^{i+1} g(x, \Phi(x)).$$

For more details see the following remark.

Remark 4.2.1. *The question, whether functions y_i, $i = 1, 2$ are sign preserving is a complex task. It is enough to show that $y_i(x^*) \neq 0$ for any $x^* \in (0, 1]$. The interval $(0, 1]$ is enough due to the domain structure.*

Let us first consider simplified Young-Laplace equation as it was used in [31]. There it was derived for the case the magnetization is at saturation on free surface. That corresponds to the choice $cL(\xi h_s) \equiv 1$. Then the derivative $\frac{\partial cL(\xi h_s)}{\partial s}$ vanishes and the Young-Laplace equation (4.15) *is simplified to*

$$\begin{aligned} h_s(x^*, y_i(x^*)) &= \widehat{\Phi}_i(x^*), \quad i = 1, 2, \\ \widehat{\Phi}_i(x^*) &:= h_s(0, y_i(0)) - Fr_m \int_0^{x^*} \omega_i^2(x, y_i(x))dx, \\ Pm &= h(0, y_2(0)) - h(0, y_1(0)), \quad U(y_1(0), y_2(0)) = U_0. \end{aligned} \tag{4.18}$$

One can see that $\widehat{\Phi}_i(x)$ is a decreasing function of x. It means magnetic field strength h_s is also a decreasing function of x. Then we can use the fact that isolines of h_s are Cassini ovals [31], which proves that the free surface cannot cross x-axis on interval $(0, 1]$, i.e. $y_i(x, h_s)$ is sign preserving.

However, for problem (4.15) it is not possible to show in general that $\Phi_i(x)$ is a decreasing function. That is why we leave this question open.

The Young-Laplace equation (4.15) then can be written as follows

$$\begin{gathered} y_i(x^*) = (-1)^{i+1} g(x^*, \Phi_i(x^*)), \quad x^* \in [0, \zeta_i], \quad i = 1, 2, \\ \mathrm{Pm} = \int\limits_{y_1(0)}^{y_2(0)} cL(\xi h_s) \frac{\partial h}{\partial y}\, dy, \quad U(y_1(0), y_2(0)) = U_0 \end{gathered} \tag{4.19}$$

with $\Phi_i(\cdot)$ defined by

$$\begin{aligned} \Phi_i(x^*) := \frac{1}{cL(\xi h_s)}\Big|_{(x^*, y_i(x^*))} \Bigg[cL(\xi h_s) h_s \Big|_{(0, y_i(0))} - \mathrm{Fr}_m \int\limits_0^{x^*} (\omega_i)^2 dx \\ + \int\limits_0^{x^*} \frac{\partial (cL(\xi h_s))}{\partial x} h_s dx + \int\limits_{y_i(0)}^{y_i(x^*)} \frac{\partial (cL(\xi h_s))}{\partial y} h_s dy \Bigg]. \end{aligned} \tag{4.20}$$

At this point it is important to say some words about the solution process. We solve the pair of Laplace (2.75a) and Young-Laplace (2.75d) equations one by one repeatedly, until iterations converge. See Section 4.5 for more details. Each solution of the Young-Laplace equation generates new mesh Ξ (4.4). Therefore it generates a sequence of grids Ξ^j with index j corresponding to the iteration number. We split each grid Ξ^j into four subgrids with respect to boundary parts. We need further grids Ξ^j_s and $\Xi^j_{f,i}$ corresponding to boundary parts Γ_s and $\Gamma_{f,i}$, respectively. In addition we change the order of nodes for $\Xi^j_{f,i}$ as follows

$$\Xi^j_{f,i} := \{(x_k, y_k) \in \widehat{\Gamma}^j_{f,i,h} \,:\, x_0 = 0, \quad x_{n-1} < x_n \quad \forall n > 0\}_{k=0}^{k=N_{f,i}}, \quad i = 1, 2, \tag{4.21}$$

where j is the grid index for iterations of Laplace and Young-Laplace equations according to (4.72).

For given grids $\Xi^j_{f,i}$, $i = 1, 2$ and Ξ^j_s, and values of integrands in (4.19), (4.20) at quadrature points one can approximate integrals by the quadrature rule. Then we obtain the following relations for points y_i^{j+1} on a free surface

$$y_i^{j+1} = (-1)^{i+1} g(x^{j+1}, \Phi_i^j(x^j)), \quad (x^{j+1}, y_i^{j+1}) \in \Xi_i^{j+1}, \quad i = 1, 2, \tag{4.22}$$

where $\Phi_i^j(\cdot)$ is related to $\Phi_i(\cdot)$ in (4.20) with the following changes

$$\Phi_i^j(x^*) := \frac{1}{cL(\xi h_s)}\Big|_{(x^*,y_i^j(x^*))}\Bigg[cL(\xi h_s)h_s\Big|_{(0,y_i^j(0))} - \mathrm{Fr}_m\int\limits_0^{x^*}(\omega_i^j)^2dx + \int\limits_0^{x^*}\frac{\partial(cL(\xi h_s))}{\partial x}h_s dx + \int\limits_{y_i^j(0)}^{y_i^j(x^*)}\frac{\partial(cL(\xi h_s))}{\partial y}h_s dy\Bigg]. \tag{4.23}$$

The equation (4.22) gives a relation between coordinates x and y of point on a free surface $(x,y)\in\Xi_{f,i}^{j+1}$. In order to find y one should know x, that is why we introduce special grid for x. Let us denote the sequences of coordinate x

$$\Theta_i^j := \{x_k\in[0,\zeta_i^j]\ :\ x_0=0\}_{k=0}^{k=N_{f,i}},\quad i=1,2. \tag{4.24}$$

The point ζ_i^{j+1} can be found from equation (4.22) using the known shape of the concentrator described by (2.26)

$$y^2(\zeta)=\tan^2\beta(\zeta^2-1).$$

Substituting $y(\zeta)$ into (4.22) and extracting ζ we obtain

$$\zeta_i^{j+1}=\sqrt{\left(\frac{\sin\beta}{\Phi_i^j(\zeta_i^j)}\right)^2+\cos^2\beta},\quad i=1,2. \tag{4.25}$$

Grids Θ_i^j are constructed for two parts of free surface by an arbitrary known rule, e.g. uniformly, according to the arc length or depending on curvature [30]. Then for given $x_k\in\Theta_i^j$ one can solve equation (4.22) and find a pair $(x_k,y_k)\in\Xi_{f,i}^{j+1}$. Doing it sequentially we construct the whole new grid $\Xi_{f,i}^{j+1}$. The full discretization then reads as follows

Find new grids $\Xi_{f,i}^{j+1}$ from the old ones $\Xi_{f,i}^j$ from the following equations

$$\begin{gathered} y_{i,k}^{j+1}=(-1)^{i+1}g(x_k^{j+1},\Phi_i^j(x_k^j)),\quad x_k^{j+1}\in\Theta_i^{j+1},\quad i=1,2,\\ \mathrm{Pm}=\int\limits_{y_{1,0}^{j+1}}^{y_{2,0}^{j+1}}cL(\xi h_s)\frac{\partial h}{\partial y}\,dy,\quad U(y_{1,0}^{j+1},y_{2,0}^{j+1})=U_0. \end{gathered} \tag{4.26}$$

Here functions Φ_i^j are given by (4.23), grids Θ_i^{j+1}, $i=1,2$ are defined by (4.24). The integral in condition for the pressure drop is approximated by a quadrature rule.

Finally the discrete domain Ω^j can be constructed according to (2.77)

$$\begin{aligned}\Omega^j := \big\{(x,y)\in\mathbb{R}^2\ :\ x>0,\quad & y^2>(x^2-1)\tan^2\beta,\\ & y_1^j(x)<y\quad\text{for}\quad x\in(0,\zeta_1^j),\quad y<y_2^j(x)\quad\text{for}\quad x\in(0,\zeta_2^j)\big\}.\end{aligned} \tag{4.27}$$

The only difference is that $y_i^j(x)$ here is not a solution of the continuous problem (2.75d), but a linear or cubic spline interpolation of the pointwise given curve Θ_i^j, $i = 1, 2$.

The scheme (4.26) is used in case when the particle concentration is given. If it is not determined, we can use the simplified system (4.18).

4.3 Planar Navier-Stokes-type equation

We formulate the finite element discretization of the variational problem (3.17) in finite element spaces X_h and M_h for $\mathbf{u}$ and p, respectively.

Find a pair $(u_h, p_h) \in X_h \times M_h$ such that

$$\begin{aligned} a_h(u_h, w_h) + N_h(u_h, u_h, w_h) + b_h(p_h, w_h) &= \langle f, w_h \rangle \qquad \forall w_h \in X_h, \\ b_h(q_h, u_h) &= 0 \qquad \forall q_h \in M_h, \end{aligned} \tag{4.28}$$

where two bilinear and a trilinear forms are defined as follows

$$\begin{aligned} a_h(u_h, w_h) &:= \frac{2}{\mathrm{Re}} \int_{\Omega_h} \mathbb{D}(u_h) : \mathbb{D}(w_h)\, dx, \\ b_h(p_h, w_h) &:= -\int_{\Omega_h} p \ \mathrm{div}\ w_h\, dx, \\ N_h(u_h, \mathrm{v}_h, w_h) &:= \int_{\Omega_h} [(u_h \cdot \nabla)\mathrm{v}_h]\, w_h\, dx. \end{aligned} \tag{4.29}$$

The solvability of the problem (4.28) needs the same steps as for the continuous problem, i.e. the coercivity of the bilinear form $a_h(\cdot, \cdot)$ on X_h and fulfillment of the LBB-condition for the bilinear form $b_h(\cdot, \cdot)$ for the pair of spaces X_h, M_h. On the other hand the error estimates should be obtained. Both these parts are in strong matter dependent on the choice of the finite element spaces X_h and M_h as well as on the type of the boundary conditions and their implementation.

We refer for example to [18] for the detailed study of the discretization of Navier-Stokes equation with Dirichlet boundary conditions for different pairs of finite elements. However, there are much less information for analysis of problems with slip boundary conditions. We take as a basis the following related works. In [2, 44] the problem (4.28) with only slip boundary conditions was investigated. Both papers used the Taylor-Hood element on polygonal approximations Ω_h of Ω. In [44] the non-optimal error estimates of $O\left(h^{1/2}\right)$ was obtained in $H^1(\Omega)$ and $L^2(\Omega)$ norms for velocity and pressure, respectively. That error bound was improved in [2] to $O\left(h^{3/2}\right)$ in the same norms. These two approaches differ in the implementation of the boundary condition $\mathbf{v} \cdot \mathbf{n} = 0$ on $\partial\Omega$. In [44] it is implemented only for the vertices on the boundary Ω. It means that the middle points of edges lying on the discrete boundary $\partial\Omega_h$ were ignored. In [2] the concept of "exact triangulation" is used to implement a discrete version of $\mathbf{v} \cdot \mathbf{n} = 0$ on $\partial\Omega_h$. The technique similar to one

in [2] was used in [27] to obtain the error bound $O\left(h^{3/2}\right)$ for the isoparametric Taylor-Hood elements for the coupled problem including the Navier-Stokes equation with mixed Dirichlet and slip boundary conditions.

In order to have an optimal error estimate we use $\mathcal{P}^2/\mathcal{P}^1$ Taylor-Hood finite elements. So the finite element spaces X_h and M_h are defined as follows

$$\begin{aligned} X_h =&\{w_h \in \left(C^0(\Omega_h)\right)^2 \mid w_h\big|_T \in \mathcal{P}_2(T)^2,\ w_h(p)\cdot \mathbf{n}(G_h(p)) = 0 \quad \forall p \in \mathcal{N}_{h,f},\\ & w_h(p) = 0 \quad \forall p \in \mathcal{N}_{h,D}\},\\ M_h =&\{q_h \in C^0(\Omega_h) \mid q_h\big|_T \in \mathcal{P}_1(T), \quad \int_{\Omega_h} q_h = 0\}, \end{aligned} \tag{4.30}$$

where $\mathcal{N}_{h,f}$ and $\mathcal{N}_{h,D}$ are the sets of all vertices and midpoints lying on $\Gamma_{f,h}$ and $\Gamma_{s,h}\cup\Gamma_{c,h}$, respectively.

We cannot directly follow the proof of existence and uniqueness of a solution used for the continuous problem (3.17). In discrete case the boundary conditions are applied pointwise, which implies $\langle w_h, n_h\rangle_{\Gamma_h} \neq 0$. Hence, the inequality (3.20) cannot show the coercivity of $a_h(\cdot,\cdot)$ directly. The LBB-condition in discrete case is also a complex task and should be proven for a chosen pair of finite element spaces. Lemma 3.3 in [2] proves the coercivity of the bilinear form $a_h(\cdot,\cdot)$ and the LBB-condition for $b_h(\cdot,\cdot)$ for the discretization of the Navier-Stokes equation with slip boundary conditions by Taylor-Hood finite elements. Using our extension of Lemma 3.1 (see Lemma 4.3.1 below) one can derive the same for the problem (4.28). The mentioned results and standard theory [18] imply that the discrete problem (4.28) has a unique solution for $(\mathrm{Re})^2\|f\|_0$ being small enough.

The main points of the proof of the error estimate in [2] are as follows. The concept of "exact triangulation" was used in order to have better approximation on the boundary and also resolve the problem that (v,p) and (v_h,p_h) lie in different spaces. The "exact triangulation" provides a mapping G_h, which is a homeomorphism between $\widetilde{\Omega}_h$ to Ω. For detailed description of a construction of such triangulation and analysis of its approximation properties please refer to [7, 24].

We introduce in addition for any pair $(w_h, q_h) \in X_h \times M_h$ the following functions

$$(\overline{w}_h, \overline{q}_h) := \left(w_h \circ G_h^{-1}, q_h \circ G_h^{-1} - \frac{1}{|\Omega|}\int_\Omega q_h \circ G_h^{-1}\right) \in X \times M. \tag{4.31}$$

The desired error estimate looks as follows

$$\|v - \overline{v}_h\|_1 + \|p - \overline{p}_h\|_0 \leq C h^{\frac{3}{2}} \tag{4.32}$$

for (v,p) being a solution of the continuous problem (3.17) and (v_h,p_h) a solution of the discrete problem (4.28).

The following boundary estimate plays an important role in the proof of (4.32). It was proven in [2] only for the problem with slip boundary conditions and here we extend it for the case of mixed Dirichlet and slip boundary conditions.

Lemma 4.3.1 (Corollary of Lemma 3.1 [2]). *There exists $h_0 > 0$ s.t. for all $0 < h < h_0$ and all $\overline{w}_h \in X_h$*

$$\|\overline{w}_h \cdot \mathbf{n}\|_{0,\partial\Omega} \leq c h^{\frac{3}{2}} \|\overline{w}_h\|_1.$$

Proof. We split the boundary according to its decomposition and write

$$\|\overline{w}_h \cdot \mathbf{n}\|^2_{0,\partial\Omega} = \int_{\Gamma_c \cup \Gamma_s} |\overline{w}_h \cdot \mathbf{n}|^2 \, d\gamma + \int_{\Gamma_f} |\overline{w}_h|^2 \cdot \mathbf{n} \, d\gamma.$$

The boundary integral over $\Gamma_c \cup \Gamma_s$ vanishes due to the boundary conditions. In [2] the desired error estimate is proven for the case of slip boundary condition applied on the whole boundary. As the proof is given separately for each $\partial\Omega \cap T$, $T \in \mathcal{T}_h$, we can apply it for a part of the boundary Γ_f. Which implies the result of the lemma. ■

One of the difficult points of the proof of the error estimate is that the regularity properties of (u, p) are not satisfied for our domain Ω. In particular the following properties were used

$$\|u\|^2_3 + \|p\|^2_2 \leq C\|f\|^2_1,$$

which are satisfied for Ω in class C^4 [41]. This inequality was used in the proof of the error estimate (4.32). We then can assume sufficient regularity of u and p and bound their norms by some constants. One can also note that analysis in [2] does not use the quasi-uniform assumption on the triangulation, so does our extension. That allows us to apply the adaptive mesh refinement, if we need, without loss of approximation properties.

Now we want to give some implementation notes for our discretization. The problem (3.17) should be discretized in $X_h \times M_h$ defined by (4.30). This needs for all discrete functions $v_h \in X_h$ holding $v_h = 0$ on $\Gamma_{c,h} \cup \Gamma_{s,h}$ and $v_h(p) \cdot \mathbf{n}(G_h(p)) = 0$ for all $p \in \mathcal{N}_{h,f}$. These conditions provide certain difficulties in constructing the basis of X_h. It is easier at first to discretize the problem in a larger space and then satisfy the restrictions of X_h. Let us define

$$W_h := \{w_h \in \left(C^0(\Omega_h)\right)^2 \, : \, w_h\big|_T \in \mathcal{P}_2(T)^2\},$$

for which $X_h \subset W_h$ holds.

The basis of W_h is written as $\{\varphi_i\}_{i=1}^{2N_U}$ which is defined through one-dimensional basis $\{\phi_i\}_{i=1}^{N_U}$

$$\varphi_i = \begin{cases} \begin{pmatrix} \phi_i \\ 0 \end{pmatrix}, & i \in \{1, \ldots, N_U\}, \\ \\ \begin{pmatrix} 0 \\ \phi_{i-N_U} \end{pmatrix}, & i \in \{N_U + 1, \ldots, 2N_U\}. \end{cases} \tag{4.33}$$

The basis of M_h is given by $\{\psi_i\}_{i=1}^{N_P}$. Every discrete function $w_h \in W_h$ and $q_h \in M_h$ can

be decomposed into a sum of weighted basis functions

$$w_h = \sum_{i=1}^{2N_U} w_i \varphi_i, \tag{4.34}$$

$$q_h = \sum_{i=1}^{N_P} q_i \psi_i. \tag{4.35}$$

For every node of the mesh p_k there is only one basis function ϕ_l not vanishing in it, i.e. $\phi_l(p_k) = \delta_{lk}$ with δ_{lk} being the Kronecker symbol. So the value of w_h in p_k is determined by only two components of decomposition (4.34) $z_l\varphi_l$ and $z_{l+N_U}\varphi_{l+N_U}$.

Using representations (4.34), (4.35) for solution and test functions, the problem (4.28) can be discretized into a system of the following equations

$$\begin{aligned} a(\sum_{i=1}^{2N_U} u_i\varphi_i, \varphi_j) + N_h(\tilde{u}_h, \sum_{i=1}^{2N_U} u_i\varphi_i, \varphi_j) \\ +(\sum_{i=1}^{N_P} p_i\psi_i, \nabla\cdot\varphi_j) = (f_h, \varphi_j), \quad j = 1, \cdots, 2N_U, \end{aligned} \tag{4.36a}$$

$$(\psi_j, \sum_{i=1}^{2N_U} u_i \nabla\cdot\varphi_i) = 0, \qquad j = 1, \cdots, N_P, \tag{4.36b}$$

where $\tilde{u}_h$ is the known function involved to linearize the system. We use well known fixed-point iteration for solving the Navier-Stokes equation, so that on each iteration step it is approximated by a linear problem. It reads as follows

For a given initial step u^0 find a pair (u^{j+1}, p^{j+1}), $j > 0$ sequentially solving

$$\begin{aligned} a_h(u^{j+1}, w) + N_h(u^j, u^{j+1}, w) + b_h(p^{j+1}, w) = (f_h, w) \qquad \forall w \in X_h, \\ b(q, u^{j+1}) = 0 \qquad \forall q \in M_h. \end{aligned} \tag{4.37}$$

The iteration process stops, when (u^j, p^j) converges to some pair (u, p). On each iteration step the problem (4.37) is linear. For more details please refer to [43].

Further we consider the discretization of the linearized problem (4.36). We can apply the boundary conditions included into X_h to obtain the final discretization in $X_h \times M_h$. At first we impose the Dirichlet boundary conditions and fix the constant for pressure, applying

$$\begin{aligned} u_h(p) &= 0 \quad \text{for all } p \in \mathcal{N}_{h,D}, \\ p_h(p_i) &= 0 \quad \text{for a single } i \in \{1, \ldots, N_P\}. \end{aligned}$$

This overwrites the $|\mathcal{N}_{h,D}| + 1$ lines of the system.

The next step is to apply slip boundary conditions as the second restriction of X_h space. Let $p \in \mathcal{N}_{h,f}$ be a boundary node on $\Gamma_{f,h}$ corresponding to basis functions φ_l and φ_{l+N_U}. One has to satisfy in that point for u_h and v_h conditions like

$$w_h(p) \cdot \widetilde{\mathbf{n}}_h(p) = 0 \quad \text{for all } p \in \mathcal{N}_{h,f} \tag{4.38}$$

with

$$\widetilde{\mathbf{n}}_h(p) = \mathbf{n}(G_h(p)). \tag{4.39}$$

As we discussed before, this needs the construction of the "exact triangulation" operator, which is quite difficult to handle. However, in [3] the normal was chosen as a weighted average

$$\widetilde{\mathbf{n}}_h(p) = \frac{m_h(p)}{|m_h(p)|}, \quad m_h(p) := \sum_{\Gamma_i \in O_h \,:\, p \in \Gamma_i} |\Gamma_i| n_h^i, \tag{4.40}$$

where $O_h = \{T \cap \Gamma_h \,:\, T \in \mathcal{T}_h,\, T \cap \Gamma_{f,h} \neq \varnothing\}$ and n_h^i is a unit outer normal to Γ_i. It was shown that the choice of a normal according to (4.40) leads to the same convergence rate $O(h^{3/2})$ as for (4.39). Therefore, we use the simpler normal (4.40) in our implementation and ignore the construction of the "exact triangulation".

Using functions representation (4.34) and structure of the basis (4.33) we can apply the no penetration condition (4.38) to a solution and test function as follows. For the solution function it is applied simply as a linear combination

$$u_l n_{k,1} + u_{l+N_U} n_{k,2} = 0,$$

where $n_{k,i}$, $i = 1, 2$ denotes first and second component of the normal $\widetilde{\mathbf{n}}_h(p_k)$, u_l and u_{l+N_U} are the coefficients of u_h in representation (4.34). Formulating it with basis functions we come to

$$-n_{k,2}(u_l\varphi_l, \varphi_l) + n_{k,1}(u_{l+N_U}\varphi_{l+N_U}, \varphi_{l+N_U}) = 0. \tag{4.41}$$

Making the linear combination of equations number l and $l + N_U$ with coefficients $-n_{k,2}$ and $n_{k,1}$, respectively, and using linearity we obtain

$$a(\sum_{i=1}^{2N_U} u_i\varphi_i, \bar{\varphi}_l) + b(\sum_{i=1}^{2N_U} u_i\varphi_i, \tilde{u}_h, \bar{\varphi}_l) + (\sum_{i=1}^{N_P} p_i\psi_i, \nabla \cdot \bar{\varphi}_l) = (f_h, \bar{\varphi}_l) \tag{4.42}$$

with

$$\bar{\varphi}_l = -n_{k,2}\varphi_l + n_{k,1}\varphi_{l+N_U} = \begin{pmatrix} -n_{k,2} \\ n_{k,1} \end{pmatrix} \phi_l.$$

One can see that $\bar{\varphi}_l \cdot n_k = 0$. It means that this manipulation gives us the basis function satisfying no penetration condition (4.38).

Finally, we replace equations (4.36a) with numbers $j = l$ and $j = l + N_U$ by equations (4.41) and (4.42). Repeating these steps for all $p_k \in \Gamma_{f,i}$ we write a problem for modified functions $\widetilde{u}_h$, $\widetilde{w}_h \in X_h$, which completes the implementation of the discrete problem (4.28).

4.4 Convection-Diffusion equation

We recall the continuous problem which we want to discretize. The classical formulation of the problem is a generalization of (3.21), (3.23)

Find $u \in C^2(\Omega) \cap C^1(\overline{\Omega})$ such that

$$\begin{aligned} -\Delta u + \nabla \cdot (\boldsymbol{\alpha} u) &= f \quad \text{in } \Omega, \\ (\nabla u - \boldsymbol{\alpha} u) \cdot \mathbf{n} &= 0 \quad \text{on } \Gamma \end{aligned} \tag{4.43}$$

with $\mathbf{n}$ denoting a unit outer normal to Γ. The weak formulation of the problem (4.43) is given by (3.26)

Find $u \in H^1(\Omega)$ such that

$$(\nabla u - \boldsymbol{\alpha} u, \nabla w) = \langle f, w \rangle \quad \text{for all } w \in H^1(\Omega). \tag{4.44}$$

Solution of both problems must satisfy the mass conservation condition (3.22)

$$\frac{1}{|\Omega|} \int_\Omega u \, dx = 1. \tag{4.45}$$

The main properties of the continuous problem are provided by Theorem 3.3.2. A discrete method which preserves these properties was first introduced in [10], where a finite volume approach was applied for different types of fluxes. Namely, centered flux, widely used in fluid mechanics upwind flux [36], and Scharfetter-Gummel flux, which is common for semiconductor framework [26, 38]. These fluxes were parametrized by a single function $B(\cdot)$ with several assumptions on it, which guaranteed the properties of the discretization. The scheme was constructed on a so called "admissible mesh".

In [21] the mixed finite element finite volume approach was suggested. This approach was considered before in [13, 14, 15, 20, 36] with some changes. The weak formulation there was split into two terms which were discretized separately. The weighting function $\lambda(\cdot)$ appeared naturally into approximated problem. Holding some assumptions on $\lambda(\cdot)$ allowed to refer to [10] for the main properties of the discretization. The weakly acute triangulation (that is, no angle is greater than $\pi/2$) was used as the basic domain decomposition.

Let us introduce the following notation. Let $P = \{p_i,\ i = 1, \ldots, N\}$ be the set of vertices of the triangulation $\mathcal{T}_h$. A dual domain associated with p_i is defined by

$$D_i := \bigcup_{T \cap p_i \neq \varnothing} \{p \in T \ : \ |p_i p| < |p p_j| \text{ for all vertices } p_j \in T\}, \tag{4.46}$$

where $|\cdot|$ is the length of a line segment. The dual domain decomposition of Ω_h is then given by

$$\mathcal{D}_h = \{D_i\}_{i=1}^N.$$

One should note that $T \in \mathcal{T}_h$ is a closed set, while D_i is open for $p_i \notin \Gamma$ and neither open nor closed for $p_i \in \Gamma$. We introduce an index set

$$\Lambda_i = \{j \neq i \ : \ \exists T \in \mathcal{T}_h \text{ such that } p_i, p_j \in T\}.$$

The intersection of $\overline{D}_i$ and $\overline{D}_j, j \in \Lambda_i$ is a face of $\overline{D}_i$ denoted by Γ_{ij}, which is, according to mesh construction, orthogonal to a line segment $p_i p_j$. Its length is denoted by $d_{ij} := |\Gamma_{ij}|$. The distance between two neighbor mesh points is by $h_{ij} = |p_i p_j|$, $j \in \Lambda_i$. In that definition one should avoid the situation when $|\Gamma_{ij}| = 0$. For that reason we redefine

$$\Lambda_i = \{j \neq i \ : \ \exists T \in \mathcal{T}_h \text{ such that } p_i, p_j \in T, \quad |\Gamma_{ij}| \neq 0\}. \tag{4.47}$$

The constructed secondary grid is related to the grids defined in [10] and [21]. Redefining $D_i := \overline{D}_i$ we obtain for a weakly acute triangulation a grid equal to one in [21]. For inner nodes p_i such that $p_i \notin \Gamma_h$ the all assumptions of an "admissible mesh" defined in [10] are satisfied. However grid points of the mesh $\mathcal{D}_h$ lie on the boundary Γ_h and control volumes D_i may be nonconvex due to the boundary. Both conditions come into contradiction with the definition of an "admissible mesh". To show this difference we present an "admissible mesh" from [10] making its definition more similar to $\mathcal{D}_h$

$$\begin{aligned} G_{ij} &:= \{p \in \Omega_h \ : \ |p_i p| < c_{ij}|p p_j| \text{ for all vertices } p_i, p_j, \ j \in \Theta_j\}, \\ M_i &:= \bigcap_{j \in \Theta_i} G_{ij}, \quad i = 1, \cdots, N, \end{aligned} \tag{4.48}$$

where $c_{ij} = 1/c_{ji} > 0$, $\Theta_i \subseteq \{1, \cdots, N\} \setminus \{i\}$ are index sets, Ω_h is a polygonal approximation of Ω. The sets of points P, indices Θ_i and constants $c_{ij}, j \in \Theta_i$ are chosen so that $\bigcup_{i=1}^N \overline{M}_i = \overline{\Omega}$, $M_i \cap M_j = \varnothing$, $i \neq j$, and for any open line segment $\sigma \subset \Gamma_h \cap \partial M_i$ (boundary edge) the line orthogonal to it and going trough p_i crosses σ. One can show that P taken as vertices of Delaunay triangulation, $\Theta_i = \Lambda_i$ and $c_{ij} = 1$ for all $i = 1, \cdots, N, j \in \Lambda_i$ generates decomposition by pairwise disjoint polygons covering Ω_h (conclusion from proof of Lemma 4.4.5). An "admissible mesh" is then defined as follows

$$\mathcal{M} = \{M_i\}_{i=1}^N.$$

We define Λ_i, Γ_{ij}, d_{ij} and h_{ij} for $\mathcal{M}$ in the same manner as we did for $\mathcal{D}_h$.

In the following subsections we discuss the possible discretizations of the convective-diffusive type problem in classical (4.43) or weak (4.44) formulation.

4.4.1 Finite volume method

Here we discuss the finite volume discretization [10] applied to the problem (4.43) on an "admissible mesh" $\mathcal{M}$ of a polygonal domain Ω_h. Integrating both sides of the equation

and using Gauss's theorem we obtain

$$\int_{\Omega_h} \nabla \cdot (\nabla u - \boldsymbol{\alpha} u)\ dx = \sum_{i=1}^{N} \int_{D_i} \nabla \cdot (\nabla u - \boldsymbol{\alpha} u)\ dx = \sum_{i=1}^{N} \int_{\partial D_i} (\nabla u - \boldsymbol{\alpha} u) \cdot \mathbf{n}\, d\gamma$$
$$= \sum_{i=1}^{N} \sum_{j \in \Lambda_i} \int_{\Gamma_{ij}} (\nabla u - \boldsymbol{\alpha} u) \cdot \mathbf{n}_{ij}\, d\gamma + \int_{\Gamma_h} (\nabla u - \boldsymbol{\alpha} u) \cdot \mathbf{n}\, d\gamma,$$

where $\mathbf{n}_{ij}$ and $\mathbf{n}$ are unit normals to Γ_{ij} and Γ_h pointing out of D_i and Ω_h, respectively. The integral over the boundary Γ_h vanishes due to the boundary condition.

The idea of a finite volume method is to write a flux balance over ∂D_i by approximating

$$\int_{\Gamma_{ij}} (\nabla u - \boldsymbol{\alpha} u) \cdot \mathbf{n}_{ij}\, d\gamma.$$

In [10] several known numerical fluxes were used as an approximation of surface integrals, namely centered, upwind and Scharfetter-Gummel fluxes. These fluxes were generalized using a generic function $B(\cdot)$. The general approximation in [10] can be written as follows

$$\sum_{j \in \Lambda_i} \int_{\Gamma_{ij}} (\nabla u - \boldsymbol{\alpha} u) \cdot \mathbf{n}_{ij}\, d\gamma \approx \frac{d_{ij}}{h_{ij}} \left(B(-N_{ij} h_{ij}) u(p_i) - B(N_{ij} h_{ij}) u(p_j) \right),$$

where N_{ij} defined by

$$N_{ij} := -\frac{1}{d_{ij}} \int_{\Gamma_{ij}} \boldsymbol{\alpha} \cdot \mathbf{n}_{ij}\, d\gamma \tag{4.49}$$

denotes the flux of $\boldsymbol{\alpha}$ through Γ_{ij} and the function $B(\cdot)$ must satisfy the following conditions in order to prove important properties of the scheme.

$$B \text{ is Lipschitz-continuous on R}, \tag{B1}$$
$$B(0) = 1 \text{ and } B(s) > 0 \text{ for all } s \in \mathrm{R}, \tag{B2}$$
$$B(s) - B(-s) = -s \text{ for all } s \in \mathrm{R}. \tag{B3}$$

Since the balance of fluxes holds for each control volume independently, we obtain a system of linear equations. The solution space in that case is given by a piecewise constant function

$$Z_h = \{ g(x)\ :\ g(x) \equiv \text{const},\ x \in D_i \}.$$

Defining by u_i the value of u_h on D_i the finite volume discretization of the problem (4.43) is given by

Find a piecewise constant function $u_h \in Z_h$ such that

$$\sum_{j \in \Lambda_i} \frac{d_{ij}}{h_{ij}} \left(B(-N_{ij} h_{ij}) u_i - B(N_{ij} h_{ij}) u_j \right) = f_i, \quad i = 1, \cdots, N, \tag{4.50}$$

where the discrete right hand side $f_i = \int_{D_i} f \, dx$. Writing a one parameter family of problems (3.30) in classical formulation we have

$$\begin{aligned} -\Delta u + \nabla \cdot (\boldsymbol{\alpha} u) + \gamma u &= f \quad \text{in } \Omega, \\ (\nabla u - \boldsymbol{\alpha} u) \cdot \mathbf{n} &= 0 \quad \text{on } \Gamma. \end{aligned} \tag{4.51}$$

The problem (4.51) is discretized like (4.50) adding the term $\gamma |D_i| u_i$ on the left hand side. We obtain

Find a piecewise constant function $u_h \in Z_h$ such that

$$\sum_{j \in \Lambda_i} \frac{d_{ij}}{h_{ij}} \left(B(-N_{ij} h_{ij}) u_i - B(N_{ij} h_{ij}) u_j \right) + \gamma |D_i| u_i = f_i, \quad i = 1, \cdots, N. \tag{4.52}$$

The properties of this discretization proven in [10] can be summarized in a theorem

Theorem 4.4.1 (composition of Theorem 2.5, 2.6 [10])**.** *Let $\mathcal{M}$ be an "admissible mesh" of Ω_h. For $B(\cdot)$ satisfying* (B1)-(B3) *the finite volume discretizations* (4.50) *and* (4.52) *have the following properties*

(i) Problem (4.52) *has a unique solution for $\gamma > 0$.*

(ii) Problem (4.50) *with $f \equiv 0$ has a one dimensional solution space spanned by $\hat{u}_h \in Z_h$ such that $\hat{u}_h(p_i) > 0$ for all $i = 1, \cdots, N$.*

(iii) Problem (4.50) *has a unique solution $u_h \in Z_h$ satisfying $\int_{\Omega_h} u_h = 0$ only in case $\sum_{i=1}^{N} f_i = 0$.*

In addition in [10] the convergence results were presented, showing that

$$u_h \to u \text{ as } h \to 0$$

for u and u_h being chosen as

- Solutions of the continuous (4.51) and the discrete (4.52) problems, respectively.
- Two unique elements with L^2 norms equal to 1 in kernels of problems (4.43) and (4.50), respectively.
- Two unique solutions with L^2 norms equal to 0 of problems (4.43) and (4.50) with $\langle f, 1 \rangle = 0$, respectively.

In all these results discrete Sobolev inequality was proven

$$\|u\|_{0,q} \leq C(|u|_{1,\mathcal{M}} + \|u\|_{0,2}) \tag{4.53}$$

with $q < +\infty$ and constant $C = C(\Omega_h, \zeta, q)$. The norm $|\cdot|_{1,\mathcal{M}}$ denotes the discrete H^1-seminorm given by

$$|u|_{1,\mathcal{M}} = \left(\frac{1}{2} \sum_{i=1}^{N} \sum_{j \in \Lambda_i} \frac{d_{ij}}{h_{ij}} (u_i - u_j)^2 \right).$$

The important assumption for the proof of discrete Sobolev inequalities is that there exists a constant ζ such that

$$d(p_i, \sigma) \geq \zeta |\sigma| \quad \forall \sigma \subset \partial D_i, \tag{4.54}$$

where σ denotes any edge of ∂D_i, $d(p_i, \sigma)$ a distance from the point p_i to the edge σ. One can notice that (4.54) cannot be satisfied for $\mathcal{D}_h$, since this mesh allows points p_i to lie on the boundary Γ_h, which gives $d(p_i, \sigma) = 0$ for $\sigma \subset \partial D_i \cap \Omega_h$ and contradicts to (4.54).

4.4.2 Mixed approach on a weakly acute triangulation

In this subsection we discuss the discretization from [21]. We denote by $\mathcal{T}_h$ a weakly acute triangulation, i.e. each angle of any triangle is less or equal to $\pi/2$. The weak formulation is split into two terms which are discretized by two different methods. The diffusive term $(\nabla u, \nabla w)$ is discretized by standard Galerkin with $\mathcal{P}^1$ finite elements on a triangulation $\mathcal{T}_h$. The convective term $(\boldsymbol{\alpha} u, \nabla w)$ is approximated by a finite volume method on a dual (secondary) grid $\mathcal{D}_h$ defined at the beginning of this section.

We introduce the discrete problem corresponding to the weak formulation of the convection-diffusion problem (4.44)

Find $u_h \in W_h$ such that

$$(\nabla u_h, \nabla w_h) + b_h(u_h, w_h) = \langle f, w_h \rangle \quad \text{for all } w_h \in W_h, \tag{4.55}$$

where on the left hand side stand discretizations of diffusive and convective terms, respectively. A finite element space is defined by

$$W_h := \{ w_h \in C^0(\Omega_h) \ : \ w_h\big|_T \in \mathcal{P}^1 \}. \tag{4.56}$$

Expressing u_h via basis of W_h we obtain by a direct computation

$$(\nabla u_h, \nabla \varphi_i) = -\sum_{j \in \Lambda_i} \frac{d_{ij}}{h_{ij}} (u_j - u_i). \tag{4.57}$$

The discretization of a convective term is started like in [36] with the identity

$$(\boldsymbol{\alpha} u, \nabla w) \equiv (\nabla \cdot (\boldsymbol{\alpha} w), u) - (\nabla \cdot \boldsymbol{\alpha}, uv). \tag{4.58}$$

We define the characteristic function of the dual domain D_i

$$\chi_i(p) = \begin{cases} 1, & p \in D_i, \\ 0, & p \notin D_i \end{cases}$$

and the lumping operator l_h

$$l_h w := \sum_{i=1}^{N} w(p_i)\chi_i. \tag{4.59}$$

Applying the lumping operator l_h and Gauss's theorem to (4.58) we obtain

$$\begin{aligned}(\boldsymbol{\alpha}u, \nabla w) &\approx (\nabla\cdot(\boldsymbol{\alpha}w), l_h u) - (\nabla\cdot\boldsymbol{\alpha}, l_h(uw)) \\ &= \sum_{i=1}^{N}\int_{D_i} [\nabla\cdot(\boldsymbol{\alpha}w)u(p_i) - \nabla\cdot\boldsymbol{\alpha}u(p_i)w(p_i)] \\ &= \sum_{i=1}^{N}\sum_{j\in\Lambda_i}\int_{\Gamma_{ij}} [\boldsymbol{\alpha}wu(p_i) - \boldsymbol{\alpha}u(p_i)w(p_i)]\cdot\mathbf{n}_{ij}d\gamma,\end{aligned}$$

where $\mathbf{n}_{ij}$ denotes the unit normal to Γ_{ij} pointing out of the dual domain D_i. We approximate w in each integral over Γ_{ij} using an upwind parameter λ_{ij}

$$w \approx \lambda_{ij}w(p_i) + (1-\lambda_{ij})w_(p_j).$$

It leads us to

$$\begin{aligned}(\boldsymbol{\alpha}u,\nabla w) &\approx -\sum_{i=1}^{N}\sum_{j\in\Lambda_i} d_{ij}N_{ij}u(p_i)(1-\lambda_{ij})\left[w(p_j)-w(p_i)\right] \\ &= \sum_{i=1}^{N}\sum_{j\in\Lambda_i} d_{ij}N_{ij}(1-\lambda_{ij})u(p_i)w(p_i) - \sum_{k=1}^{N}\sum_{l\in\Lambda_k} d_{kl}N_{kl}(1-\lambda_{kl})u(p_k)w(p_l) \\ &= \sum_{i=1}^{N}\sum_{j\in\Lambda_i} d_{ij}N_{ij}(1-\lambda_{ij})u(p_i)w(p_i) + \sum_{l=1}^{N}\sum_{k\in\Lambda_l} d_{lk}N_{lk}\lambda_{lk}u(p_k)w(p_l) \\ &= \sum_{i=1}^{N}\sum_{j\in\Lambda_i} d_{ij}N_{ij}w(p_i)\left[(1-\lambda_{ij})u(p_i)+\lambda_{ij}u(p_j)\right],\end{aligned}$$

where N_{ij} is the flux across Γ_{ij} defined by (4.49). Taking $u = u_h$, $w = w_h$ and expressing them via the basis of W_h we obtain

$$(\boldsymbol{\alpha}u_h, \nabla\varphi_i) \approx \sum_{j\in\Lambda_i} d_{ij}N_{ij}\left[(1-\lambda_{ij})u_i + \lambda_{ij}u_j\right]. \tag{4.60}$$

Summing up the discretization of two terms we end up with the discrete problem

Find $u_h \in W_h$ such that

$$\sum_{j\in\Lambda_i}\frac{d_{ij}}{h_{ij}}\left(\left[1-N_{ij}h_{ij}(1-\lambda_{ij})\right]u_i + \left[1+N_{ij}h_{ij}\lambda_{ij}\right]u_j\right) = f_i, \quad i=1,\cdots,N, \tag{4.61}$$

where $f_i = \int_{D_i} f\,dx$, W_h is defined by (4.56). We can also write (4.61) as a system of linear equations $Au_h = f$, where matrix entries a_{ij} are given by

$$a_{ij} = \begin{cases} \displaystyle\sum_{k\in\Lambda_i} \frac{d_{ik}}{h_{ik}}\Big(1 - N_{ik}h_{ik}[1-\lambda_{ij}]\Big) & j = i, \\ \displaystyle -\frac{d_{ij}}{h_{ij}}\Big(1 + N_{ij}h_{ij}\lambda_{ij}\Big) & j \in \Lambda_i, \\ 0 & \text{otherwise.} \end{cases} \tag{4.62}$$

In [21] the upwind parameter λ was given by $\lambda_{ij} = \Phi(N_{ij}h_{ij})$ with $\Phi(\cdot)$ being a weighting function controlling the amount of upwinding and satisfying

$$\Phi(t) = 1 - \Phi(-t)\ \forall t > 0 \ \text{ and } \ 0 \le \Phi(t) \le 1 \quad \forall t \in \mathbb{R}, \tag{H1}$$

$$t\left[\Phi(t) - \frac{1}{2}\right] \ge 0 \quad \forall t \in \mathbb{R}, \tag{H2}$$

$$\Psi(t) := t\Phi(t) \text{ is Lipschitz continuous on } \mathbb{R}, \tag{H3}$$

$$\Psi(t) > 1 - \frac{1}{t} \ \text{ for } t > 0 \ \text{ and } \ \Psi(t) < -\frac{1}{t} \ \text{ for } t < 0. \tag{H4}$$

It was also shown in [21] that defining $B(t) = 1 + t\Phi(t)$ and making simple transformation, the discretization (4.61) on a dual grid $\mathcal{D}_h$ of a weakly acute triangulation becomes identical to (4.50) on an "admissible mesh" $\mathcal{M}$. In addition assumptions (B1)-(B3) on $B(\cdot)$ are equivalent to (H1), (H3), (H4) on $\Phi(\cdot)$. That closeness allows to prove the existence and uniqueness of a solution of the discrete problem by just referring to [10]. The assumption (H2) allows to transfer coercivity results from the continuous problem to the discrete one, see [21] for more details.

The most important results listed in [21] can be summarized as follows

Theorem 4.4.2. *Let the weighting function $\Phi(\cdot)$ satisfy the assumptions* (H1)-(H4) *then the following holds*

(i) For $\boldsymbol{\alpha}$ such that $\boldsymbol{\alpha}\cdot\mathbf{n} \le 0$ on $\partial\Omega$, $\operatorname{div}\boldsymbol{\alpha} \ge 0$ in Ω, and sufficiently small mesh size h the bilinear form $a_h(u_h, v_h) := (\nabla u_h, \nabla v_h) + b_h(u_h, v_h)$ is coercive on W_h.

(ii) The kernel of the matrix A defined by (4.62) *is one-dimensional and is spanned by a vector $\hat{u}_h$ such that either $(\hat{u}_h)_i > 0$ or $(\hat{u}_h)_i < 0$ for all i.*

(iii) The nonhomogeneous problem (4.61) *has a unique solution $u_h \in W_h$ with $\int_{\Omega_h} u_h = 0$ if and only if $\sum_{i=1}^N f_i = 0$.*

Part (ii) may be interpreted like the problem (4.61) with $f \equiv 0$ has a solution unique up to a multiplicative constant.

As it was mentioned before, the convergence analysis in [10] uses discrete Sobolev inequalities (4.53), whose proof cannot be followed directly for the mesh $\mathcal{D}_h$. Moreover, the order of convergence was not estimated there. The different approach was used in [21]

which also provides the convergence rate. At first it was shown that the discrete inf-sup constant is uniformly bounded from below

$$\beta_h := \inf_{u\in\widetilde{W}_h} \sup_{w\in\widetilde{W}_h} \frac{a_h(u_h, w_h)}{\|u_h\|_1 \|w_h\|_1} \geq \beta_0 > 0$$

for all h small enough. The space $\widetilde{W}_h$ is space W_h (4.56) with incorporated integral condition (4.45)

$$\widetilde{W}_h = \{w_h \in W_h \ : \ \int_{\Omega_h} w_h dx = 0\}.$$

Using the bound of the inf-sup constant the error estimate was proven

$$\|u - u_h\|_1 \leq Ch(\|u\|_2 + \|f\|_0). \tag{4.63}$$

4.4.3 Mixed approach on a Delaunay triangulation

In this section we want to extend the results from [21] to a more flexible Delaunay triangulation. We start with definitions of Delaunay triangulation and Voronoi polygon and propose a Voronoi diagram as the dual domain decomposition to Delaunay triangulation.

Definition 4.4.3 (Definition from [11])**.** *Let P be a set of points in the plane. A triangulation $\mathcal{T}$ is Delaunay triangulation of P if for each edge σ of $\mathcal{T}$ there exists a circle C with the following properties:*

(1) The endpoints of edge σ are on the boundary of C.

(2) No other vertex of P is in the interior of C.

In other words it can be described as an empty circumcircle property, which is well explained in [40]: "The circumcircle of a triangle is the unique circle that passes through its three vertices. The Delaunay triangulation of a set of vertices is the triangulation (usually, but not always, unique) in which every triangle has an empty circumcircle – meaning that the circle encloses no vertex of the triangulation". We denote the Delaunay triangulation of Ω_h as $\mathcal{T}_D$.

The definition of a planar ordinary Voronoi polygon is given as follows

Definition 4.4.4 (Definition V2 in [28])**.** *Let $P = \{p_1, \cdots, p_n\} \subset \mathbb{R}^2$, where $2 < n < \infty$ and $p_i \neq p_j$ for $i \neq j$. We call the region given by*

$$D(p_i) = \{p \ : \ \|pp_i\| < \|pp_j\| \text{ for all } j \neq i\}$$

the planar ordinary Voronoi polygon associated with p_i (or the Voronoi polygon of p_i), and the set given by

$$\widetilde{\mathcal{D}_h} = \{D(p_1), \cdots, D(p_n)\}$$

the planar ordinary Voronoi diagram generated by P (or the Voronoi diagram of P).

Here and further we name a planar ordinary Voronoi polygon simply Voronoi polygon for simplicity. Every Voronoi polygon can be defined as an intersection of half-planes. From this immediately follows that every Voronoi polygon is a convex set up to the boundary of a discretized domain.

We propose the Voronoi diagram of the polygonal domain Ω_h, not necessary convex, as a domain decomposition. Let us denote such a decomposition as $\widetilde{\mathcal{D}_h}$. It can be constructed as a dual mesh to the Delaunay triangulation. The Delaunay triangulation in its turn can be made automatically by well known implementation Triangle [39]. One can notice that a dual domain decomposition $\mathcal{D}_h$ of a weakly acute triangulation is a special case of Voronoi diagram $\widetilde{\mathcal{D}_h}$ constructed on vertices of Delaunay triangulation.

The vertices of Voronoi polygons are circumcenters of Delaunay triangles. In general case triangles satisfying the Delaunay condition are not acute, so the circumcenter may not be located inside the triangle itself. It can provide some problems on the boundary, but Triangle [39] can construct a triangulation such that circumcenters of all triangles lie inside triangulation. We further assume that this property holds for $\mathcal{T}_D$.

We repeat the discretization steps (4.57) and (4.60) to show that the scheme from [21] can be applied on a more general Delaunay triangulation and start with some useful notation. We define with indices i, j, k three vertices p_i, p_j, p_k of a triangle T. Angles, corresponding to these vertices of triangle, are denoted by $\alpha_i, \alpha_j, \alpha_k$, respectively. The edge of between two vertices p_i and p_j is p_ip_j with length $h_{ij} = |p_ip_j|$. Moreover, we denote the circumcenter of a triangle T by p_c, and the center of edge p_ip_j by p_m.

The first term of the discrete form $a_h(\cdot,\cdot)$ is derived directly

$$\begin{aligned}(\nabla u_h, \nabla\varphi_i) &= \sum_{T\in\mathcal{T}_D\,:\,p_i\in T} (\nabla u_h, \nabla\varphi_i)_T \\ &= \sum_{T\in\mathcal{T}_D\,:\,p_i\in T} \left((u_j-u_i)\,(\nabla\varphi_j, \nabla\varphi_i)_T + (u_k-u_i)\,(\nabla\varphi_k, \nabla\varphi_i)_T\right).\end{aligned} \tag{4.64}$$

One can show by simple computations that

$$(\widehat{\nabla\varphi_i, \nabla\varphi_j})\big|_T = \pi - \alpha_k.$$

Using representation $|\nabla\varphi_i| = h_{jk}/2|T|$ we come to

$$(\nabla\varphi_i, \nabla\varphi_j)_T = \frac{h_{ik}h_{jk}}{4|T|}\cos(\widehat{\nabla\varphi_i, \nabla\varphi_j})\big|_T = \frac{h_{ik}h_{jk}}{4|T|}\cos\alpha_k.$$

Applying formula for area of triangle $|T| = \frac{1}{2}|p_ip_k||p_jp_k|\sin\alpha_k$ we end up with

$$(\nabla\varphi_i, \nabla\varphi_j)_T = -\frac{1}{2}\cot\alpha_k. \tag{4.65}$$

The second scalar product in (4.64) $(\nabla\varphi_k, \nabla\varphi_i)_T$ is evaluated in the same way. This formula is a 2D special case of a more general one listed in [49]. Vector $\nabla\varphi_i$ is directed along the height of the triangle from side to vertex. Using simple geometry one can obtain

$$\cot\alpha_k = 2\frac{d_k}{h_{ij}}. \tag{4.66}$$

Here we used d_k related to the length of a mid perpendicular to a circumcenter $p_c p_m$

$$d_k := \begin{cases} |p_c p_m|, & \alpha_k \le \pi/2, \\ -|p_c p_m|, & \alpha_k > \pi/2. \end{cases} \tag{4.67}$$

Let us define index sets corresponding to each boundary component Γ_{ij}

$$I_{ij} = I_{ji} := \{k \,:\, p_k \in P,\, k \neq i, j,\, \exists T \in \mathcal{T}_D \text{ such that } p_i, p_j, p_k \in T\},$$

which contains one index in case $p_i p_j \subset \Gamma_h$ and two indices otherwise.

Substituting the evaluation of scalar products (4.65)–(4.67) into (4.64) we obtain

$$\begin{aligned} (\nabla u_h, \nabla \varphi_i) &= -\sum_{T \in \mathcal{T}_D \,:\, p_i \in T} \left((u_j - u_i) \frac{d_k}{h_{ij}} + (u_k - u_i) \frac{d_j}{h_{ik}} \right) \\ &= -\sum_{j \in \Lambda_i} \sum_{k \in I_{ij}} \frac{d_k}{h_{ij}} (u_j - u_i) = -\sum_{j \in \Lambda_i} \frac{\widetilde{d}_{ij}}{h_{ij}} (u_j - u_i), \end{aligned} \tag{4.68}$$

where Λ_i is defined by (4.47) and $\widetilde{d}_{ij}$ is given by

$$\widetilde{d}_{ij} := \begin{cases} d_{k_1} + d_{k_2}, & k_1, k_2 \in I_{ij}, k_1 \neq k_2, \\ d_k, & k \in I_{ij}, |p_i p_j| \subset \Gamma_h \end{cases} \tag{4.69}$$

with d_k defined by (4.67). It was proven in [49] that such a discretization on Delaunay triangulation satisfies the maximum principle by showing that $\widetilde{d}_{ij} \ge 0$. However, in order to refer to the scheme (4.61) from [21] one should show in addition that $\widetilde{d}_{ij} = d_{ij} = |\Gamma_{ij}|$ for all i, j.

Lemma 4.4.5. *For a Delaunay triangulation $\mathcal{T}_D$ of the domain Ω_h and piecewise linear basis functions φ_i, $i = \overline{1, N}$ of W_h (4.56) the discretization of the diffusive term $(\nabla u_h, \nabla \varphi_i)$ (4.68) is equivalent to (4.57) on a weakly acute triangulation, i.e. $\widetilde{d}_{ij} = |\Gamma_{ij}|$.*

Proof. At first we distinguish two cases, where $p_i p_j$ is a boundary edge and an inner, respectively.

1) Assume $p_i p_j$ is a boundary edge. Then according to (4.69) $\widetilde{d}_{ij} = d_k$. As we assumed before, the circumcenter p_c lies within the triangulation $\mathcal{T}_D$, which implies $\alpha_k \le pi/2$. And as a consequence we have by (4.67) $\widetilde{d}_{ij} = |p_m p_c| = |\Gamma_{ij}|$.

2) Let $p_i p_j$ be an inner edge, i.e. there exist $T_1, T_2 \in \mathcal{T}_D$ such that $T_1 \cap T_2 = \Gamma_{ij}$. We choose $k_1, k_2 \in I_{ij}$ such that $p_{k_1} \in T_1$, $p_{k_2} \in T_2$. There are three possible cases

- $d_{k_1} \ge 0$ and $d_{k_2} \ge 0$;
- $d_{k_1} \le 0$ and $d_{k_2} < 0$;
- $d_{k_1} \cdot d_{k_2} < 0$.

In case $d_{k_1}, d_{k_2} \geq 0$ both triangles are weakly acute, which immediately implies $\widetilde{d}_{ij} = |\Gamma_{ij}|$. The case $d_{k_1} \leq 0$ and $d_{k_2} < 0$ cannot occur since it implies the circumcircle of T_1 containing p_{k_2}, which comes into contradiction with the Definition 4.4.3 of a Delaunay triangulation. It remains to prove the statement for $d_{k_1} \cdot d_{k_2} < 0$. Without loss of generality we consider $d_{k_1} > 0$ and $d_{k_2} < 0$. It means that both vertices p_{k_1}, p_{k_2} lie on the same side of mid-perpendicular of the edge $p_i p_j$. According to Definition 4.4.3 there is no point in P which is inside of a circumcircle of any triangle $T \in \mathcal{T}_D$. One can conclude that

$$|p_{k_1} p_{c_2}| < |p_{k_1} p_{c_1}|.$$

Finally, using (4.69) and (4.67) one can show

$$\widetilde{d}_{ij} = d_{k_1} + d_{k_2} = |p_m p_{c_1}| - |p_m p_{c_2}| = |p_{k_1} p_{c_1}| - |p_{k_1} p_{c_2}| = |p_{c_1} p_{c_2}| = |\Gamma_{ij}|,$$

which completes the proof. ■

The discretization of the convective term $b_h(\cdot, \cdot)$ directly repeats the derivation of (4.60). The only difference for $\mathcal{T}_D$ is that Γ_{ij} and $p_i p_j$ may not cross each other, which nevertheless allows to apply the lumping operator (4.59). The final discretization has exactly the same form as (4.61)

Find $u_h \in W_h$ such that

$$\sum_{j \in \Lambda_i} \frac{d_{ij}}{h_{ij}} \left([1 - N_{ij} h_{ij} (1 - \lambda_{ij})] \, u_i + [1 + N_{ij} h_{ij} \lambda_{ij}] \, u_j \right) = f_i, \quad i = 1, \cdots, N. \tag{4.70}$$

One should note, that there is a difference in construction of d_{ij} between these two methods, that comes from different triangulations. But due to equivalent definitions, the properties can also be transfered, including solvability result in Theorem 4.4.2 and the error estimate (4.63).

4.4.4 Implementation notes

The discretization of the problem (4.70) in space W_h leads to a system of linear equations

$$A u_h = 0, \tag{4.71}$$

with matrix $A = (a_{ij})_{ij}$ defined by (4.62). The right hand side can be written as $f = (0)_i$. According to Theorem 4.4.2 matrix A has a one-dimensional kernel, and solution of (4.71) exists and is unique up to a multiplicative constant. In order to have it unique we fix the solution $\hat{u}_h$ at an arbitrary point p_k. It is done by changing the corresponding row of the system

$$\tilde{a}_{kj} = \begin{cases} 0, & k \neq j, \\ 1, & k = j \end{cases} \quad \text{for all } j,$$
$$\tilde{f}_k = 1.$$

We want to show that k can be chosen arbitrary, i.e. by deleting any equation in (4.70) we obtain a linear independent system. We prove this statement for matrix formulation (4.71). Let us assume that the j-th row is deleted and the rest of the system is linearly dependent. Then there exists a vector $\lambda \neq 0$, which has zero on j-th position, such that $A\lambda = 0$. On the other hand, the kernel of A is one-dimensional and spanned by a strictly positive vector. Hence, $\lambda \equiv 0$ that leads to a contradiction. This proves that every $n-1$ rows of matrix A are linearly independent. Moreover, adding an arbitrary non negative and non trivial vector $\mathbf{a}$ to a system of $n-1$ rows of matrix A, one obtains a linearly independent system, since such a vector $\mathbf{a}$ is not orthogonal to the kernel of A.

One should note that such a procedure does not provide a solution satisfying the mass conservation condition (4.45). So we have to do one more step. We find the normalization constant for the solution of the modified system $\widetilde{A}u_h = \widetilde{f}$

$$C_N = \frac{1}{\Omega_h} \int_{\Omega_h} u_h \, dx.$$

Then the final solution is given then by $\widetilde{u}_h = u_h \, C_N$. The closer C_N is to 1, the better computational accuracy we have. Therefore, one should choose a point at which the value of the normalized solution $\widetilde{u}_h$ is close to 1. To find the index of this point, precomputation of u_h can be used.

4.5 Solution strategy

In this section we discuss the solution of the whole system (2.75), (2.76), which was discretized above. The equations are partially coupled, but the discretization of each equation is performed separately. Therefore, an additional technique is required. We suggest iterative solving of equations by updating solutions on each step. We split the system (2.75) into two subsystems. The first one consists of Young-Laplace and Laplace equations, the second one of Navier-Stokes and convection-diffusion equations. This decoupling follows in a natural way from the structure of equations. One can perform iterations between these pairs later. The iteration process starts with the pair of Young-Laplace (2.75d) and Laplace (2.75a) equations, which describe the position of free surfaces and the azimuthal velocity, respectively. Since the particle concentration is unknown, the simplified version of the Young-Laplace equation (4.18) is used. The subsystem can be illustrated as follows

$$\begin{aligned} y_i^{j+1}(x^*) &= (-1)^{i+1} g(x^*, \widehat{\Phi}_i^j(x^*)), \quad x^* \in [0, \zeta_i^j], \quad i = 1, 2, \\ \Delta\omega^{j+1} &= 0 \quad \text{in } \Omega^{j+1}. \end{aligned} \tag{4.72}$$

Here, y_i^j and ω^j are sequences of solutions of the Young-Laplace and Laplace equations, respectively. The discretizations of these equations are presented above in this chapter. The equation is written in a continuous way and the boundary conditions as well as conditions on the Young-Laplace equation for simplicity are omitted. The Young Laplace

equation is discretized by (4.26), the function $\widehat{\Phi}_i^j$ is derived from (4.18) in the same way as Φ_i^j given by (4.23). The Young-Laplace equation produces a grid of boundary nodes Ξ_i^{j+1} from a given grid Ξ_i^j, $i = 1, 2$ and azimuthal velocity ω^j. Afterwards, the grid Ξ^{j+1} for the Laplace equation is constructed by (4.4) and includes all the points of Ξ_i^{j+1}, $i = 1, 2$ and points on the solid boundaries Γ_s, Γ_c. Once ω^{j+1} is obtained, the values of $\widehat{\Phi}_i^j(\cdot)$ can be evaluated on the grid Ξ_i^{j+1}. We continue the iterations until the convergence is reached. The initial guess is $\omega^0 = 0$, for which $\widehat{\Phi}_i^0$ becomes an analytically given function, so that the first grids Ξ_i^0, $i = 1, 2$ can be constructed.

After a final step j^*, the domain Ω is determined by (4.27) using $y_i^{j^*}$, $i = 1, 2$. After that Ω is approximated by a polygonal domain Ω_h, which is then partitioned by the Delaunay triangulation. We solve the second subsystem on a discrete domain Ω_h defined above.

At first, the Laplace equation is discretized one more time with $\mathcal{P}^2$ finite elements, the finite element solution is used later in the discretization of the Navier-Stokes equation. The coupled system of the Navier-Stokes (2.75b) and convection-diffusion (2.75c) equations is linearized as follows

$$\begin{gathered}
\left(\mathbf{v}^k \cdot \nabla\right) \mathbf{v}^k - \operatorname{div} \sigma(\mathbf{v}^k, p^k) = \mathbf{e}_1 \delta \omega^2 + \frac{\delta}{\mathrm{Fr}_m} L\left(\xi h_s\right) c^{k-1} \nabla h_s \quad \text{in } \Omega, \\
\nabla \cdot \mathbf{v}^k = 0 \quad \text{in } \Omega, \\
-\frac{1}{\mathrm{Pe}} \nabla \cdot \left(\nabla c^k - c^k \xi L\left(\xi h_s\right) \nabla h_s\right) + \mathbf{v}^k \cdot \nabla c^k = 0 \quad \text{in } \Omega, \quad \int\limits_{\Omega} c^k \, dx = |\Omega|.
\end{gathered} \tag{4.73}$$

Here $\mathbf{v}^k$ and c^k are sequential numerical solutions of the Navier-Stokes and convection-diffusion equations, respectively. We omit for simplicity the boundary conditions (2.76b), (2.76c) and linearization technique for the Navier-Stokes equation (4.37). The Navier-Stokes equation is discretized using the $\mathcal{P}^2/\mathcal{P}^1$ Taylor-Hood finite elements, whereas the convection-diffusion equation is solved with the mixed Finite Element–Finite Volume technique. We continue iterations until the convergence is reached.

Later, the iteration process between two mentioned pairs can be performed with the help of a solution of the convection-diffusion equation. This, however, involves additional implementation challenges and is beyond the scope of the current work.

Chapter 5

Numerical results

In this chapter we present numerical calculations for the mathematical model described in previous chapters. We start with some model problems and compare results with ones appeared in other researches.

All the calculations were made in in-house project MoonMD with some improvements. MoonMD provides mesh construction by using well known algorithm Triangle [39, 40] and a wide range of different finite element methods for Navier-Stokes and convection-diffusion equations. As an extra we have added the following implementations

- Discretization of the Young-Laplace equation as an integral equation;
- Boundary element method for the Laplace equation;
- Slip boundary condition for the Navier-Stokes equation;
- Discretization of the convective term of the convection-diffusion equation with Finite Volume Method;
- Algorithm for local mesh refinement.

5.1 Free surface computations

We start the solution process of the mathematical model (2.75) finding the numerical solution of the coupled problem of the Young-Laplace equation and the Laplace equation for azimuthal velocity (4.72). The solution technique was discussed in details in Sections 4.1, 4.2. Since the particle concentration is unknown it is considered to be uniform. It leads us to a discretization of the simplified Young-Laplace equation (4.18)

$$y_{i,k}^{j+1} = (-1)^{i+1} g(x_k^{j+1}, \widehat{\Phi}_i^j(x_k^j)), \quad x_k^{j+1} \in \Theta_i^{j+1}, \quad i = 1, 2,$$

$$\widehat{\Phi}_i(x^*) := h_s(0, y_i(0)) - \mathrm{Fr}_m \int_0^{x^*} \omega_i^2(x, y_i(x)) dx,$$

$$\mathrm{Pm} = h(0, y_{2,0}) - h(0, y_{1,0}), \quad U(y_1(0), y_2(0)) = U_0,$$

which corresponds to the problem in [31]. The sequences $\Theta^j_{f,i}$ (4.24) are generated by a uniform fragmentation of $[0, \zeta^j_i]$

$$\Theta^j_{f,i} := \{x_k = kh_i \in [0, \zeta^j_i]\}_{k=0}^{k=N}, \quad h_i = \frac{\zeta^j_i}{N}, \quad i = 1, 2$$

with ζ^j_i denoted according to (4.25)

$$\zeta^j_i = \sqrt{\left(\frac{\sin\beta}{\widehat{\Phi}^j_i(\zeta^j_i)}\right)^2 + \cos^2\beta}, \quad i = 1, 2.$$

The discrete domain is then determined as follows

$$\begin{aligned}\Omega_h := \big\{(x, y) \in \mathbb{R}^2 \ : \ & x > 0, \quad x < x_h(y), \\ & y_1(x) < y \quad \text{for} \quad x \in (0, \zeta_1), \quad y < y_2(x) \quad \text{for} \quad x \in (0, \zeta_2)\big\}.\end{aligned} \tag{5.1}$$

Here $x_h(y)$ is a polyline approximation of a right branch of hyperbola (2.26) between $y_1(\zeta_1)$ and $y_2(\zeta_2)$, functions $y_i(x)$ are understood as polylines constructed from the discrete curves $(x_k, y_{i,k})$, $i = 1, 2$, $k = \overline{0, N}$, index j is omitted for simplicity.

Choosing arbitrary mesh on $\Gamma^j_{h,s}$, which is a straight line, and using the polygonal boundary of Ω_h we construct grid Ξ by (4.4) for boundary element method. After that we solve the discrete problem for the Laplace equation (4.7) with coefficients (4.13), (4.14).

For the first step we should determine $\widehat{\Phi}^0$ which is taken for $\omega^0 = 0$ and can be also interpreted as $\mathrm{Fr}_m \to 0$. The stopping criteria is

$$\sum_{i=1}^{2}\sum_{k=0}^{N}(x^{j+1}_k - x^j_k)^2(y^{j+1}_{i,k} - y^j_{i,k})^2 < \varepsilon^2,$$

were ε denotes the tolerance.

In Tables 5.1 and 5.2 one can see the number of iterations needed to obtain a solution of the coupled system for zero ($\mathrm{Pm} = 0$) and critical ($\mathrm{Pm} = \mathrm{Pm}^*$) pressure drops, respectively. The remaining parameters are the domain area $U = 5$ and tolerance $\varepsilon = 10^{-9}$. We do not show examples for $\mathrm{Fr}_m > 0.5$, because in this case a better initial guess is needed.

Points per component	$\mathrm{Fr}_m = 0.1$	$\mathrm{Fr}_m = 0.25$	$\mathrm{Fr}_m = 0.5$
5	13	31	87
10	13	27	60
25	13	27	57
50	13	27	58
100	14	27	59

Table 5.1: Number of iterations between Young-Laplace and Laplace equations, Pm= 0.

As one can see, the number of points per component has almost no influence on the number of iterations. However, the more points on the boundary, the better interpolation we can achieve. So we choose 50 points per boundary component for further computations. The obtained free surface shapes are in good agreement with the results presented in [31].

Points per component	$\mathrm{Fr}_m = 0.1$	$\mathrm{Fr}_m = 0.25$	$\mathrm{Fr}_m = 0.5$
5	19	47	152
10	19	37	65
25	19	36	63
50	19	37	61
100	19	37	57

Table 5.2: Number of iterations between Young-Laplace and Laplace equations, Pm=Pm*.

5.2 Problem for azimuthal velocity

We present here computations for the azimuthal velocity obtained as a solution of the Laplace equation (2.75a)

$$\Delta\omega = 0 \tag{5.2}$$

with corresponding boundary conditions (2.76a). On Figure 5.1 the azimuthal velocity for different geometries, i.e. different Froude numbers Fr_m, is presented. These solutions are obtained by the Finite Element method and used for later calculus in Navier-Stokes equation.

Comparing results with ones presented in [31], which were calculated by the Boundary Element method, one can see that they are in a good agreement.

5.3 Navier-Stokes model problem

In that example we ignore the coupling between the Navier-Stokes and convection-diffusion equation (4.73) as it was done in [31]. The Navier-Stokes equation (2.75b) then is written as follows

$$\begin{aligned} (\mathbf{v}\cdot\nabla)\,\mathbf{v} - \operatorname{div}\,\sigma(\mathbf{v},p) &= \mathbf{e}_x\delta\omega^2, \\ \nabla\cdot\mathbf{v} &= 0 \end{aligned} \qquad \text{in } \Omega. \tag{5.3}$$

In [31] the Navier-Stokes equation was solved in vorticity–stream function formulation. We repeat the tests for velocity–pressure formulation using the same parameters and compare the results. On Figures 5.2, 5.3 one can see the representation of secondary flow as the main point of interest. Comparing the numerical tests we conclude that the structure of the secondary flow as well as its magnitude match the results in [31].

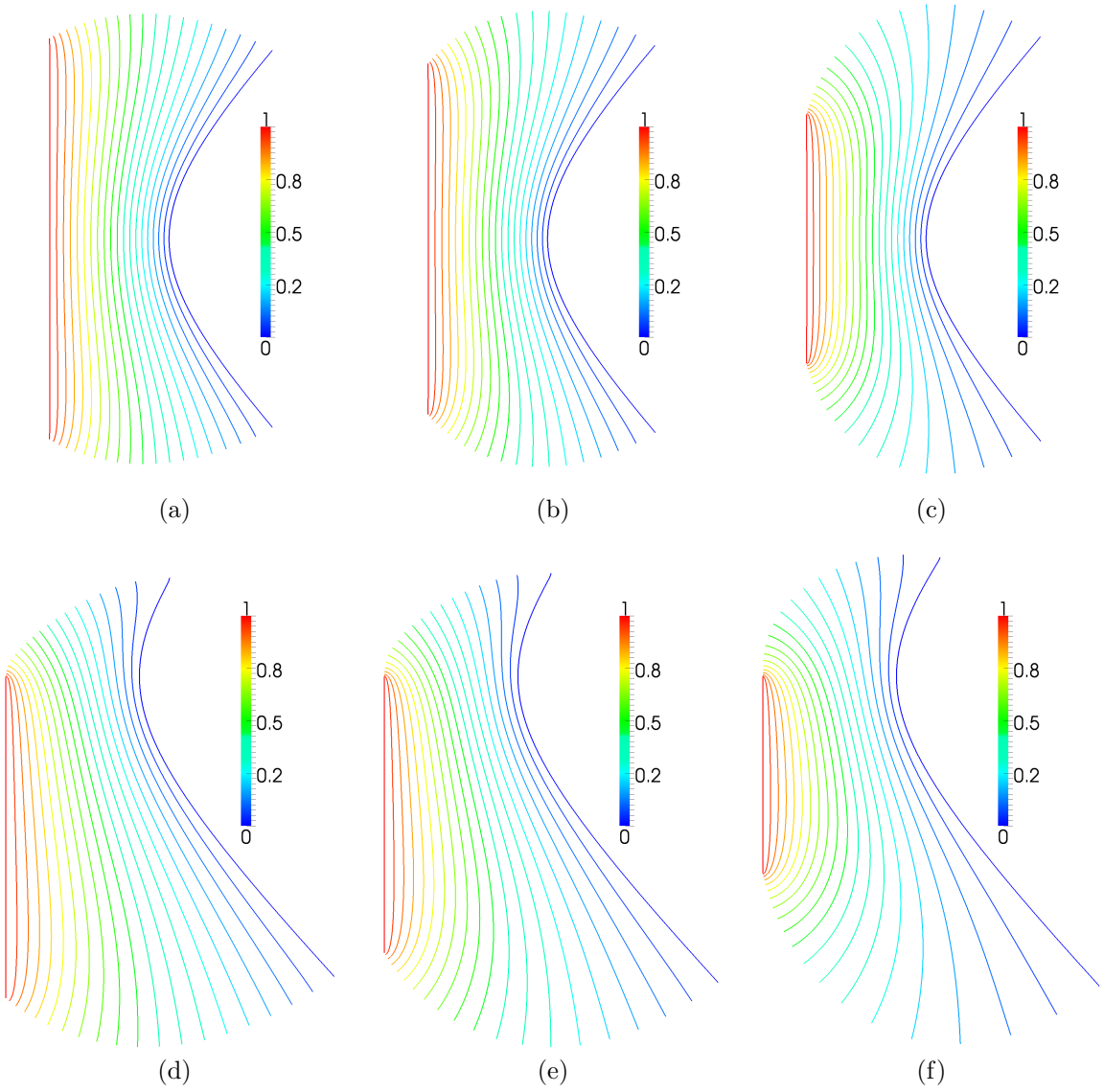

Figure 5.1: Isolines of the azimuthal velocity for zero (a-c) and critical (d-f) pressure drops. $\mathrm{Fr}_m = 0.1; 0.25; 1$, $\mathrm{Re} = 63.2456; 100; 200$, from left to right.

5.4 Convection-Diffusion model problems

We start with simple tests for the general convective-diffusive type problem (3.25) with zero right hand side

$$\begin{aligned} -\nabla \cdot (\nabla c - \boldsymbol{\alpha} c) &= 0 \quad \text{in } \Omega, \\ (\nabla c - \boldsymbol{\alpha} c) \cdot \mathbf{n} &= 0 \quad \text{on } \Gamma. \end{aligned} \tag{5.4}$$

The homogeneous problem means we compute the kernel $\widehat{c}$ of the associated operator with $\int_{\Omega_h} \widehat{c}\, dx/|\Omega_h| = 1$. The problems with known analytical solutions are chosen, in order to

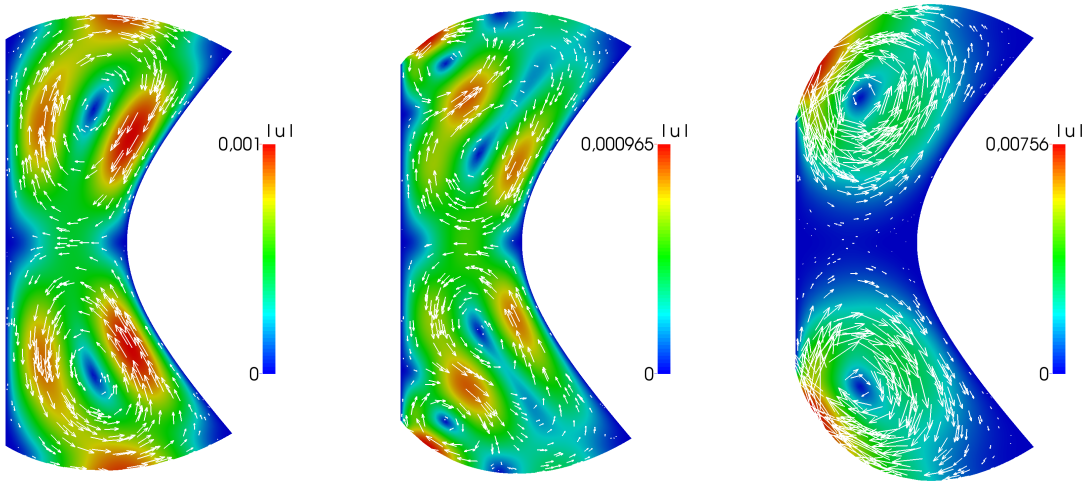

Figure 5.2: Secondary flow for no pressure drop. $\mathrm{Fr}_m = 0.1; 0.25; 1$, $\mathrm{Re} = 63.2456; 100; 200$, from left to right.

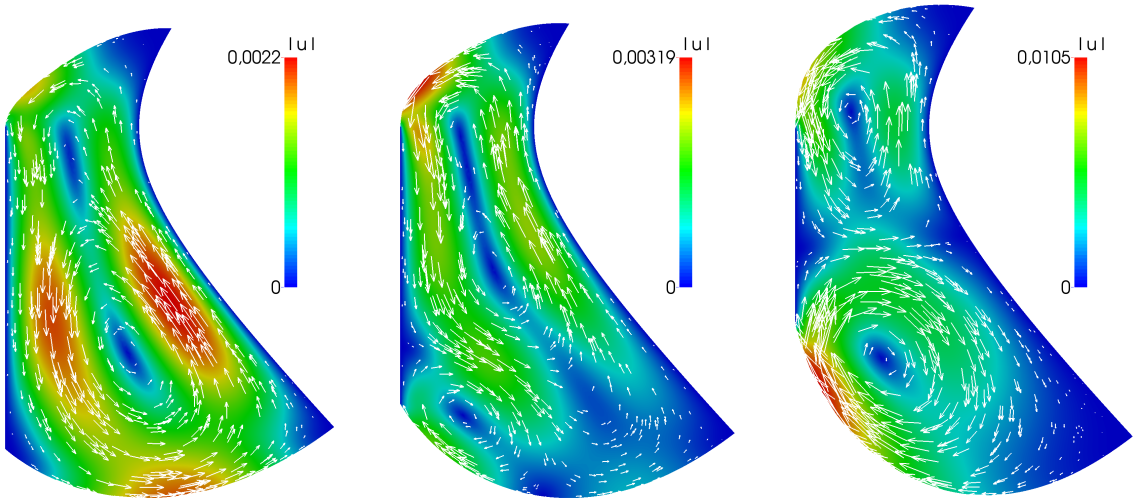

Figure 5.3: Secondary flow for critical pressure drop. $\mathrm{Fr}_m = 0.1; 0.25; 1$, $\mathrm{Re} = 63.2456; 100; 200$, from left to right.

estimate convergence rates. We test discretizations by a mixed Finite Element–Finite Volume technique on a weakly acute triangulation (4.61) and on Delaunay triangulation (4.70).

5.4.1 Academic test problems

We repeat the tests cases 1 and 2 from [21] on weakly acute and Delaunay triangulations. The problem is considered in a unit square domain $\Omega = (0,1) \times (0,1)$. We denote the decomposition of the domain Ω by a weakly acute triangulation as $\Omega_{h,a}$ and by Delaunay

triangulation as $\Omega_{h,D}$. The discrete domain $\Omega_{h,a}$ on level 0 consists of two triangles. Next level meshes are constructed by sequential refinement of each triangle into four ones of equal area. The mesh $\Omega_{h,D}$ is constructed by the Delaunay triangulation of the domain Ω for a given set of the boundary points. Since we want these meshes to be as similar as possible, we define $\partial\Omega_{h,D} := \partial\Omega_{h,a}$. In order to have the similar number of degrees of freedom, the constraint on the maximum triangle area was taken as $\frac{3}{4}h^2$, where h is a distance between two neighboring boundary nodes (mesh size of $\partial\Omega_{h,D}$).

On Figures 5.4 one can see discrete domains $\Omega_{h,a}$ and $\Omega_{h,D}$ for different levels, respectively.

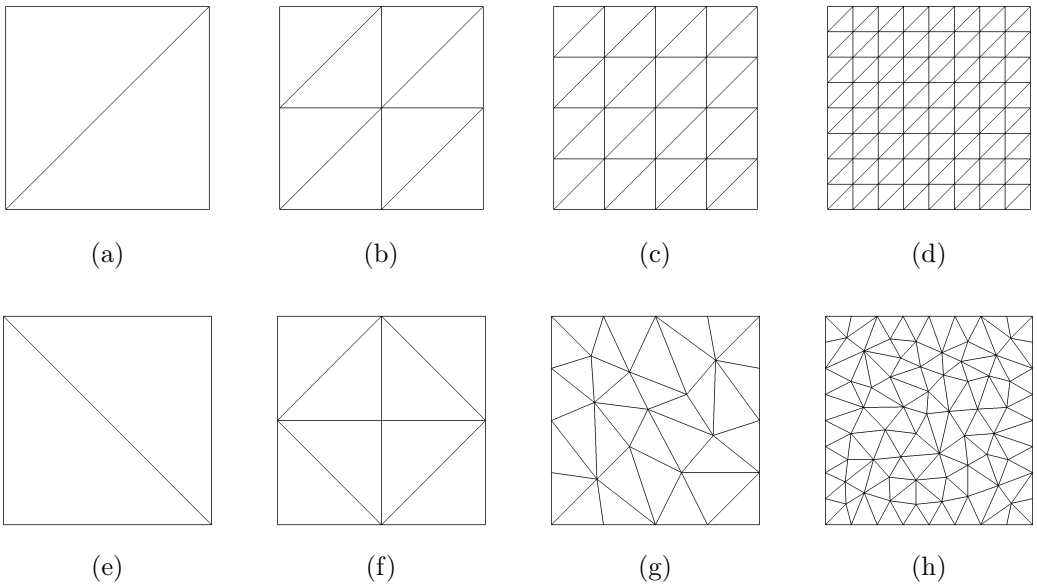

Figure 5.4: Meshes on level 0 to 3 from left to right on $\Omega_{h,a}$ (a-d) and $\Omega_{h,D}$ (e-h)

In Table 5.3 one can see comparison of the meshes on different levels. In most cases $\Omega_{h,D}$ has a slightly larger number of DOFs and cells than $\Omega_{h,a}$, in some cases the numbers for both meshes are equal. In the following examples we provide the errors in L^2 and H^1 norms as well as minimum and maximum values.

Test case 1. The first example takes a strong but constant convection field

$$\boldsymbol{\alpha} = \nabla\Psi(x,y)^T = (40,0)^T, \quad \Psi(x,y) = 40x,$$

which does not satisfy the coercivity condition (3.29). The scaled analytical solution is given by

$$c(x,y) = \frac{40}{1-\exp(-40)}\exp(-40(1-x)).$$

In Table 5.4 the minimum and maximum values of discrete solutions are given. Like in [21] we consider also a numerical solution obtained by a standard Galerkin Finite Element method. One can see that this method provide huge oscillations of solution on

	$\Omega_{h,a}$		$\Omega_{h,D}$	
level	DOFs	cells	DOFs	cells
0	4	2	4	2
1	9	8	9	8
2	25	32	26	34
3	81	128	81	128
4	289	512	293	520
5	1089	2048	1131	2132
6	4225	8192	4404	8550
7	16641	32768	17411	34308
8	66049	131072	69727	138428
9	263169	524288	277522	552994
10	1050625	2097152	1109514	2214930

Table 5.3: Number of degrees of freedom and triangles of $\Omega_{h,a}$ and $\Omega_{h,D}$ on different levels.

coarser meshes, while the mixed Finite Element–Finite Volume discretization provides positive values for the weakly acute and Delaunay triangulations on all mesh levels. The used upwind function is Scharfetter-Gummel. The errors of the discrete solutions are presented on Figure 5.5.

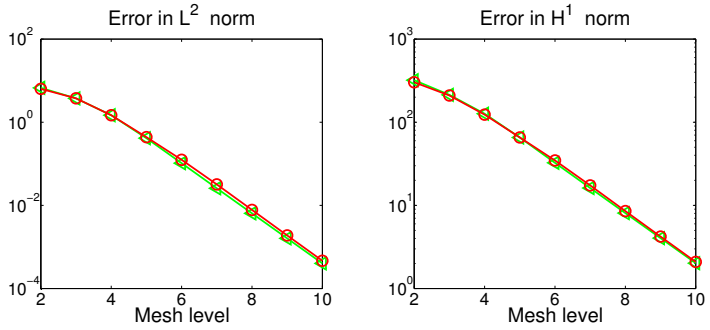

Figure 5.5: Errors for test case 1. On $\Omega_{h,a}$ - green triangles, on $\Omega_{h,D}$ - red circles.

Test case 2. The second example corresponds to a nonconstant convection field

$$\boldsymbol{\alpha} = \nabla\Psi(x,y)^T, \quad \Psi(x,y) = \log(1+x+y-2xy).$$

One can show that $\nabla \cdot \boldsymbol{\alpha} < 0$ and $\boldsymbol{\alpha} \cdot \mathbf{n}$ changes sign along Γ, i.e. the coercivity conditions (3.29) are not satisfied. The scaled solution is given by

$$c(x,y) = \frac{2}{3}(1+x+y-2xy).$$

The errors in H^1 and L^2 norms are presented on Figure 5.6.

level	Minimum value			Maximum value		
	$\Omega_{h,a}$ FE–FV	$\Omega_{h,D}$ FE–FV	$\Omega_{h,a}$ Galerkin	$\Omega_{h,a}$ FE–FV	$\Omega_{h,D}$ FE–FV	$\Omega_{h,a}$ Galerkin
2	3.39837e-17	3.44112e-17	-68.2520	7.99927	8.0999	96.6648
3	6.70638e-17	6.43539e-17	-33.1906	15.7858	15.1479	62.2907
4	1.15322e-16	1.16186e-16	-9.77680	27.1451	27.3484	49.9365
5	1.50793e-16	1.51329e-16	-5.28308e-17	35.4944	35.6206	44.1083
6	1.64610e-16	1.64407e-16	2.99895e-17	38.7468	38.6991	41.5351
7	1.68565e-16	1.68534e-16	1.13334e-16	39.6776	39.6705	40.5251
8	1.69589e-16	1.69594e-16	1.53708e-16	39.9188	39.9199	40.1679
9	1.69848e-16	1.69850e-16	1.65706e-16	39.9797	39.9803	40.0511
10	1.69913e-16	1.69913e-16	1.68859e-16	39.9949	39.9951	40.0151

Table 5.4: Test case 1. Minimum and maximum values of the discrete solutions for different meshes and methods.

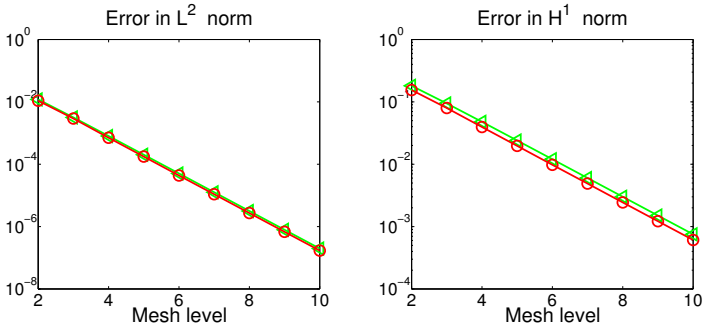

Figure 5.6: Errors for test case 2. On $\Omega_{h,a}$ - green triangles, on $\Omega_{h,D}$ - red circles.

Conclusions. The both examples show that more general Delaunay triangulation does not decrease the accuracy of numerical solution. In both cases the errors for two meshes show similar values and qualitative behavior. Convergence rates in H^1 norm satisfy the theoretical predictions. The errors in L^2 norm have second order of convergence due to the choice of Scharfetter-Gummel upwinding.

5.4.2 Seal-related problem

In this section we find a discrete solution of the Convection-Diffusion equation in the domain, corresponding to the seal shape. We want to find two discrete solutions of the problem with the same method but on different meshes. Using the fact that the convection-diffusion equation (2.75c), (2.76c) has an exact solution in case of no flow [33], we can measure the errors. The equation (5.4) with $\boldsymbol{\alpha}$ given by (3.24) and zero velocity

field is as follows

$$\begin{aligned} \nabla \cdot (\nabla c - c\xi L(\xi h_s) \nabla h_s) = 0 \quad &\text{in } \Omega, \\ (\nabla c - \boldsymbol{\alpha} c) \cdot \mathbf{n} = 0 \quad &\text{on } \Gamma, \end{aligned} \tag{5.5}$$

where $L(\cdot)$ denotes the Langevin function (2.30), ξ the dimensionless Langevin parameter (2.31), h_s is an analytical expression of the magnetic field strength (2.27).

The analytical solution has the following form [33]

$$c = \frac{\varphi |\Omega|}{\int_\Omega \varphi \, dx} \tag{5.6}$$

with φ denoted by

$$\varphi(h_s) = \exp\left(\int_0^{\xi h_s} L(\gamma) \, d\gamma \right) = \frac{\sinh(\xi h_s)}{\xi h_s}.$$

The exact solution (5.6) represents the concentration of magnetic particles in a ferrofluid seal in no flow case. One can expect a high pick at the region where h_s reaches its maximum, especially for high values of ξ. Knowing form of h_s given by (2.27) and the fact, that the domain Ω is bounded by two analytical curves, one can conclude that the maximum is obtained at the point $(1, 0)$ corresponding to the pick of the concentrator.

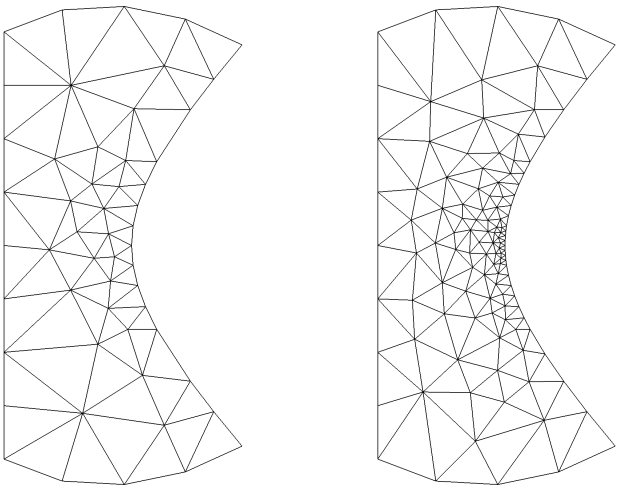

Figure 5.7: Examples of meshes with and without local mesh refinements.

The local mesh refinement can be used there in order to improve the numerical solution. On Figure 5.7 one can see the example of the mesh with and without local mesh refinement. Using the exact solution (5.6) we can also measure the errors. One can see these results for two choices of ξ on Figure 5.8.

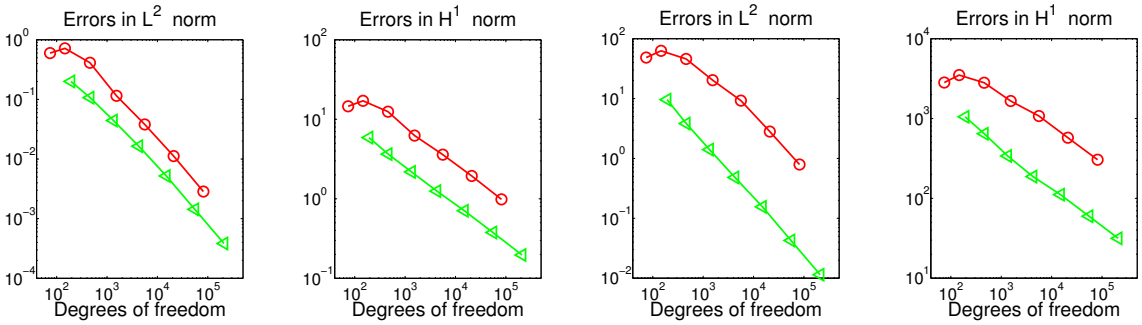

(a) (b) (c) (d)

Figure 5.8: Errors in L^2 and H_1 norms for different values of ξ, $\xi = 10$ (a,b), $\xi = 50$ (c,d)

5.5 Coupled NSE–CDE system

The system of Navier-Stokes (2.75b) and convection-diffusion equation (2.75c)

$$\begin{aligned} (\mathbf{v}\cdot\nabla)\,\mathbf{v} - \operatorname{div}\,\sigma(\mathbf{v},p) &= \mathbf{e}_x\delta\omega^2 + \frac{\delta}{\mathrm{Fr}_m}cL(\xi h_s), \\ \nabla\cdot\mathbf{v} &= 0, \\ -\frac{1}{\mathrm{Pe}}\nabla\cdot\left(\nabla c - c\xi L(\xi h_s)\nabla h_s\right) + \mathbf{v}\cdot\nabla c &= 0 \end{aligned} \tag{5.7}$$

is solved iteratively, one equation after another. At this point we use calculations of free surface providing the domain Ω, and azimuthal velocity ω, which were done in Sections 5.1 and 5.2, respectively. We use shapes for either zero or critical pressure drops.

For a better convergence of iterations the relaxation technique was used. Let us define the solution operators $N(\mathbf{v}, c)$ and $S(c)$ of the Navier-Stokes and convection-diffusion equations, respectively. The choice of operators corresponds to some fixed constants, i.e. Reynolds, Péclet, magnetic Froude number, and Langevin coefficient. Then one can use relaxation in the following way

$$\begin{aligned} \mathbf{v}_i &= N(\widetilde{\mathbf{v}}_{i-1}, \widetilde{c}_{i-1}) \\ \widetilde{\mathbf{v}}_i &= \beta_1\mathbf{v}_i + (1-\beta_1)\mathbf{v}_{i-1} \\ c_i &= S(\widetilde{\mathbf{v}}_i) \\ \widetilde{c}_i &= \beta_2 c_i + (1-\beta_2)c_{i-1}, \end{aligned} \tag{5.8}$$

where β_1, $\beta_2 \in (0, 1]$ are relaxation constants, $\mathbf{v}_i$ and c_i solutions on the i-th iteration step, $\widetilde{\mathbf{v}}_i$ and $\widetilde{c}_i$ relaxed solutions.

The initial choice of concentration and secondary flow is taken as follows. The particle concentration is uniform ($c_0 = 1$) and the secondary flow is zero ($\mathbf{v}_0 = 0$). The first numerical tests have shown that provided iteration technique converges to a solution not for all parameter values. To improve the convergence we use intermediate steps. It means we change the parameter values in order to lower the coupling between equations. The

obtained solution is later used as an improved initial guess. In order to have a better overview of convergence for different parameter values, all the presented results were commuted separately, every time starting with the initial guess $c_0 = 1$, $\mathbf{v}_0 = 0$.

5.5.1 Local mesh refinement

The local mesh refinement can increase the accuracy of the discrete solution in problematic regions, providing generally a better solution. Local refinement is applied at regions which were defined empirically. It happens that in these areas the secondary flow is especially low and can miss the correct direction. Probably here lies the answer, why the more accurate secondary flow helps to achieve a better precision of particle distribution.

On Figure 5.9 one can see the difference between regular mesh and mesh with local refinement. The regions of refinement can be divided into three categories: the area near concentrator, corners, central area on the shaft. Some of them are bounded with boxes and marked with numbers 1, 2, 3, respectively.

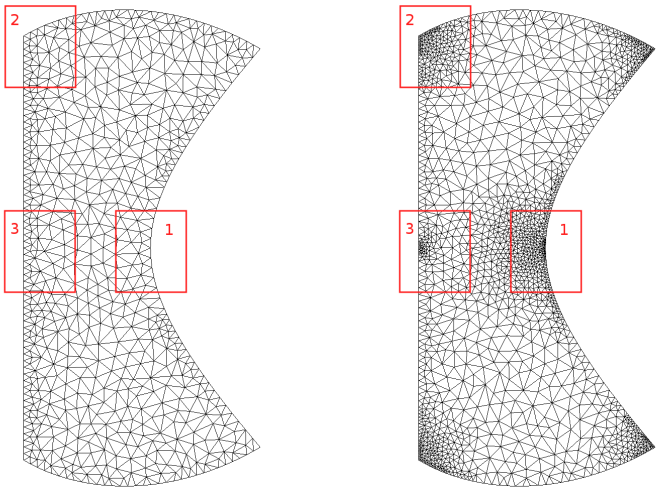

(a) (b)

Figure 5.9: Mesh structure with (a) and without (b) local mesh refinement.

On Figure 5.10 solutions on the regular and refined meshes are presented. On Figures 5.11, 5.12, 5.13 one can see how the local mesh refinement improves the solution of convection-diffusion equation locally. All solutions are presented with color scheme of a solution on the refined mesh for a better view.

5.5.2 Coupled system for no pressure drop

We present typical solutions obtained for a wide parameter range in case of no pressure drop. Zero pressure drop causes the domain Ω to be symmetric with respect to x-axis. We choose the parameter values according to evaluations in Section 2.4. The Reynolds

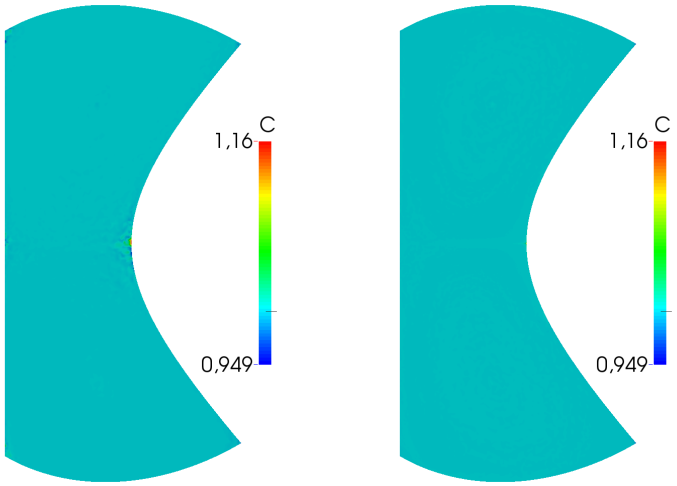

(a) (b)

Figure 5.10: Solutions on regular (a) and locally refined (b) meshes.

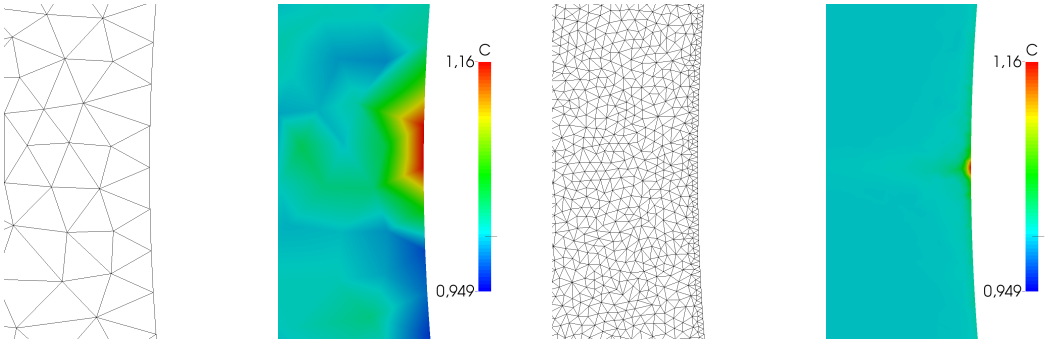

(a) (b) (c) (d)

Figure 5.11: Difference in computations of particle distribution, region 1. Regular mesh (a–b) and locally refined (c–d).

number is fixed to 100 as an average of the given values. Langevin parameter ξ changes in a small region, which is nevertheless enough for a significant influence on the solution of the coupled system. The magnetic Froude number Fr_m is related to the domain shape and varied in a given range, that is between 0.1 and 1. For values of Péclet number greater than 10^9 we observe in some cases numerical instability. That is why the lower values of the parameter are considered.

On Figure 5.14 one can compare the secondary flow and particle concentration computed for the coupled system (5.7) with the solution of independent problems (5.3) and (5.5). In Table 5.5 the maximum of particle concentration, as one of the most important characteristics, for the coupled system is listed. Empty cells mean the coupled solution was not obtained for that choice of constants.

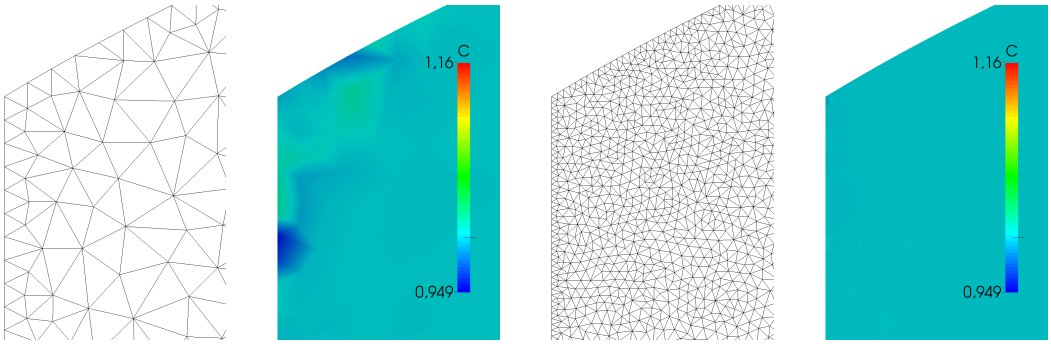

(a) (b) (c) (d)

Figure 5.12: Difference in computations of particle distribution, region 2. Regular mesh (a–b) and locally refined (c–d).

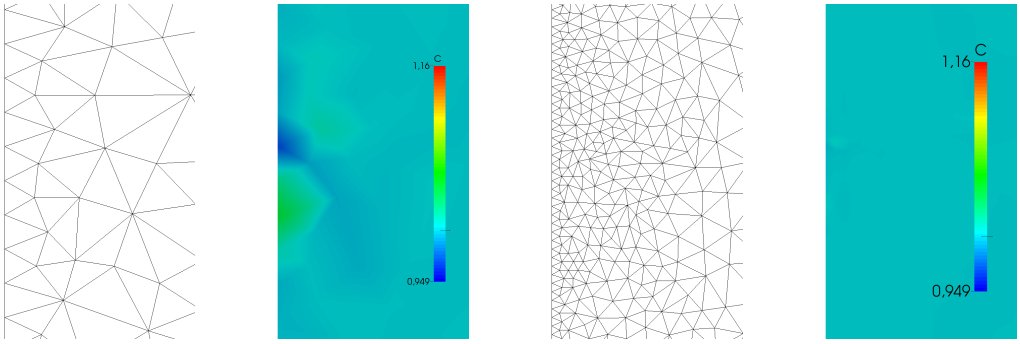

(a) (b) (c) (d)

Figure 5.13: Difference in computations of particle distribution, region 3. Regular mesh (a–b) and locally refined (c–d).

Analyzing the results in the table, one can conclude that the coupled system converges either for almost uniform particle concentration (right part, large Péclet number) or for non disturbed particle concentration (left part, small Péclet number).

The secondary flow on Figure 5.14 is almost equivalent in structure and magnitude for both the concentration independent Navier-Stokes equation (5.3) and the Navier-Stokes equation in the coupled system (5.7). At the same time graphs for particle concentration differ much more. On Figures 5.15 one can see difference of secondary flows for the mentioned cases. We plot the magnitude $|\mathbf{v}|$ over the line $((0,0);(1,0))$, which splits the domain into two equal parts. One can observe on the figure that two secondary flows differ only slightly in magnitude along this line. But in region approximately between 0.9 and 1, where the highest particle concentration is reached, secondary flow for the coupled system is up to several orders lower than for concentration independent problem. It can be expressed in the way that high particle concentration prevents fluid motion.

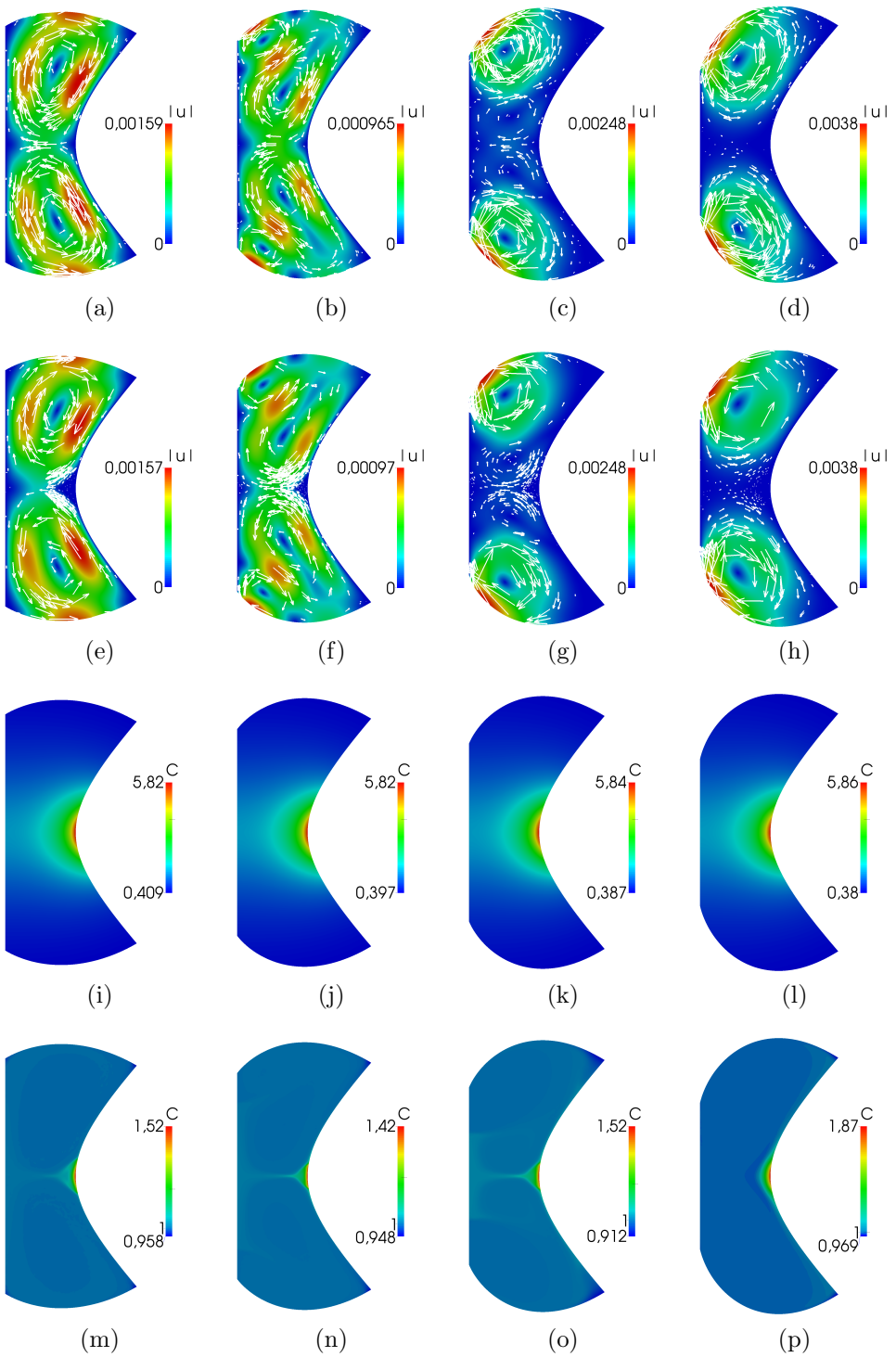

Figure 5.14: Computations of secondary flow (a–h) and particle concentration (i–p) as concentration independent (a–d), (i–l) and coupled (e–h), (m–p) problems. Re = 100, Pe = 10^7, $\xi = 6$, $\mathrm{Fr}_m = 0.1; 0.25; 0.5; 1$ from left to right. Zero pressure drop.

	$\mathrm{Pe} = 10^5$	$\mathrm{Pe} = 10^6$	$\mathrm{Pe} = 10^7$	$\mathrm{Pe} = 10^8$	$\mathrm{Pe} = 10^9$	$\mathrm{Pe} = 10^{10}$
$\mathrm{Fr}_m = 0.1$						
$\xi = 2$	1.246	1.127	1.061	1.026	1.011	1.007
$\xi = 6$	–	–	1.523	1.149	1.064	1.036
$\xi = 10$	–	–	–	1.312	1.117	–
$\mathrm{Fr}_m = 0.25$						
$\xi = 2$	1.227	1.122	1.060	1.027	1.012	1.009
$\xi = 6$	5.607	–	1.420	1.163	1.064	1.028
$\xi = 10$	–	–	–	1.309	1.127	1.054
$\mathrm{Fr}_m = 0.5$						
$\xi = 2$	1.305	1.137	1.067	1.031	1.013	1.032
$\xi = 6$	4.908	–	1.522	1.190	1.072	–
$\xi = 10$	16.80	–	–	1.370	1.147	–
$\mathrm{Fr}_m = 1$						
$\xi = 2$	1.235	1.178	1.148	1.067	1.024	1.019
$\xi = 6$	3.881	2.482	1.867	–	–	1.058
$\xi = 10$	13.39	–	–	–	–	1.109

Table 5.5: The maximum of the concentration achieved for the coupled system, $\mathrm{Re} = 100$, no pressure drop ($\mathrm{Pm} = 0$).

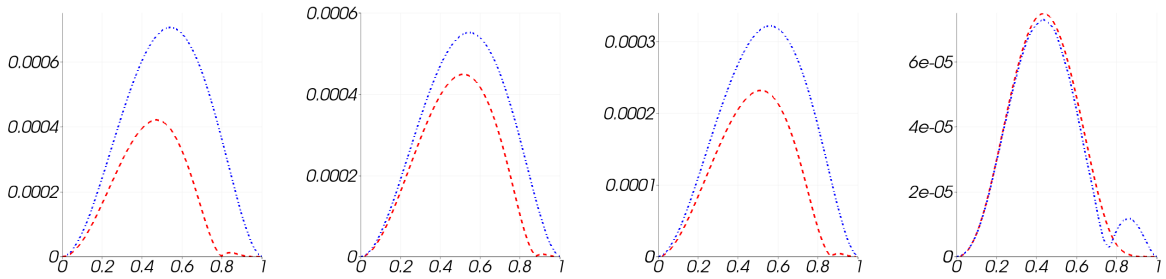

(a) (b) (c) (d)

Figure 5.15: Magnitude of the secondary flow for the coupled system and independent from particle concentration measured over line $((0,0);(1,0))$, $\mathrm{Re} = 100$, $\mathrm{Pe} = 10^7$, $\xi = 6$, $\mathrm{Fr}_m = 0.1; 0.25; 0.5; 1$ from left to right. Red dashed line - coupled system, blue dotted line - independent problem.

5.5.3 Coupled system for critical pressure drop

We solve the coupled system once more for different domain geometry, which is set by critical pressure drop. We considered the same set of parameters. However, these results are less interesting, since we have got almost uniform particle concentration even for low Péclet numbers and almost not dependent on the magnetic Froude number. On Figure 5.16 one can see that with changing Fr_m globally different secondary flows provide very similar location of an area of high particle concentration together with the similar magnitude.

We present the Figure 5.17 comparing the secondary flow for the coupled system and concentration independent case. The difference in flows is much lower than in case of no pressure drop, that is Figure 5.15. However, one can still observe the high difference in a region of varying concentration. The values are calculated along the line from the origin to the right-up corner.

5.5.4 Particle concentration on a free surface

One of our goals is to understand whether iterations between two subsystems (4.72) and (4.73) are required. In Section 5.1 we solved (4.72) with simplified Young-Laplace equation (4.18), since the particle concentration is unknown at that point. However, if particle concentration is sufficiently uniform along the free surface, we can conclude that iterations between subsystems are unnecessary and our solution is close to the solution of the whole system (2.75). The following figures show that fluid motion makes the ferrofluid on free surfaces much closer to uniform, comparing to the solution of velocity independent convection-diffusion equation (5.5).

Either for critical or for zero pressure drop we draw the particle concentration along the upper free surface. In case of zero pressure drop we do it because of symmetry, in case of critical - because on the upper surface the particle distribution is less uniform. On Figure 5.18 the typical distribution of magnetic particles on a free surface in case of no fluid motion is presented. As one can see, for sufficiently high Langevin parameter ξ, i.e. high magnetic field intensity, fluid becomes up to ten times more dilute, then uniform.

On Figure 5.19 pictures for the solutions of the coupled system (4.73) for different values of magnetic Froude number and Langevin parameter are considered. One can see, that graphs look very similar either for different pressure drops, or different parameter values. The particles concentration becomes almost uniform except the small area near the concentrator, which in its turn will hardly change the behavior of ferrofluid in case of iterations between subsystems (4.72) and (4.73).

5.5.5 Different fluid volume

In this subsection we present the results obtained for different fluid volumes. We model only the case of zero pressure drop, since we find it more interesting. All the previous results were obtained for the volume $U_0 = 5$. We consider two volumes 2 and 10 in addition to have a better overview of the problem. The result of convergence along with

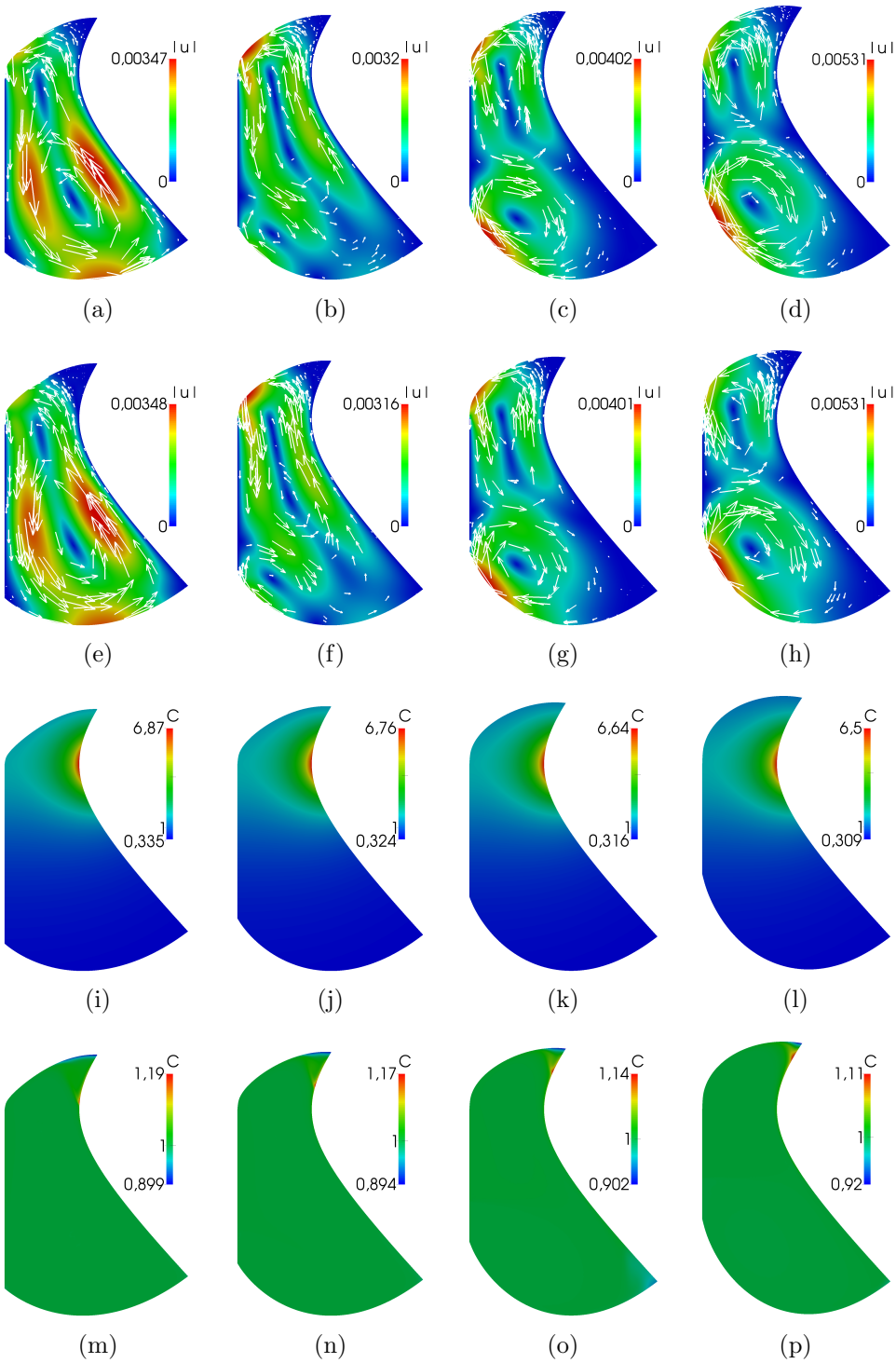

Figure 5.16: Computations of secondary flow (a – h) and particle concentration (i – p) as independent (a – d), (i – l) and coupled (e – h), (m – p) problems. Re = 100, Pe = 10^7, $\xi = 6$, $\mathrm{Fr}_m = 0.1; 0.25; 0.5; 1$ from left to right. Critical pressure drop.

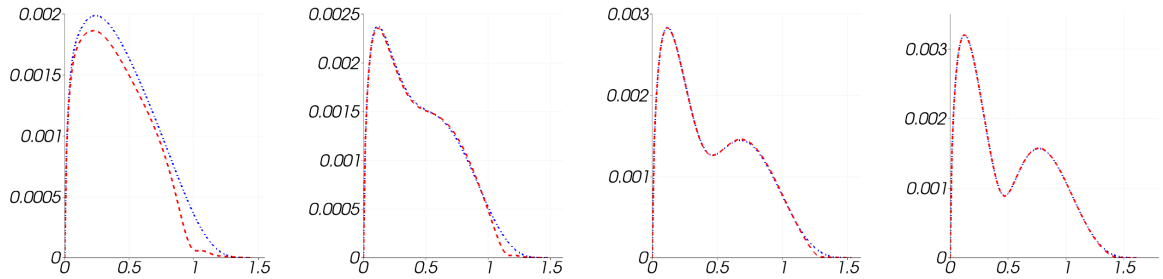

Figure 5.17: Magnitude of the secondary flow for the coupled system and independent from particle concentration measured over line from the origin to the right-up corner, Re = 100, Pe = 10^7, $\xi = 6$, $\mathrm{Fr}_m = 0.1; 0.25; 0.5; 1$ from left to right. Red dotted line - coupled system, blue dashed line - independent problem.

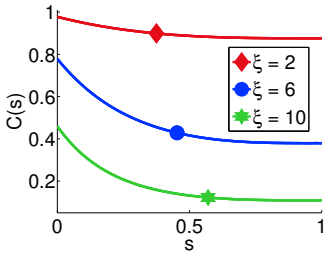

Figure 5.18: Distribution of magnetic particles along the upper free surface, no fluid motion.

the final particle concentration are presented in Tables 5.7 and 5.8. The results for the fluid volume $U_0 = 2$ are calculated only for values of magnetic Froude number lower than 0.5, since for higher values our method becomes unstable. A better choice of the boundary points for the Young-Laplace equation may help with this problem.

One can see in Table 5.6 that the maximum concentration of magnetic particles in a non-disturbed state is directly dependent on the fluid volume. This effect has been also observed in [33]. But with increasing of the Péclet number, i.e. the influence of a fluid motion, the situation changes significantly. It is especially seen for the case $U_0 = 10$. With Péclet number greater than 10^6 the solution demonstrates lower particle concentration together with incredible convergence comparing to case $U_0 = 5$, Table 5.5.

	$U_0 = 2$	$U_0 = 5$	$U_0 = 10$
$\xi = 2$	1.31	1.44	1.55
$\xi = 6$	3.66	5.82	8.76
$\xi = 10$	9.36	19.2	35.5

Table 5.6: Approximate maximum of concentration for given parameters.

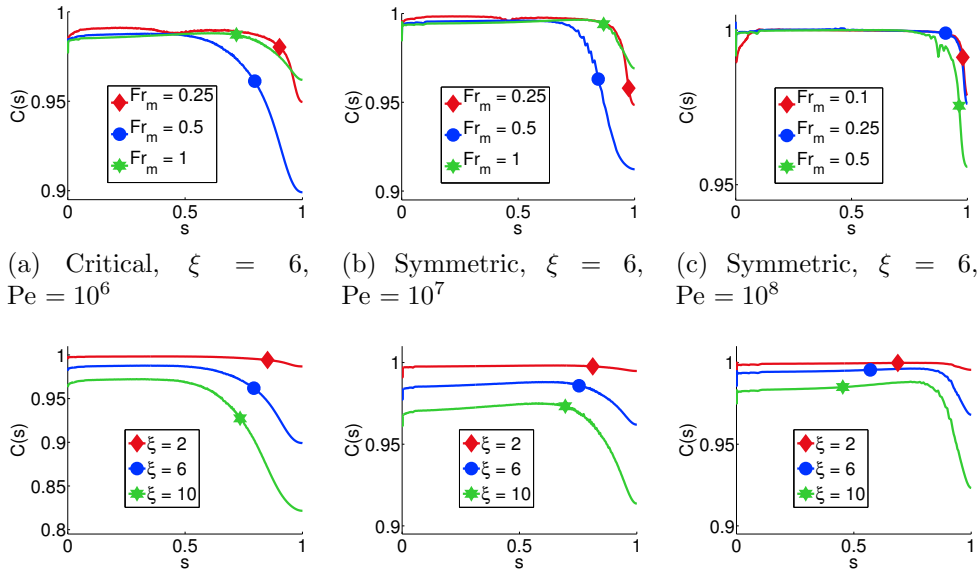

(a) Critical, $\xi = 6$, $\mathrm{Pe} = 10^6$ (b) Symmetric, $\xi = 6$, $\mathrm{Pe} = 10^7$ (c) Symmetric, $\xi = 6$, $\mathrm{Pe} = 10^8$

(d) Critical, $\mathrm{Fr}_m = 0.5$, $\mathrm{Pe} = 10^6$ (e) Critical, $\mathrm{Fr}_m = 1$, $\mathrm{Pe} = 10^6$ (f) Symmetric, $\mathrm{Fr}_m = 1$, $\mathrm{Pe} = 10^7$

Figure 5.19: Distribution of magnetic particles along the upper free surface, solutions of the coupled system (4.73).

	$\mathrm{Pe} = 10^5$	$\mathrm{Pe} = 10^6$	$\mathrm{Pe} = 10^7$	$\mathrm{Pe} = 10^8$	$\mathrm{Pe} = 10^9$	$\mathrm{Pe} = 10^{10}$
$\mathrm{Fr}_m = 0.1$						
$\xi = 2$	1.313	1.262	1.163	–	–	–
$\xi = 6$	–	–	–	–	–	–
$\xi = 10$	–	–	–	–	–	–
$\mathrm{Fr}_m = 0.25$						
$\xi = 2$	1.228	1.069	1.03	1.014	1.012	1.012
$\xi = 6$	3.698	–	–	1.069	1.03	–
$\xi = 10$	9.515	–	–	1.134	1.056	–

Table 5.7: Maximum of the concentration achieved for the coupled system, $\mathrm{Re} = 100$, $U_0 = 2$.

The pictures showing the secondary flow for different Froude numbers are presented on Figures 5.20 and 5.21.

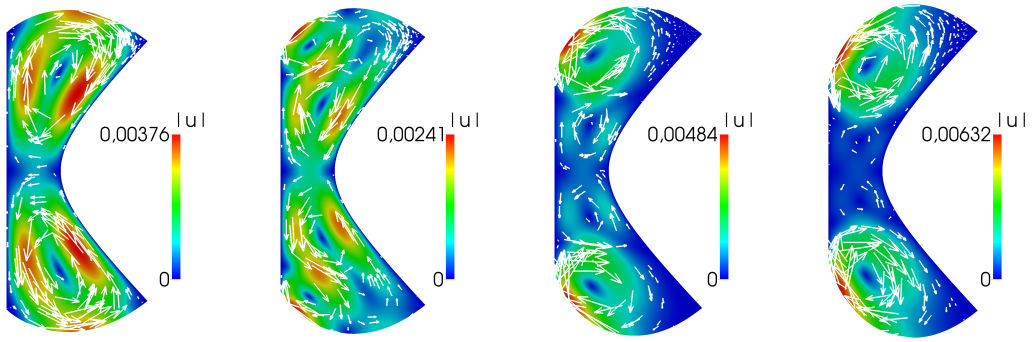

Figure 5.20: Secondary flow provided by the problem (5.3), Re = 100, $U_0 = 10$, $\mathrm{Fr}_m = 0.1; 0.25; 0.5; 1$ form left to right.

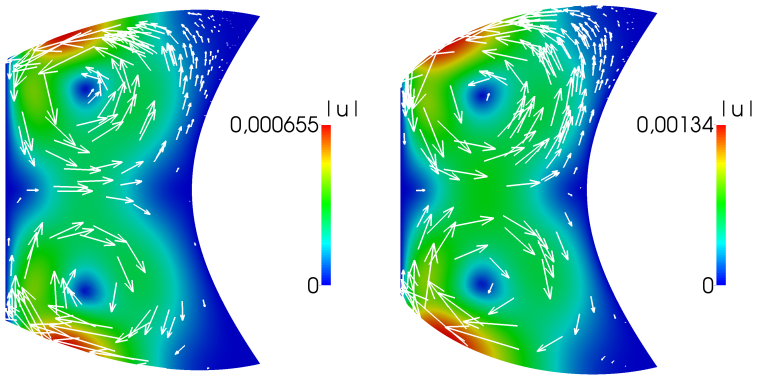

Figure 5.21: Secondary flow provided by the problem (5.3), Re = 100, $U_0 = 2$, $\mathrm{Fr}_m = 0.1; 0.25$ form left to right.

	$\mathrm{Pe} = 10^5$	$\mathrm{Pe} = 10^6$	$\mathrm{Pe} = 10^7$	$\mathrm{Pe} = 10^8$	$\mathrm{Pe} = 10^9$	$\mathrm{Pe} = 10^{10}$
$\mathrm{Fr}_m = 0.1$						
$\xi = 2$	1.23	1.119	1.056	1.024	1.01	1.007
$\xi = 6$	–	–	1.409	1.139	1.058	1.038
$\xi = 10$	–	–	–	1.273	1.107	–
$\mathrm{Fr}_m = 0.25$						
$\xi = 2$	1.2	1.106	1.052	1.024	1.019	1.019
$\xi = 6$	–	–	1.331	1.14	1.051	1.021
$\xi = 10$	–	–	1.826	1.269	1.105	1.039
$\mathrm{Fr}_m = 0.5$						
$\xi = 2$	1.201	1.106	1.052	1.024	1.025	1.028
$\xi = 6$	5.979	1.893	1.336	1.131	1.049	1.03
$\xi = 10$	–	–	1.712	1.275	1.096	1.038
$\mathrm{Fr}_m = 1$						
$\xi = 2$	1.216	1.11	1.055	1.025	1.011	1.011
$\xi = 6$	5.342	1.87	1.333	1.132	1.052	1.02
$\xi = 10$	21.66	5.331	1.746	1.274	1.099	1.037

Table 5.8: Maximum of concentration achieved for the coupled system, $\mathrm{Re} = 100$, $U_0 = 10$.

Chapter 6

Summary

In this thesis a mathematical model of the ferrofluid rotary seal is considered. This model is based on the existing studies. While deriving one can make particular assumptions, which essentially simplify the system of equations. However, the influence of these simplifications reduces the model accuracy. Therefore, a more complex and, at the same time, more general model may reveal better properties. We derive such a model and provide a robust numerical discretization of it.

The constructed mathematical model consists of an integro-differential and three partial differential equations, and is hard to handle. Each equations of the system was studied separately. Simple discretization of the Young-Laplace equation followed previous studies. Discretization of the Laplace equation was done twice with Boundary Element and Finite Element methods. The Boundary Element method is more convenient for incorporation with the Young-Laplace equation. However, the Finite Element discretization was used for a better connection with the remaining numerical approximations. The Navier-Stokes equation with slip boundary conditions was solved in a velocity-pressure formulation. For the convection-diffusion equation a mixed Finite Element–Finite Volume method on a weakly acute triangulation was suggested. This mixed discretization is related to an existing Finite Volume discretization, which allowed to prove the unique solvability and other important properties of the scheme. Moreover, the stability of it was shown. Further investigations allowed to extend this discretization to a more general Delaunay triangulation with preserving its properties.

We did the validation of the discretizations, comparing our computations with ones given in other studies. Due to complexity of the whole system we introduced the decoupling procedure. The system of equations was split into two subsystems, each of which was solved iteratively. The main part of it is a nonlinear subsystem of the Navier-Stokes and the convection-diffusion equations. Their interaction has not been considered up to now in the related studies. Finally, we calculated the result of coupling of two effects of fluid motion and particle concentration. The obtained results showed that this interaction plays an important role and cannot be neglected.

In a future work we would like to improve the following aspects. Numerical calculations

indicated a particular directions in which the further investigations can be done. In particular, the parameter range of good convergence of the iterative scheme can be studied in more details. The introduced iteration method can be improved, or a new one can be suggested, in order to provide a better convergence. Another possible approach is the derivation of a more complex mathematical model, which describes more physical effects. It may add new equations, complicate the investigated equations, or even introduce a time-dependent system.

Bibliography

[1] I. Anton, I. De Sabata, L. Vékás, I. Potencz, and S. E. Magnetic fluid seals: some design problems and application. *Journal of Magnetism and Magnetic Materials*, 65:379–381, 1987.

[2] E. Bänsch and K. Deckelnick. Optimal error estimates for Stokes and Navier-Stokes equations with slip-boundary condition. *Mathematical Modelling and Numerical Analysis*, 33:923–938, 1999.

[3] E. Bänsch and B. Höhn. Numerical treatment of the Navier-Stokes equations with slip boundary condition. *SIAM J. Sci. Comput.*, 21:2144–2162, 2000.

[4] V. Bashtovoi, V. Polevikov, A. Suprun, A. Stroots, and S. Beresnev. Influence of Brownian diffusion on the statics of magnetic fluid. *Magnetohydrodynamics*, 43:17–25, 2007.

[5] S. Beresnev, V. Polevikov, and L. Tobiska. Numerical study of the influence of diffusion of magnetic particles on equilibrium shapes of a free magnetic fluid surface. *Commun Nonlinear Sci Numer Simulat*, 14:1403–1409, 2009.

[6] B. Berkovsky, V. Medvedev, and M. Krakov. *Magnetic Fluids [In russian]*. Khimiya, Moscow, 1989.

[7] C. Bernardi. Optimal finite-element interpolation on curved domains. *SIAM J. Numer. Anal.*, 26(5):1212–1240, 1989.

[8] D. Braess. *Finite Elements*. Cambridge University Press, New York, 2007.

[9] M. Cappelezzo, C. Capellari, S. Pezzin, and L. Coelho. Stokes-Einstein relation for pure simple fluids. *J. Chem. Phys.*, 126:224516, 2007.

[10] C. Chainais-Hillairet and J. Droniou. Finite-volume schemes for noncoercive elliptic problems with Neumann boundary conditions. *IMA J. Numer. Anal.*, 31:61–85, 2011.

[11] L. P. Chew. Constrained Delaunay triangulations. *Algorithmica*, 4(1-4):97–108, 1989.

[12] J. Droniou and J.-L. Vázquez. Nonconercive convection-diffusion elliptic problems with Neumann boundary conditions. *Calc. Var.*, 34:413–434, 2009.

[13] M. Feistauer, J. Felcman, and M. Lukáčová-Medviďová. Combined finite element–finite volume solution of compressible flow. *J. Comput. Appl. Math.*, 63(1-3):179–199, 1995. International Symposium on Mathematical Modelling and Computational Methods Modelling 94 (Prague, 1994).

[14] M. Feistauer, J. Felcman, and M. Lukáčová-Medviďová. On the convergence of a combined finite volume–finite element method for nonlinear convection-diffusion problems. *Numer. Methods Partial Differential Equations*, 13(2):163–190, 1997.

[15] M. Feistauer, J. Felcman, M. Lukáčová-Medviďová, and G. Warnecke. Error estimates for a combined finite volume–finite element method for nonlinear convection-diffusion problems. *SIAM J. Numer. Anal.*, 36(5):1528–1548, 1999.

[16] V. Fertman, N. V.A., and S. A.K. Numerical study of the hydrodynamics of high-speed magnetic fluid seals. *Journal of Magnetism and Magnetic Materials*, 39:133–136, 1983.

[17] R. K. Flitney. *Seals and sealing Handbook*. Elsevier Science, Oxford, 2007.

[18] V. Girault and P. Raviart. *Finite Element Methods for Navier-Stokes Equations*. Springer-Verlag, New York, Berlin, Heidelberg, 1986.

[19] C.-w. Guo and S.-c. Feng. Sealing mechanism of magnetic fluids. *Journal of Shanghai University (English Edition)*, 10(6):522–525, 2006.

[20] T. Ikeda. *Maximum principle in finite element models for convection-diffusion phenomena*, volume 4 of *Lecture Notes in Numerical and Applied Analysis*. Kinokuniya Book Store Co., Ltd., Tokyo, 1983. North-Holland Mathematics Studies, 76.

[21] K. Kavaliou and L. Tobiska. A finite element method for a noncoercive elliptic problem with Neumann boundary conditions. *Computational Methods in Applied Mathematics*, 12:168–183, 2012.

[22] M. S. Krakov and I. V. Nikiforov. Influence of the meridional flow and thermomagnetic convection on characteristics of magnetic fluid seal. *Technical Physics*, 56(12):1745–1753, 2011.

[23] L. Landau and E. Lifshitz. *Hydrodynamics [In russian]*. Nauka, Moscow, 1986.

[24] M. Lenoir. Optimal isoparametric finite elements and error estimates for domains involving curved boundaries. *SIAM J. Numer. Anal.*, 23:562–580, 1986.

[25] L. Loitsianskii. *Gas and Fluid Mechanics [In russian]*. Gos. isdatelstvo technikoteoreticheskoj literatury, Moscow, Leningrad, 1950.

[26] P. A. Markowich. *The stationary semiconductor device equations*. Computational Microelectronics. Springer-Verlag, Vienna, 1986.

[27] T. Mitkova. *Lösbarkeit und Finite-Elemente-Approximation eines mathematischen Modells für die Strömung in Magnetfluiddichtungen.* PhD thesis, Otto-von-Guericke Universität, Magdeburg, 2004.

[28] A. Okabe, B. Boots, K. Sugihara, and S. Chiu. *Spatial Tessellations - Concepts and Applications of Voronoi Diagrams.* John Wiley, Chichester, 2000.

[29] V. Polevikov. Stability of a static magneto-fluid seal under the action of an external pressure drop. *Izv. Ros. Akad. Nauk, Mekh. Zhidk. Gaza.*, (3):170–93, 1997.

[30] V. Polevikov. Methods for numerical modeling of two-dimensional capillary surfaces. *Computational Methods in Applied Mathematics*, 4:66–93, 2004.

[31] V. Polevikov and L. Tobiska. Modeling of a dynamic magneto-fluid seal in the presence of a pressure drop. *Fluid Dynamics*, 36:890–898, 2001.

[32] V. Polevikov and L. Tobiska. On the solution of the steady-state diffusion problem for ferromagnetic particles in a magnetic fluid. *Mathematical Modelling and Analysis*, 13:233–240, 2008.

[33] V. Polevikov and L. Tobiska. Influence of diffusion of magnetic particles on stability of a static magnetic fluid seal under the action of external pressure drop. *Commun Nonlinear Sci Numer Simulat*, 16:4021–4027, 2011.

[34] A. F. Pshenichnikov, E. A. Elfimova, and A. O. Ivanov. Magnetophoresis, sedimentation, and diffusion of particles in concentrated magnetic fluids. *The Journal of chemical physics*, 134(18):184508, 2011.

[35] V. Rakhuba, V. Samoilov, and V. Chernobai. Dynamics of high-speed magnetic fluids seals. *Journal of Magnetism and Magnetic Materials*, 39:152–154, 1983.

[36] H.-G. Roos, M. Stynes, and L. Tobiska. *Robust numerical methods for singularly perturbed differential equations: convection-diffusion-reaction and flow problems*, volume 24. Springer Science & Business Media, 2008.

[37] R. Rosensweig. *Ferrohydrodynamics.* Cambridge University Press, Cambridge, 1985.

[38] D. L. Scharfetter and H. K. Gummel. Large-signal analysis of a silicon read diode oscillator. *Electron Devices, IEEE Transactions on*, 16(1):64–77, 1969.

[39] J. R. Shewchuk. Triangle: Engineering a 2D Quality Mesh Generator and Delaunay Triangulator. In M. C. Lin and D. Manocha, editors, *Applied Computational Geometry: Towards Geometric Engineering*, volume 1148 of *Lecture Notes in Computer Science*, pages 203–222. Springer-Verlag, May 1996. From the First ACM Workshop on Applied Computational Geometry.

[40] J. R. Shewchuk. Delaunay refinement algorithms for triangular mesh generation. *Computational geometry*, 22(1):21–74, 2002.

[41] V. A. Solonnikov and S. V. E. A certain boundary value problem for the stationary system of Navier-Stokes equations. *Proc. Steklov Inst. Math.*, 125:186–199, 1973.

[42] O. Steinbach. *Numerical Approximation Methods for Elliptic Boundary Value Problems*. Springer Science & Business Media, New York, 2008.

[43] S. Turek. *Efficient solvers for incompressible flow problems*, volume 6 of *Lecture Notes in Computational Science and Engineering*. Springer-Verlag, Berlin, 1999. An algorithmic and computational approach.

[44] R. Verfürth. Finite element approximation of steady Navier-Stokes equations with mixed boundary conditions. *IMA J. Nume. Anal.*, 19:461–475, 1985.

[45] R. Verfürth. Finite element approximation of incompressible Navier-Stokes equations with slip boundary condition. *Numer. Math.*, 50:697–721, 1987.

[46] R. Verfürth. Finite element approximation of incompressible Navier-Stokes equations with slip boundary condition ii. *Numer. Math.*, 59:615–636, 1991.

[47] A. Vislovich and V. Polevikov. Effect of the centrifugal and capillary forces on the shape of the free surface of a magneto-fluid seal. *Magnitn. Gidrodinamika*, 1:77–86, 1994.

[48] A. Vislovich and V. Polevikov. Numerical simulation of the destruction of magneto-fluid seal with a rotating outer profiled cylinder. *Inzh.-Fiz. Zhurn.*, 70:105–110, 1997.

[49] J. Xu and L. Zikatanov. A monotone finite element scheme for convection-diffusion equation. *Mathematics of Computation*, 68:1429–1446, 1999.